University of Nebraska Medical Center
BREAKTHROUGHS FOR LIFE

University of Nebraska Medical Center
DigitalCommons@UNMC

Theses & Dissertations

Graduate Studies

Spring 5-7-2022

Development of Perfluorocarbon Nanoemulsions for Delivery of Therapeutic Nucleic Acids

Ling Ding
University of Nebraska Medical Center

Follow this and additional works at: https://digitalcommons.unmc.edu/etd

Recommended Citation

Ding, Ling, "Development of Perfluorocarbon Nanoemulsions for Delivery of Therapeutic Nucleic Acids" (2022). *Theses & Dissertations*. 620.
https://digitalcommons.unmc.edu/etd/620

This Dissertation is brought to you for free and open access by the Graduate Studies at DigitalCommons@UNMC. It has been accepted for inclusion in Theses & Dissertations by an authorized administrator of DigitalCommons@UNMC. For more information, please contact digitalcommons@unmc.edu.

Development of perfluorocarbon nanoemulsions for delivery of therapeutic nucleic acids

by

Ling Ding

A DISSERTATION

Presented to the Faculty of
the University of Nebraska Graduate College
in Partial Fulfillment of the Requirements
for the Degree of Doctor of Philosophy

Pharmaceutical Sciences
Graduate Program

Under the Supervision of Professor David Oupický

University of Nebraska Medical Center
Omaha, Nebraska

March 2021

Supervisory Committee:

David Oupický, Ph.D.
Daren L. Knoell, Ph. D.
Todd A. Wyatt, Ph. D.
Tatiana K. Bronich, Ph.D.

Acknowledgements

First and foremost, I would like to express my most sincere thanks to my supervisor Prof. David Oupický for his continued support during the four years of my PhD study. It would not have been possible without his support. I have been encouraged and inspired by his unlimited passion to science, wild knowledge, and critical thinking.

I would also like to appreciate the continue guidance and professional suggestions that from my committee members, Prof. Tatiana K. Bronich, Prof. Todd A. Wyatt, Prof. Daren L. Knoell.

My thanks also go to Siyuan Tang for all the kind help with the animal studies, and Deanna D. Mosley for the help with ciliary beat frequency experiment. My thanks also go to Dr. Weimin Tang and Dr. Huizhen Jia for their kind help and suggestions. I would also like to thank Dr. Ao Yu and Dr. Diptesh Sil for helping me with chemistry. I would also thanks to our lab manager Karen Pennington for her organization. I especially thank all of my former and current lab members, and out of lab for their kind help, suggestions, and encouragement throughout the four-year.

Lastly, I would like to thank my parent, my husband, my son, and my friends for their sincere company, unlimited spiritual support, love and encouragement throughout my studies and my life.

Abstract

Development of perfluorocarbon nanoemulsions for delivery of therapeutic nucleic acids

Ling Ding

University of Nebraska Medical Center, 2021

Supervisor: David Oupický, Ph.D.

Local pulmonary administration of therapeutic siRNA represents a promising approach to the treatment of lung fibrosis, which is currently hampered by inefficient delivery. Pancreatic cancer (PC) is a fatal human cancer whose progression is highly dependent on the nervous tumor microenvironment. siRNA delivery has been well studied as a promising therapeutic agent for several disease, including the pulmonary fibrosis and cancer. Perfluorocarbon nanoemulsions have been studied in the treatment of various diseases as drug delivery systems. We report development of perfluorooctylbromide (PFOB) nanoemulsions as a platform to facilitate delivery and penetration of a therapeutic siRNA to pulmonary fibrosis lung and orthotopic pancreatic tumors. PCX@PFOB emulsion, which contained the polymeric CXCR4 antagonist PCX with PFOB, is a dual functional emulsion to inhibit CXCR4 and deliver siRNA. This dissertation hypothesized that inhibition of CXCR4 by PCX@PFOB emulsion combined with siRNA delivery cooperatively enhances the pulmonary fibrosis and PC treatment.

In chapter 1, an overview of pulmonary siRNA delivery and the recent progress and challenges are given, together with introduction to PC.

Chapter 2 describes PAMD@PFOB/siRNA emulsion polyplexes (EPs) combined with CXCR4 inhibition and STAT3 silencing. We proposed that the EPs overcome two major pulmonary siRNA delivery barriers: cell membrane and mucus layer. The results show that the EPs are capable of efficiently silencing the expression of STAT3 and inhibiting chemokine receptor CXCR4 – two validated targets in pulmonary fibrosis. Both *in vitro* and *in vivo* results demonstrate that the nanoemulsions improve mucus penetration and facilitate effective cellular delivery of siRNA. Pulmonary treatment of mice with bleomycin-induced pulmonary fibrosis showed strong inhibition of the progression of the disease and significant prolongation of animal survival.

Chapter 3 explores P@P EPs to target the tumor-neuronal interaction for PC treatment via NGF silencing by EPR-independent delivery of nanoparticles. P@P EPs exhibited deep tumor penetration that was dependent on exocytosis, and enhanced NGF gene silencing *in vitro* and *in vivo* when compared with control polycation/siRNA polyplexes, leading to the effective and safe suppression of tumor growth in orthotopic pancreatic cancer.

In Chapter 4, conclusion and future directions are described.

Table of Contents

List of Figures

List of Schemes

List of Tables

List of Abbreviations

AEC I - Type I alveolar epithelial cells

AEC II - Type II alveolar epithelial cells

AHP - Acute hepatic porphyria

AKI - Acute kidney injury

ALI – Acute lung injury

ALI - Air-liquid interface

ARF1 - ADP-ribosylation factor

ASL - Airway surface layer

BALF - Bronchoalveolar lavage fluid

BLM - Bleomycin

BPE - Bovine pituitary extract

C/LR - Caveolae/lipid raft dependent endocytosis

CAFs - Cancer-associated fibroblasts

CAMs - Cell adhesion molecules

CBF - Ciliary beat frequency

CDKN2A - Cyclin dependent kinase inhibitor 2A

CF – Cystic fibrosis

Chi3l1 - Chitinase-3-like-1

CME - Clathrin mediated endocytosis

COPD - Chronic obstructive pulmonary disease

CPPs - Cell penetrating peptides

Cpz - Chlopromazine

CTB - CellTiter-Blue

CTGF - Connective tissue growth factor

CXCR4 - C-X-C chemokine receptor type 4

CyD - Cytochalasin D

DEX-NGs - Dextran nanogels

DLS - Dynamic light scattering

DMEM - Dulbecco's modified Eagle medium

DMSO - Dimethyl sulfoxide

DOPE - 1,2-dioleoyl-sn-glycero-3-phoshoethanolamine

DOTAP - 1,2-dioleoyl-3-trimethylammonium-propane

DPIs - Dry powder inhalers

DPPC - Dipalmitoyl phosphatidylcholine

DRG - DGR dorsal root ganglion

DSPC – Distearoylphosphatidylcholine

EC - Endometrial cancer

ECM - Extracellular matrix

EGF - Epidermal growth factor

EMT - Epithelial-to-mesenchymal transition

EP300 - E1A binding protein P300

EPs - Emulsion polyplexes

EXO-1 - 2-(4-Fluorobenzoylamino)-benzoic acid methyl ester

FBS - Fetal bovine serum

FEV1 - Forced expiratory volume

FRET - Fluorescence resonance energy transfer

H&E - Hematoxylin and eosin

HCC - Hepatocellular carcinoma

HMBA - Hexamethylenebisacrylamide

HPLFs - Human primary lung fibroblasts

HPMCs - Human peritoneal mesothelial cells

HSCs - Hepatic stellate cells

HSP47 - Heat shock protein 47

HYP - Hydroxyproline

IF - Immunofluorescence

IHC - Immunohistochemical

ILD - Interstitial lung disease

IP - Intraperitoneal

IPF - Idiopathic pulmonary fibrosis

IV - Intravenous

JAK2 - Janus kinase 2

LHRH - Luteinizing hormone-releasing hormone

LNPs - Lipid-based NPs

LPC - Lysophosphatidylcholine

LPHPs - Large porous hollow particles

MAPK-RAS - Mitogen-activated protein kinase signaling

MCC - Mucociliary clearance

MDI - Metered-dose inhalers

MFI - Mean fluorescence intensity

MP - Macropinoctytosis

MPLFs - Mouse primary lung fibroblasts

MPPs - Mucus-penetrating particles

MSN - Mesoporous silica nanoparticles

MTECs - Mouse tracheal epithelial cells

NAC - N-acetyl cysteine

NDC - Non disease control

NGF - Nerve growth factor

NLCs - Nanostructured lipid carriers

NLRP3 - NLR family pyrin domain containing 3

Nys - Nystatin

PAI-1 - Plasminogen activator inhibitor-1

PBS - Dulbecco’s phosphate buffered saline

PC - Pancreatic cancer

PCL - Periciliary layer

PCX - Polymeric CXCR4 antagonists

PDT - Photodynamic therapy

PEG - Polyethylene glycol

PEI - Polyethyleneimine

PFC - Perfluorocarbon

PFOB - Perfluorooctylbromide

PGP 9.5 - Protein Gene Product 9.5

PI - Propidium Iodide

PI3K - Phosphaphatidylinositol 3-kinase

PLA - Poly lactic acid

PLGA - Poly(lactic-co-glycolic) acid

PLGA-PEG - Poly lactic acid-co-glycolic acid- polyethylene glycol

pMDI - Pressurized metered-dose inhaler

pMDIs - Pressurized metered-dose inhalers

PNI - Perineural invasion

PS - Pulmonary surfactant

PSC - Pancreatic stellate cells

p-STAT3 - Phosphorylation at tyrosine 705

PTT - Photodynamic therapy

PTX - Paclitaxel

rhDNase - Recombinant human DNase

RNAi - RNA interference

RSV - Respiratory syncytial virous

RSV - Respiratory syncytial virus

RT - Room temperature

RT-PCR - Real Time Polymerase Chain Reaction

SAVA - Sisson Ammons Video Analysis

SDF-1 - Stromal cell-derived factor-1

SFD - Spray freeze drying

STAT3 - Signal transducer and activator of transcription 3

TB - Tuberculosis

TEM - Transmission electron microscopy

TGF-β - Transforming growth factor beta

TME - Tumor microenvironment

TrkA - Tyrosine kinase A

UCHL-1 - Ubiquitin C-terminal hydrolase 1

VIPER - Virus-inspired polymer for endosomal release

VSVG - Vesicular stomatitis virus

W/D - Wet/dry

α-SMA - α-smooth muscle actin

Chapter 1. Introduction

1. Pulmonary siRNA delivery for lung disease: Review of recent progress and challenges

Please note that this part of the dissertation was published in the Journal of Controlled Release (Ling Ding et al, 2020). As the first author, I wrote this review. Prof. Oupicky, Prof. Knoell, Prof. Wyatt, and Siyuan Tang helped with editing the manuscript. All the co-authors agree with including their work in this dissertation.

Lung diseases are a significant global public health problem creating a large economic burden [1]. Because the lung directly interfaces with the external environment, inhaled drug delivery to therapeutically address pulmonary diseases has been a longstanding goal. In addition to endogenous stimuli, the lungs are susceptible to inhalation injury and multiple related diseases as an organ exposed directly to harmful substances [2-4]. Pulmonary delivery offers the potential to address unmet medical needs in lung-related disease including allergy [5], asthma [6], idiopathic pulmonary fibrosis (IPF) [7], cystic fibrosis (CF) [8], both viral and bacterial infections [9], acute lung injury (ALI) [10], chronic obstructive lung disease (COPD) [11], and lung cancer [12].

Inhalation-based delivery of small interfering RNA (siRNA) designed for efficient, targeted delivery to specific cells within the lungs holds great promise but remains yet to be realized. In general, inhalation drug delivery systems, if designed effectively, reduce the overall dose required to treat pulmonary disorders in comparison to oral or parenteral

delivery systems. They also avoid first-pass metabolism, reducing dose and risk of toxicity from metabolic byproducts. It provides a reproducible and possibly more economical platform that can be provided to diverse patient populations within a variety of settings and on a daily basis if necessary. The now commonly used dry powder inhalation (DPI) devices used to treat asthma or COPD serve as excellent examples [13].

Active targeting of the lung using siRNA has been a postulated approach for a variety of lung diseases. siRNAs induce gene silencing by a sequence-specific posttranscriptional process known as RNA interference (RNAi) [14]. With the first siRNA medication (Patisiran) approved in the USA and EU [15], the field of siRNA delivery received a strong stimulus to expand the scope of RNAi therapeutics to other diseases [16]. Patisiran is a nanoparticle formulation containing a chemically modified siRNA encapsulated with lipid excipients for delivery to hepatocytes. The lipid nanoparticles are composed of ionizable cationic lipids (DLin-MC3-DMA), phospholipid (DSPC), cholesterol, and polyethylene glycol modified lipids (PEG2000-C-DMG), that are combined via rapid mixing under acidic conditions. The siRNA is modified with eleven 2'-methoxy-modified sugar residues and four 2'-deoxythymidine residues to improve the stability and to avoid off-target effects [17]. Another RNAi drug GIVLAARI™ (givosiran) was approved in November 2019 for the treatment of acute hepatic porphyria (AHP) [18]. The treatments based on siRNA provide potential benefits compared to traditional drugs, including target specificity and ability to inhibit the expression of mutant proteins without affecting wild type ones [16]. For RNAi-based therapies, a suitable delivery strategy is critical for optimum therapeutic effect. In

many diseases like cancer, amyloidosis, viral infections, hypercholesterolemia, and acute kidney injury (AKI), systemic delivery is necessary for siRNA to reach a specific target. There are more than 25 systemically administered siRNA drug candidates are under clinical trials [19, 20]. However, systemic delivery of therapeutic siRNA targeting tissues other than the liver has proven challenging. Local delivery of siRNA provides potentially better gene silencing at the target site and circumvents the first-pass effect thus resulting in lower doses and reduced off-target effects [21]. There are thirteen clinical trials that utilize local siRNA delivery as of the fall of 2020 [20]. Direct delivery of siRNA into the lungs is non-invasive and allows for self-medication [22]. Addressing pulmonary delivery barriers and intracellular delivery of siRNA is critical for success of pulmonary siRNA delivery. The use of nanoparticles to deliver siRNA can help to overcome anatomical barriers, mucociliary clearance (MCC), intracellular siRNA uptake limitations, and macrophage alveolar clearance. For optimum siRNA pulmonary delivery, siRNAs need to be deposited to the target region of the lungs and released at the target cells. An ideal siRNA delivery system should: (1) condense siRNA into a stable particle, (2) protect siRNA from nuclease degradation, (3) improve cellular uptake and promote endosomal escape to release siRNA to the cytoplasm of target cells, and (4) specifically silence the target gene with low off-target effects and toxicity [3]. In this review, we highlight the progress of pulmonary siRNA delivery over the past decade.

1.1. Pulmonary barriers that affect siRNA delivery

Efficient delivery of siRNA directly to the lungs with the intent to treat lung diseases is relatively complex despite the convenience of established inhalation delivery strategies. Depending on the desired location of delivery for a given disease state (upper airway, lower airway, alveolar region, systemic absorption) a number of considerations that include packaging, particle size, morphology, geometry, surface properties, cell target, and host defense mechanisms must be taken into consideration. There are three mechanisms of drug deposition in the respiratory system: impaction, sedimentation, and diffusion. From a particle point of view, if the intended location of drug deposition is the alveolar region, it will require navigation past 23 branching segments [23]. Therefore, the formulation must be designed with an optimal aerodynamic particle size that can be maintained and afford deep penetration into the lung. In particular, large particles with aerodynamic diameters greater than 6 μm deposit on the back of the larynx in the upper airways, never reaching the lower airway. If the intent is to deliver siRNA to the bronchiolar or alveolar region, then smaller particles are required. Likewise, if particles are designed with an aerodynamic diameter less than 1 μm they are predominantly exhaled due to Brownian motion, never achieving deposition [24, 25]. Accordingly, the optimal aerodynamic diameter for efficient lung deposition typically is in a range between 1-5 μm.

Considering that innate host barrier defense mechanisms are designed to keep foreign particles out of the lungs, carefully consideration of these natural defense mechanisms is necessary when formulating pulmonary siRNA therapeutics. Perhaps the

biggest obstacle to particulate drug delivery is the mucociliary transport system, including the mucociliary clearance and phagocytosis by macrophages. A variety of epithelial cell subtypes forms a continuous barrier, sealed by tight junctions, that secrete mucus and other host defense factors into the lumen that work in concert with oscillating ciliary projections particularly in the upper airway and bronchiolar regions [26]. Together this system works to capture foreign particles and escalate them up and out of the airway. Further, excessive mucus production is a characteristic encountered in many inflammatory-based lung diseases including, but not limited to, CF, chronic bronchitis and asthma thereby potentially making it more difficult for a particle to avoid capture or to traverse this barrier in order to reach intended target cells [27]. The deeper a particle penetrates into the lung, the more frequently it will encounter alveolar macrophages that are designed to phagocytose and destroy foreign particles, as this too may be modified further in certain disease states (discussed in more detail later). Finally, the epithelial barrier is bound together via multiple tight junctions designed to maintain a patent airway. The epithelium is in a polarized state such that the expression of surface bound proteins may be restricted to or predominantly expressed on the apical or basolateral surface, thus making it more or less accessible for receptor-targeted approaches [28].

The pulmonary surfactant (PS) and macrophages in the airspace are another obstacle to affect the pulmonary siRNA delivery. The alveolar macrophages are phagocytes residing in the airspace that play a critical role in homeostasis, host defense and tissue remodeling. In the following section, we will focus on the details of the most

important pulmonary barriers to siRNA delivery and on how to strategically overcome the barriers in order to improve siRNA delivery efficiency.

1.1.1. Pulmonary surfactant (PS)

PS is a surface-active material covering the entire alveolar surface, which is secreted by specialized alveolar type II epithelial cells (AEC II). The main physiological role of PS is to maintain low surface tension upon expiration to prevent alveolar collapse. PS has been extensively studied because of the functional role in mammalian breathing [29, 30]. Inhaled gene vectors that make it to the alveoli must retain their stability and function in the presence of PS which are abundant in the airspace. Natural human PS has a complex composition of ~8% of surfactant proteins and ~92% of lipids by mass. The protein part consists of four surfactant proteins which can be structurally divided into two parts: the larger hydrophilic SP-A and SP-D, and the smaller hydrophobic SP-B and SP-C [31]. The hydrophilic surfactant proteins, also known as collectins, participate in the opsonization process to promote pathogen and particle uptake by phagocytic cells [32]. The hydrophobic surfactant proteins regulate the interfacial surfactant absorption dynamics, which improve the lipid transfer and membrane fusion process. The lipid fraction mainly contains zwitterionic phosphatidylcholine (~60-70 wt%), anionic phosphatidylglycerol (~10 wt%), and neutral lipids, of which cholesterol is the most abundant (~8-10 wt%) [29, 30]. From an inhalation therapy perspective, PS is primarily considered as one of the extracellular barriers in the deep lung which needs to be overcome to gain access to the underlying target cells [33, 34]. Poractant alfa, a modified PS from swine, and beractant,

bovine PS, are commercially available for treating neonatal respiratory distress syndrome [35].

1.1.2. Alveolar macrophages

Alveolar macrophages are phagocytes residing in the airspace that play a critical role in homeostasis, host defense, and tissue remodeling. There are 12-14 macrophages in each alveolus and the numbers may vary in pathological states, such as observed increases in smokers [36]. Following inhalation, particles can be rapidly cleared by alveolar macrophages via opsonin-independent scavenger receptors or by opsonin-dependent mechanisms, which trigger the release of pro-inflammatory cytokines TNF-α and IL-1β and initiate the production of further inflammatory mediators, consequently leading to the acute lung toxicity [37, 38]. In alveoli, phagocytosis by macrophages and migration towards the mucociliary escalator contribute to the overall elimination. Although macrophages are less efficient in the phagocytosis of nanoparticles than microparticles [39, 40], siRNA-containing nanoparticles may aggregate in the presence of PS, which increases their susceptibility to macrophage clearance. In the case of polymeric nanoparticles, studies have shown that particles with hydrophobic surfaces are more susceptible to phagocytosis by macrophages than those with hydrophilic surfaces [41].

The alveolar macrophages in the bronchoalveolar lumen play a critical role in lung inflammatory pathologies and therefore constitute attractive target for siRNA therapeutics. However, delivery of siRNA to macrophages presents a significant challenge, because the fully differentiated alveolar macrophages are difficult to transfect. Several strategies have

been devised to overcome this challenge. PLGA microparticles with encapsulated siRNA were successfully aerosolized and resulted in strong macrophages transfection [42]. Macrophage uptake of anionic PLGA-lipid hybrid microparticles was greater than uptake of positively and negatively charged precursor PLGA particles [43]. Lynn et al. developed a hybrid core-shell nanoparticle that mediated efficient *in vivo* delivery of siRNA to alveolar macrophages [44]. Duo et al. evaluated an inhaled exosomes to deliver siRNA to activate or inhibit alveolar macrophages, which can modulate pulmonary immune response, and results proved that only lung macrophages efficiently take up exosomes *in vivo* [45]. Despite the promising results, better understanding of how environmental damage affects alveolar macrophage function is necessary for the development of macrophage-targeted treatment strategies.

1.1.3. Mucociliary clearance (MCC) and periciliary layer (PCL)

MCC by ciliated epithelial cells serves as a barrier to pulmonary siRNA delivery. In the upper and central airways, epithelial cell mucus is a defense barrier against irritants such as bacteria, allergens, and other inhaled particles (Figure 1.1). Airway mucus is produced by secretory cells including goblet cells and club cells and forms an adhesive and hyper-viscoelastic barrier to impede particle deposition in the deeper lung [46, 47]. Airway mucus is composed of mucins, water, and other gel-like constituents [46]. Mucins are glycoproteins with densely glycosylated and negatively charged regions. The mucus covering the airway epithelium has been recognized as one of the greatest obstacles to siRNA delivery. Electrostatic interactions with positively charged siRNA particles may trap

the particles in the mucus layer resulting in increased MCC and decreased delivery efficacy [48]. Demeester *et al.* showed that cationic DOTAP/DOPE lipoplexes were stable when incubated with diluted CF sputum obtained from patients, but binding of mucins decreased the transfection efficacy. Mucins, however, did not cause aggregation or dissociation of the lipoplexes, indicating that mucins alter (intra)cellular steps in the transfection process [49]. Nanoparticles trapped in the mucus layer of the airways are cleared by MCC or cough-driven clearance. However, particles that rapidly penetrate through the mucus layer and into the PCL may be retained significantly longer in the lungs. The PCL is believed to be nearly stationary and presents a significantly steric barrier to particle penetration. In CF lungs, dehydration of PCL mediated by dysregulation of epithelial sodium channels in the airway epithelium can cause osmotically driven collapse of the PCL, which makes the PCL mesh tighter and thus increases further the barrier to particle transport. Overall, particles that can penetrate the mucus layer but not the PCL would also be cleared via MCC or by macrophages [39].

Multiple strategies have been studied for effective mucus layer penetration and MCC avoidance, including mucus-penetrating particles (MPPs). Unlike mucoadhesive particles, which are trapped in the luminal mucus layer and eliminated by the MCC, MPPs diffuse through mucus and avoid MCC. Surface properties of the MPPs are crucial in improving mucus penetration [38, 46, 48, 50, 51]. To favor penetration, MPPs should be small enough to avoid entrapment in the mucin mesh and have hydrophilic and neutral surface charge to avoid interactions with the hydrophobic and negatively charged groups of

mucins. However, siRNA delivery often relies on lipophilic and positively charged carriers [46]. Therefore, careful surface engineering strategies are needed. Among those, dense surface coating with polyethylene glycol (PEG) has been the most successful approach. Surface PEG affects lung distribution, mucus penetration, and lung-residence time of the siRNA particles [38, 50, 52]. Densely PEGylated DNA MPPs showed greatly enhanced particle distribution, lung retention time, and gene transfer following intranasal administration compared to similarly sized mucoadhesive nanoparticles [52]. A recently reported alternative to PEG to facilitate mucus penetration relies on a unique combination of lipophobic and hydrophobic properties of perfluoroalkyl polymers [51].

The use of adjuvants which can modulate the biological barriers is another suitable approach to overcome the barriers. Adjustment of biological barriers with properly selected adjuvants is one possible way to enhance the efficiency of pulmonary siRNA delivery. However, it is important to ensure that any adjuvant approaches do not cause significant toxicity or disrupt the normal lung function. The most widely explored method in this context has been the use of mucolytic agents that degrade or loosen primary macromolecular components of airway mucus, such as, the recombinant human DNase (rhDNase, Pulmozyme®) and N-acetyl cysteine (NAC, Mucomyst®) [53], which can significantly reduce the viscoelasticity of airway mucus. Both are clinically used in helping CF patients clearing accumulated mucus from the airways. It has been reported that pre-treatment with NAC increases mucus mesh spacing which leads to rapid diffusion and improved penetration through airway mucus [54]. Improving airway surface hydration with

osmotically active inhaled hypertonic saline provides another effective way of mucus clearance [55, 56]. Inhaled mannitol creates an osmotic drive for water to move into the airway lumen. The consequent increased hydration of the airway surface decreases the adherence of mucus to the epithelium, facilitates the coupling of mucus and cilia thereby increasing mucus clearance. Inhaled dry powder mannitol (Bronchitol®) is promising to be an effective treatment for the clearance of retained airway secretions in the patients with CF and thereby may also be useful as an adjuvant to inhaled gene therapy [57].

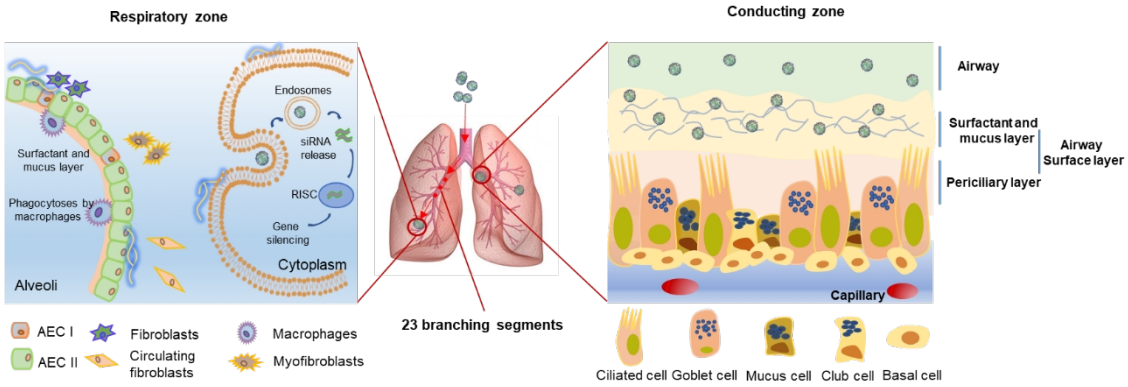

Figure 1.1 Schematic illustration of the pulmonary barriers that affect siRNA delivery

1.1.4. Cellular and intracellular barriers

To exert its therapeutic effect, siRNA must be delivered to the cytoplasm of the target cells. The cell uptake pathway associated with the siRNA delivery by non-viral vectors is endocytosis. There are four main mechanisms of endocytosis. First, clathrin-mediated endocytosis, which is the most widely studied mechanism and is involved in receptor-mediated uptake of nanoparticles. For example, transferrin receptor, low density lipoprotein receptor, and epidermal growth factor receptors have been explored to mediate endocytic uptake. Second, caveolin-dependent endocytosis, which generates cytosolic caveolar vesicles following nanoparticle binding to the cell membrane. Third, macropinocytosis, which generates large macropinosomes containing extracellular fluid and soluble proteins. Fourth, other endocytic mechanisms that rely on actin-driven membrane protrusions, which subsequently fuse with and separates from the plasma membrane to generate macropinosomes [58]. For the most obstructive lung diseases, such as COPD and CF, airway epithelial cells are the primary target for treatment. Unfortunately, these cells display low endocytic activity on the apical side [39]. Agents such as the natural airway surfactant lysophosphatidylcholine (LPC) or the calcium chelator EGTA were employed to transiently disrupt epithelial tight junctions and improve vesicular stomatitis virus (VSVG)-HIV entry *in vivo* [59]. Particles smaller than 150 nm allow for endocytosis and also limit macrophage uptake, both of which help to avoid lung clearance [60]. Upon endosomal cellular entry, siRNA must escape from the endosomes into the cytoplasm. Multiple strategies have been studied to overcome and promote the

endosomal escape of siRNA that are directly applicable to pulmonary delivery [61-66]. Active targeting using ligand moieties that bind to over-expressed receptors on the surface of target cells is a widely explored strategy to enhance cell uptake and to improve therapeutic efficiency [67]. For example, T-cell targeted pulmonary siRNA delivery using transferrin and melittin-PEI conjugate shows efficient uptake in active T cells and endosomal escape for the treatment of asthma [68]. As cholesterol is an essential component of the cell membrane and can be metabolized, it is often used as the lipid anchor for improving stability and cellular uptake as well as decreasing the cytotoxicity of the carriers [69]. Once taken up by the target cells, siRNA particles must overcome several intracellular barriers, including but not limited to the endosomes and lysosomes. These barriers are shared in numerous organs and tissues in addition to the lungs and have been extensively reviewed elsewhere [70].

1.2. Disease-dependent pathological changes and their role in pulmonary disease and impact on siRNA delivery

When considering whether a patient with a given lung disease would benefit from inhalation of siRNA there are a number of important host factors that should first be determined. Pulmonary mechanics play a vital role in deciding whether medication can be inhaled deep into the lung, retained, and made available to target cells. In the majority of asthma or COPD patients, the day-to-day fluctuation in respiration is suitable for metered-dose inhalers (MDI), DPI, or nebulizers [13]. In extreme settings of lung diseases, such as stage IV COPD with forced expiratory volume (FEV1) < 50%, severe asthma (FEV1 <

50%), or end-stage IPF with diffusion capacity of the lung for carbon monoxide (CO) (DLCO) < 50%, respiration may be severely obstructed or restricted to the extent that inhalation is ineffective because therapeutic deposition of particles cannot be achieved [71]. This would be most apparent during acute disease exacerbations.

Tissue composition must also be considered. In the case of obstructive lung diseases, such as asthma or chronic bronchitis, airway tissue composition changes significantly with increases in mucus production, hypertrophy of the basement epithelial membrane and surrounding smooth muscle, activated immune cells, and the many inflammatory factors that they produce [72]. This also leads to changes in the composition of the aqueous and mucous layers that line the airway thereby in most instances decreasing fluidity and increasing viscosity [72]. Whether siRNA particles can traverse through this complex admixture en route to target cells that lie underneath remains a major challenge in this field.

In CF, the levels of endogenous DNA and actin filaments released from necrotic neutrophils are elevated which further contributes to the dense mesh structure of the airway [73]. The elevation of oxidative stress in CF increases disulfide cross-links between mucin fibers which unfavorable changes mucus transport properties for particles [74]. The size of the CF mucus mesh ranges from 60 to 300 nm [75]. Gene delivery vectors that have been used in CF clinical trials have been shown to be incapable of efficiently penetrating CF mucus, most likely due to the positivity charged surface of the formulations that interact with negatively charged mucus.

COPD patients experience increased airway inflammation, dynamic lung hyperinflation, elevated bacterial colonization in the lower airways, and increased susceptibility to viral airway infections [76]. Significant efforts have been made to develop siRNA therapeutics targeting mRNAs involved in the pathogenesis of COPD, including RIP2, RPS3, MAP3K19, and CHST3 [7, 77]. Clinical trials using either viral or non-viral delivery vectors have failed to show clinical benefits because of inefficient transfection of target cells [39]. Poor ability of the particles to penetrate the mucus layer and aggregation caused by PS are likely other reasons for the lack of success in clinical testing. COPD and CF show activation of the alveolar macrophages, which provides additional challenge in siRNA delivery [78]. In asthma, the barrier function of the airway epithelium is impaired through defective tight junction formation. The tight junction proliferation results in increased epithelial resistance. However, the pro-inflammatory cytokines and bacterial toxins reduce the permeability of tight junctions, which means that the barrier properties of the airway epithelium may vary with disease state [79].

Respiratory infections can be caused by a wide range of microorganisms in airways, including bacteria and viruses. Respiratory infections are among the most common reasons for hospitalization, partly because many infectious diseases have become difficult to treat due to the rise of antimicrobial resistance. The respiratory syncytial virous (RSV) replicates in the superficial layer of the respiratory epithelium, local delivery of siRNA to the lungs is a rational approach to treat RSV infection [80]. There has been a clinical test of an siRNA formulation, ALN-RSV01, which was directed against mRNA that exhibits

specific anti-RSV activity [80]. Tuberculosis (TB) is a bacterial lung infection caused by Mycobacterium Tuberculosis. RNAi approaches against TB typically aim to modulate the host gene expression or host immune response instead of targeting the microorganism directly due to the lack of the requisite machinery for RNAi [81, 82]. The 2020 pandemic of the newly discovered coronavirus (SARS-CoV-2, COVID-19) spurred interest in siRNA as a possible treatment [83]. In principle, multiple proteins encoded in the viral genome can be targeted by siRNA. Zheng et al. designed 48 siRNA sequences that potentially target the entire SARS-CoV genome, including ORFs needed for the translation of key proteins [84]. Li et al. developed an siRNA which improved several symptoms of SARA-CoV, like fever, viral load, and acute alveolar damage [85]. He et al. demonstrated synergistic antiviral effects through the use of siRNA pool targeting various structural genes of the virus [86]. Since coronaviruses are positive ssRNA viruses that use ORF1a and ORF1b replicases [87], siRNA could be an efficient approach to control the virus by silencing the viral mRNA at particle stages. Future studies are called for to evaluate their potential efficiency and safety.

Finally, a significant limitation for the greater success of inhalation therapies is in the development of validated animal models of different lung disease states [2, 88]. Approaches to enhance RNA stability, tissue targeting, cell penetration and intracellular endosomal escape are critical to realize the full potentials of RNAi drugs. This is important in preclinical development to demonstrate efficacy, toxicity profiles, and ultimately the establishment of appropriate human dosing regimens and how *in vitro* models can enrich

pulmonary drug delivery research allowing for faster and more reliable clinical translation [88, 89].

1.3. Recent developments in the pulmonary siRNA delivery systems

Pulmonary siRNA delivery requires the use of suitable vectors that can safely circumnavigate the unique environment and barriers in the lungs [2, 21, 22, 90]. In addition to the delivery barriers discussed above, the stability of delivery systems is critical for efficient pulmonary siRNA delivery. For the systemic siRNA delivery, the siRNA is rapidly degraded with poor stability. Even though the nuclease levels are low in the lungs, the particles stability in the presence of mucus and PS poses an obstacle. It is critical to evaluate the impact of mucus and PS on the delivery systems. Study showed that the cationic lipid-based siRNA nanocarriers (LipofectamineTM and RNAiMAX) were incompatible with PS, however, the gene silencing potential of siRNA-loaded dextran nanogels (DEX-NGs) was maintained in the presence of PS and the intracellular siRNA delivery by DEX-NGs was enhanced [91]. Moreover, BALF contains inhibitory components for non-viral gene transfer, and a study showed that mucin absorbed more to lipoplexes than to polyplexes. However, the specific inhibitory components have not been identified. The inhibition was most likely due to the charge in the surface charge of the gene vectors [92]. The shielding of siRNA particles to circumvent interaction with the airway surface layer (ASL) environment should be a focus for pulmonary administration.

In the following sections, we will review safety considerations and focus on the main types of vectors employed in the pulmonary siRNA delivery. Because each type of delivery

vector offers a unique set of advantages and disadvantages, there is a great need for direct head-to-head comparisons of the different delivery systems to provide evidence for their relative delivery performance. A good example of such a study is the evaluation by Garbuzenko et al. of micelles, liposomes, mesoporous silica nanoparticles, cationic dendrimers, quantum dots, and PEG in their ability to accumulate in the lungs [93].

1.3.1. Safety of pulmonary delivery systems

Careful safety evaluation of siRNA delivery systems is critical for their use because of the finely tuned and sensitive immune response of the respiratory system to foreign particles. Evidence shows that the observed toxic effects related to particulate delivery systems are primarily mediated by inflammatory responses that often occur after particle-induced oxidative stress. The extent of the response is sensitive to the physicochemical properties of the particles, including their size, chemical composition, surface properties, charge, and shape [94]. The intracellular oxidative stress can regulate the expression of endothelial cell adhesion molecules (CAMs) by transcription-dependent mechanism that involves redox-sensitive transcription factors and result in the activation of the MAPK and NF-κB pathways, which leads to the release of the inflammation-related cytokine [95]. Multiple studies show that most positively charged particles induce lung inflammation following pulmonary delivery. For example, positively charged chitosan microparticles and gold and Fe_3O_4 nanoparticles caused inflammatory lesions in rodents [96]. Rats given positively charged graphene nanoplates exhibited greater pulmonary inflammation than negatively charged counterparts [97]. Mice administered with cationic liposomes and

cationic NLCs developed pulmonary inflammation, while neutral and anionic liposomes and anionic NLCs exhibited normal lung histology [97, 98]. For some particles, however, negative surface charge can elicit stronger release of proinflammatory cytokines than positively charged particles [99]. For example, in RAW264.7 macrophages, negatively charged silica nanoparticles induced the highest secretion of proinflammatory TNF-α compared to neutral and positively charged silica NPs [100]. Negative surface charge on quantum dots enhanced the mRNA levels of TNF-α in A549 cells, whereas IL-1β expression was enhanced by all quantum dots regardless of their surface charge [101]. Lipid-based delivery vectors can induce toxicity and non-specific activation of inflammatory cytokines and interferon response [102], while alveolar macrophages are not activated by exposure to polymeric microspheres [103].

To reduce non-specific toxicity to normal lungs following pulmonary delivery, nanoparticles with site-specific targeting and triggered release characteristics have been evaluated. PS-based pH-sensitive nanoparticles were cytotoxic to lung tumor cells but proved safe to healthy lung cells, indicating a possible selective toxicity can be achieved [104]. A biodegradable PLGA nanoparticles did not induce apoptosis, oxidative stress or cell cycle arrest compared with nonbiodegradable forms [105]. A block copolymer composed of PEG and PAsp(DET) achieved safe gene transfection without inducing severe lung inflammation [106]. Covalent siRNA conjugates are among the most promising delivery approaches with a usually favorable toxicity profile [107]. Further,

exosomes as a new class of delivery systems did not trigger the lung immune response and were less likely to aggregate [45].

1.3.2. Lipid-based carriers for pulmonary siRNA delivery

A majority of commercial siRNA transfection agents are based on cationic lipids and some of them have been used in pulmonary delivery [108]. Lipid-based formulations used in pulmonary siRNA delivery include liposomes, lipoplexes, and nanostructured lipid carriers (NLC) [109]. Despite their outstanding transfection efficacy, the presence of cationic lipids in many of the formulations raises toxicity concerns associated with non-specific activation of inflammatory cytokines and interferon responses [110]. The inflammation response can be minimized by incorporating PEG lipids into the formulations [111]. However, a balance must be found between the positive surface charge and PEG surface density. The exclusive use of neutral lipids such as cholesterol in the form of covalent siRNA-lipid conjugates may reduce the toxicity and inflammation associated with cationic lipids [112].

Incorporation of specific ligands to achieve receptor-targeted siRNA delivery has been explored in various delivery strategies, including pulmonary delivery. Tumor-specific receptor luteinizing hormone-releasing hormone (LHRH) has been used in NLC formulations of siRNA and paclitaxel (PTX) in pulmonary treatment of lung cancer [113]. Inhalation delivery of the targeted formulation showed limited adverse effects and clearly outperformed non-targeted formulation as well as intravenously administered control. Oligolysine epithelial-targeting peptide have been used as part of DOTMA/DOPE

formulations to deliver siRNA to mediate silencing of airway epithelial ENaC [114]. siRNA encapsulated in a vitamin A-coupled liposome efficiently suppressed HSP47 expression and induced apoptosis of myofibroblasts in the IPF model [115]. When Genzyme GL-67 cationic formulation composed of DOPE and DMPE-PEG, was clinically tested for the delivery of DNA for cystic fibrosis treatment [116], chloride abnormalities were improved and bacterial adherence in patients' lungs was reduced.

Lipids have also been widely used as components of other of siRNA delivery systems. For example, hybrid lipid-polymer nanoparticles containing PLGA and dipalmitoyl phosphatidylcholine (DPPC) have shown great potential for pulmonary siRNA delivery [117]. Similar hybrid nanoparticles have been optimized for scale-up, spray-drying production to fabricate physiochemically stable, biologically functional powders with properties optimal for pulmonary siRNA delivery [118].

1.3.3. PS for pulmonary siRNA delivery

Recent studies have shown that PS can be used to prepare nanoparticles with control over their biological fate, toxicity, pulmonary distribution, cell targeting, and intracellular delivery [44]. In the context of pulmonary siRNA delivery, PS can be used as carriers in the design of unique and bio-inspired systems to improve the siRNA distribution at the alveolar interface in the deep lung. The PS-based delivery strategy was first reported in 1994 in a study that used poly(lysine) conjugated to SP-B to deliver DNA into airway cells *in vitro* [119]. Because SP-B is positively charged, it is one of the most investigated PS for pulmonary delivery [33, 34, 120, 121].

Amphiphilic cationic KL4 peptide was developed and tested as a synthetic SP-B mimic [122]. KL4 is one of the active compounds in Surfaxin, an FDA-approved intratracheal PS suspension for the prevention of RDS [122]. The KL4 peptide formed complexes with siRNA and helped in delivery in lung epithelial cells. Compared with conventional lipoplexes, the KL4/siRNA complexes remained stable and mediated efficient siRNA transfection in the presence of PS [123].

Systematic studies have been conducted to delineate how lipid composition affects pulmonary siRNA delivery with SP [29, 30, 33, 34, 44, 91]. Hybrid nanoparticles consisting of siRNA-loaded dextran hydrogel core were coated with Curosurf® (a clinically used porcine PS) as an outer shell. The studies demonstrated that the outer layer of PS enhanced the intracellular siRNA delivery [34, 44]. SP-B was identified as the key component responsible for the enhanced siRNA delivery following pulmonary administration [30]. SP-B can also promote siRNA delivery to other cell types, suggesting a more universal carrier potential [29].

1.3.4. Polycation-based systems for pulmonary siRNA delivery

The utility of polycations as siRNA delivery systems called polyplexes has been explored for several decades. A plethora of synthetic and natural polycations have been pursued for pulmonary delivery of siRNA, including PEI and chitosan [60].

PEI has become one of the most widely studied siRNA delivery vectors because of its highly modifiable amine-rich structure that facilitates effective cellular internalization and endosomal escape [124-127]. Clinical application of PEI or its conjugates has been

so far limited by toxicity concerns [125]. Modification of PEI with neutral or anionic moieties, like PEG, perfluoroalkyls, hyaluronic acid, and attachment of targeting moieties has been shown to reduce toxicity [125-128]. Transferrin-PEI was designed to selectively deliver siRNA to activate T cells in the lung to avoid potential systemic effects [125]. An investigation by Merkel et al. showed that polyplexes formulated with PEG-PEI demonstrate better targeted delivery of siEGFP compared with PEI polyplexes via intratracheal administration [126]. In our previous study, we designed polyplexes based on CXCR4 (C-X-C chemokine receptor type 4) inhibiting PEI derivative (PEI-C) for pulmonary delivery of siRNA as a combination treatment of IPF [129]. Similarly, pulmonary co-delivery of chemotherapy and siRNA can improve therapeutic efficacy in lung cancer [130]. Doxorubicin was conjugated to PEI using a pH-sensitive cis-aconityl linker and the polymer-drug conjugate was then used to condense siBcl-2 into polyplexes [130]. The combined polyplexes exhibited enhanced antitumor efficacy compared with either monotherapy.

Chitosan is another polycation that has been evaluated for pulmonary siRNA delivery [131]. Findings showed that chitosan dry powder prepared by spray freeze drying delivered siRNA against VEGF decreased the number of metastatic lesions in the lungs [132]. A limitation of chitosan is its poor solubility at physiological pH [131, 133]. Various chemical modifications of chitosan have been used, including PEG conjugation. Piperazine substitution of chitosan increased aqueous solubility at physiological pH, lowered cytotoxicity, and increased gene silencing efficacy. The system was used for

inhalation delivery with good tolerability [131]. Xu et al. developed inhalable chitosan particles for co-delivery of doxorubicin and siRNA. The nanoparticles, which were embedded in poly-L-lactide (PLA) were highly stable and achieved deep lung deposition with excellent aerodynamic performance and sustained release of doxorubicin [134].

Cationic dendrimers have well-defined hyperbranched 3D structure with spherical shape [135]. The high density of surface groups allows for specific ligand modification for improved siRNA delivery [136]. Generation 4 PAMAM dendrimer was used for siRNA delivery using pressurized metered-dose inhaler (pMDI) [137]. The dendrimer/siRNA polyplexes were stabilized with mannitol and given with hydrofluoroalkane propellant to achieve siRNA delivery to alveolar epithelial cells. Triphenyl phosphonium modification of PAMAM dendrimers achieved successful aerosol delivery to the lungs using portable inhalers [138]. Dendrimer/siRNA polyplexes prepared using microfluidic assembly were successfully evaluated in spray-dried microparticle form [139].

Virus-inspired polymer for endosomal release (VIPER) was developed based on a polycation block to electrostatically condense siRNA into polyplexes [140]. Pulmonary administration of VIPER polyplexes in mice improved accumulation of the particles in both the bronchial and alveolar epithelium.

Compared with simple polyplexes, core-shell polymeric NPs can encapsulate siRNA in a polymer matrix to improve siRNA stability in the formulation [141]. Receptor-targeted nanoparticles comprising multifunctional mixtures of cationic segments (oligolysine epithelial-targeting peptide and the liposome DOTMA/DOPE) demonstrated effective

mucus penetration and siRNA delivery to airway epithelium with low cytotoxicity, high transfection efficiency, and increased gene expression [114].

Fluorinated polycations emerged as attractive materials for nucleic acid delivery due to their unique serum resistance associated with the lipophobic and hydrophobic features of fluorocarbons [142]. Fluorination as an effective strategy for transmucosal nucleic acid delivery using guanidinated and fluorinated bifunctional helical polypeptides was reported recently [51]. The authors found that fluorination prevented undesired dissociation and decreased the mucin aggregation, which improved mucus penetration. This was due to reduced interactions between the polyplexes and the mucins. We have recently taken advantage of the fluorinated polycations in a pulmonary delivery strategy to successfully modulate the immune response and enhance anti-PD-L1 immunotherapy in lung cancer [143].

1.3.5. Peptide-based systems for pulmonary siRNA delivery

Bioactive cationic peptides represent an interesting class of siRNA delivery systems due to the possibility to take advantage of their inherent biological activity to improve the efficacy of the delivery process. Cell penetrating peptides (CPPs) used alone or covalently conjugated to polymers are a common example. CPPs consist of short amino acid chains and can interact with the plasma membrane to allow for cellular uptake during siRNA delivery [144]. A recent study shows that the silencing of chitinase-3-like-1 (Chi3l1) expression in the lung using CPPs-siRNA complexes (dNP2-siChi3l1) inhibits lung metastasis with enhanced Th1 and cytotoxic T-lymphocyte responses [145]. However,

when compared to naked siRNA, conjugation of siRNA to transactivator of transcription and penetrating CPPs failed to increase siRNA-mediated gene knockdown in healthy mouse lung [146].

1.3.6. Emulsion-based systems for pulmonary siRNA delivery

Direct formulation delivery to a disease site provides an attractive approach to treating lung disease. In our previous work, we reported that combining CXCR4 inhibition with plasminogen activator inhibitor-1 (PAI-1) silencing could serve as a promising strategy for treating IPF [129]. However, simple cationic polyplexes poorly penetrated the lung mucus layer [49]. Perfluorocarbons (PFCs) are biocompatible materials widely used as ultrasound contrast agents, in treating lung diseases, and in organ transplantation because of their high oxygen-dissolving capacity [147-149]. We have reported that PFC emulsions could improve cellular siRNA delivery to attenuate lung cancer metastasis, IPF, and ALI [147, 148]. The PFC emulsion polyplexes formulated for pulmonary siRNA delivery improved cellular internalization and endosomal escape when compared with polyplexes. Furthermore, PFC in PLGA-PEG emulsions can serve as an agent for highly efficient organ reoxygenation [150]. A reverse water-in-PFC emulsion has been evaluated as a potential drug delivery system for pulmonary administration using pMDIs [151-153], but has not yet been used for siRNA delivery.

1.3.7. Inorganic nanoparticles for pulmonary siRNA delivery

In recent decades, various inorganic materials have been developed for therapeutic and diagnostic applications [154]. Among them, mesoporous silica nanoparticles (MSN) and hybrid lipid-calcium phosphate nanoparticles have shown promise in pulmonary siRNA delivery. MSN are well-suited for co-delivery of small molecule drugs and siRNA due to large porous surface area. LHRH-targeted MSN were tested in delivery of anticancer drugs and siRNA to treat lung cancer [155]. When compared with intravenous injection, where only 5% of the injected dose accumulated in the lung, pulmonary delivery of the MSN increased lung accumulation to 73% and prevented the absorption into the systemic circulation. Hybrid lipid-calcium phosphate nanoparticles were developed for pulmonary delivery of siRNA to abate lung inflammation [156]. The nanoparticles consisted of a calcium phosphate core coated with siRNA directed against pro-inflammatory mediators, encapsulated in PLGA, and finally coated with the outer layer of PEI. Nasal instillation of the particles led to a significant reduction of target gene expression and modulation of the inflammation response [156]. Conde et al. developed functionalized gold nanoparticles for targeted delivery of siRNA to cancer cells toward effective silencing of the specific target oncogene [157].

1.3.8. Naked siRNA for pulmonary delivery

The term “naked siRNA” refers to the delivery of siRNAs without any delivery vectors. Several studies suggested that naked siRNA delivery is compromised because of the instability and poor pharmacokinetic performance in systemic circulation. However, for

local pulmonary delivery, naked siRNA has shown promising results in the treatment of lung infections [82, 132, 158-161]. To improve siRNA stability and efficacy without using delivery systems, the siRNA was either chemically modified or conjugated to other biomolecules. Zhang et al. demonstrated that pulmonary delivery of siRNA can be achieved by intranasal administration without any vectors [162], although many of the mechanistic considerations, such as mechanism of cell uptake, are not clear. Nevertheless, the delivery of naked siRNA has been extended to clinical trials. A modified form of siRNA (ALN-RSV01) was administered using nasal spray and the treatment reduced RSV infection. In addition to liquid formulations, dry powder forms of naked siRNA also showed gene silencing effects [163, 164]. Kohie et al. showed that naked siRNA was not affected by nebulization when processing using ultrasonic, air-jet, and vibrating-mesh nebulizers [165].

1.3.9. Microparticles for pulmonary siRNA delivery

Aerosol particles with aerodynamic diameter 1-5 μm are optimal for penetration into the deep lungs and lower airways. Despite their large size (5-30 μm), large porous hollow particles (LPHPs) can achieve the desired aerodynamic size range via enhanced porosity within the particles, which aerodynamically balances the large size [166]. A main advantage of this approach is that the actual geometric size is too large for phagocytosis by alveolar macrophage, which permits therapeutics retention for longer periods of time. LPHPs show other beneficial features, including high dispersibility from an inhaler and enhanced deposition in the lungs upon inhalation. The large particle size reduces

fractional surface area of particle-particle contact in a dry powder or liquid suspension and leads to decreased tendency to aggregate. A dry powder inhalable PLGA LPHP containing insulin showed prolonged drug release and decreased macrophage uptake and mucociliary clearance *in vivo* compared with nonporous particles [167]. LPHP of PEG-PLGA containing heparin exhibited reduced the uptake by isolated rat alveolar macrophages *in vitro* than small nonporous particles [168, 169]. A 3D-printed micromixer was used for preparation of siRNA-dendrimer nanocomplexes, which were then processed into nano-embedded macroparticles and shown to retain siRNA integrity and bioactivity [139]. siRNA can be encapsulated in PLGA microparticles optimized using a double emulsion technique, and the results showed significant downregulation of the target gene expression compared to negligible knockdown using commercial transfection reagents [42, 170]. Xu et al. developed PLA porous microparticles which contained siRNA-loaded chitosan and doxorubicin by the supercritical anti-solvent process. The particles exhibited a favorable aerodynamic performance and sustained drug release that led to higher anticancer efficiency [134]. A porous silicon micro/nano composite was reported to deliver siRNA to the lungs with melanoma metastasis [171].

1.3.10. Exosomes for pulmonary siRNA delivery

Exosomes are a type of extracellular nanovesicles released from living cells. Exosomes were once thought to be a mechanism for removing unwanted proteins, but we now know that they are also involved in intercellular communication. The fact that exosomes can bind a wide range of surface receptors makes them interesting option for

therapeutic siRNA delivery. Recent studies suggest that exosomes regulate the development of lung inflammation in response to diverse stimuli, potentially providing novel therapeutic and diagnostic targets for ALI/ARDS [172, 173]. An inhaled exosomes have been developed for efficient delivery to inhibit or activate the alveolar macrophages and also generate pulmonary immune response [45]. Importantly, these serum-derived exosomes themselves did not trigger the lung immune response. Intratracheal siRNA delivery using host serum-derived exosomes attenuated LPS-induced inflammation in alveolar macrophages [45]. Intratracheal instillation deposited exosomes in alveolar regions rather than in bronchioles and macrophages were the main recipient cells. The presence of surface proteins in exosomes may facilitate uptake by specific cell types in the lungs and avoid uptake by macrophages. Exosomes from human induced pluripotent stem cells were used as siRNA delivery vectors to silence ICAM-1 expression as a potential treatment of ALI. Recent study showed the potential of exosomes in delivering siRNA in an important *in vitro* airway model [174].

1.4. Pulmonary siRNA inhalation delivery: Promise of dry powder inhalers

Therapeutic delivery via inhalation provides direct access to the target cells of siRNA therapy in a relatively non-invasive manner. Early developmental and preclinical studies of pulmonary siRNA delivery typically use intratracheal and intranasal administration for their simplicity. However, these administration routes are not usually directly translatable to clinical use due to considerable risks and discomfort for patients. Hence, the development of inhalation aerosol systems is critical for the practical translation of

experimental siRNA delivery systems from the laboratory to clinical use [175]. The three most common used commercial aerosol inhalation systems are nebulizers, pressurized metered-dose inhalers (pMDIs), and dry powder inhalers (DPIs). Nebulizers generate inhalable micro-sized liquid droplets that can carry large amounts of siRNA delivery vectors per droplet and reach virtually all areas of the lungs. Some of them have already been successfully used in clinical pulmonary nucleic acid delivery. A nebulized cationic lipid/DNA formulation has been tested in phase I clinical trial in CF [116]. More recently, two additional inhalable RNAi-based products have entered clinical trials: ALS-RSV01 [80, 176] and ExcellairTM [177]. ALS-RSV01 uses cholesterol-siRNA conjugate to treat RSV infection in lung transplant patients [176]. ExcellairTM (whose phase II trial was discontinued in 2015) was aimed at treating asthma through silencing Syk [177].

Dry powder siRNA formulations have several advantages over liquid aerosol formulations, including better stability, ease of handling, and lower cost of storage and transportation [178]. Nevertheless, the development of DPIs for pulmonary siRNA delivery remains limited due to unresolved issues related to destabilization of the siRNA and the carrier system caused by the stress of heating, freezing, or spraying [179]. Spray drying, spray freeze drying (SFD), and supercritical fluid drying are the three major dry powder techniques applicable for the use in siRNA formulations [179]. Even the naked form of siRNA could be formulated into an inhalable dry powder using co-spray-drying with mannitol and l-leucine (a dispersion enhancer), while maintaining the integrity of siRNA [163]. An early example of siRNA formulation in the form of inhalable dry powder using

spray drying technology dates back to 2010 [180]. The initial formulation was improved by incorporating DOTAP into the original PLGA matrix to improve encapsulation and transfection activity of the siRNA in the spray-dried formulations [181]. Inhalable dry powder formulations of pH-responsive peptide/siRNA complexes were successfully produced by spray drying without compromising the physical integrity and biological activity of siRNA [182]. SFD is a multi-step process including a spray-freezing step and a freeze-drying step. The powder production by the SFD maintained the physicochemical properties of polyplexes without negating transfection efficiency [183]. SFD can provide high recovery of the powders even when the formulation amount is small, which makes SFD well-suited for the task due to the relative expense of siRNA [184]. SFD process parameters and choice of excipients could be optimized to maintain integrity and biological activity of siRNA, for example by co-spraying with carbohydrates and using low inlet temperatures [181]. Similarly, co-spray drying with mannitol and L-leucine as excipients also successfully preserved siRNA integrity even in the absence of any delivery system [163]. The presence of siRNA also alters the molecular arrangement and solid-state composition of carbohydrate excipients during the spray drying process [185].

Among the polycation-based siRNA delivery systems, PEI and chitosan have been the most often used vectors for the preparation of dry powders. SFD was used to prepare chitosan formulation with siVEGF, which was successfully used for pulmonary delivery to treat metastatic lung cancer [132]. PEI/siRNA powder with a spherical and highly porous structure was also prepared by SFD with high aerosol and lung delivery performance [186].

Merkel et al. demonstrated successful spray drying of PEI polyplexes in the form of nano-embedded microparticle powder [124]. The authors optimized the spray-drying parameters to generate powder with appropriate aerodynamic properties suitable for deep lung deposition.

In several published studies, the inhalable siRNA dry powder formulations were limited by the siRNA content, which was too low to be moved to clinical study. Inhalable spray-dried powder formulation with high siRNA loading (>6% w/w) was developed using human serum albumin as a dispersion enhancer to improve aerosol performance [187]. As a dispersion enhancer, albumin favorably modifies the surface properties of the spray-dried powder leading to the fine particle fraction consistently over 50% [187]. L-leucine is often used as the dispersion enhancer, but due to its small size compared to macromolecular siRNA, the benefits of L-leucine in siRNA formulation were modest [163].

1.5. Conclusion

In this review, siRNA delivery barriers and recent approaches were described. Pulmonary delivery of siRNA has gained increased attention due to the specific physiology of the lung and characteristic properties of siRNA. However, how to translate laboratory studies to clinical practice and the difficulties that exist in evaluating this route of administration still remain a significant challenge. Even though the DPIs seem the best choice for pulmonary siRNA delivery, more studies are required in regard to dose, siRNA loading, optimal excipients, and inhaler device for maintenance of siRNA stability and biological function.

2. CXCR4 as a therapeutic target in fibrosis and pancreatic cancer

CXCR4 is a G-protein-coupled receptor which involved in several physiological processes in immune system and hematopoietic. CXCL12 is the chemokine ligand of CXCR4. CXCL12/CXCR4 axis plays important role in several disease, including cancer, fibrosis, and some injured (acute and chronic) disease [188].

2.1. CXCL12/CXCR4 axis

Chemokines are a class of small, secreted cytokines with 8-12 kD molecular weight and functions. They are known for the mediation of immune cell recruitment and regulate many of tissue and cell functions. Chemokine can be categorized into 4 subfamilies (C, CC, CXC and CX3C) based on the arrangement of the first two cysteine residue's location beside the amino terminus [189]. CXCL12, also referred to as stromal cell-derived factor-1 (SDF-1), binds to CXCR4 then induces downstream signaling pathways, including cell proliferation, migration, and cancer cells metastasis [190]. CXCL12 can be secreted by stromal cells [191], fibroblasts, and epithelial cells, which regulating hematopoietic cells trafficking and secondary lymphoid tissue architecture [192]. CXCR4 induces downstream signaling pathway via G proteins and GRKs, which subsequently induces many signaling pathways (MAPK, AKT, PI3K, ERK1/2) after binding with CXCL12, and then promoting several cellular functions, such as actin polymerization, cells skeleton rearrangement, cells survival, proliferation, and migration [190].

2.2. CXCR4 in fibrosis

CXCR4 not only overexpressed in the cancer tissue, but also in some fibrosis disease, such as, peritoneal fibrosis [193], IPF [194], liver fibrosis [195], cardiac fibrosis [196], and skin fibrosis [197], *et al*. In lung tissue, multiple type of cells express CXCR4, especially in fibrotic lungs, including fibroblasts and myofibroblasts, epithelial cells, vascular endothelial cells and some inflammatory cells (alveolar macrophages) [198]. Jade Jaffar evaluated the CXCR4+ cells in lung tissue of patients with IPF, and they found that CXCR4 is overexpressed in IPF patients than the non-disease control (NDC) [194]. Moreover, some of the study suggested that CXCL12/CXCR4 axis resides in lung fibroblasts contributed to fibrotic by directing activating lung fibroblasts [199]. Epithelial-to-mesenchymal transition (EMT) of human peritoneal mesothelial cells (HPMCs) is considered as the main mechanism involved the origination and development of the peritoneal fibrosis [200]. During the fibrosis stages, TGF-β activation results in secretion and expression of CXCL12 and its receptor CXCR4, which resulting in potential of HPMCs migration and ECM deposition in the fibrosis foci [193]. In the liver fibrosis, more of the activated hepatic stellate cells (HSCs) lead to the ECM deposition. Study proved the HSCs express CXCR4 receptor both *in vivo* and *in vitro* [201].

Some of the paper developed nanomedicine related to CXCR4 whereas CXCR4 served as the therapeutic target for treating the fibrosis disease. The following are some examples. Combined delivery of sorafenib and MEK inhibitor using CXCR4-targeting NPs can prevent ERK activation in activated HSCs and has anti-fibrotic effects in the CCl_4-

induced murine models [202]. The inhibition of the CXCL12/CXCR4 biological axis can attenuated the severe of fibrosis progression. Treatment of the mice lung fibrosis models with CXCR4 antagonists, including TN14003 [203], MSX-122 [204] and ADM3100 [205], attenuated the progression of lung fibrosis significantly. Dual-functional NPs targeting CXCR4 and delivering antiangiogenic siRNA reduce liver fibrosis [195]. Khan A designed a liposome based on the CXCR4-receptor-targeter shown promising the therapeutic effect for treating peritoneal fibrosis [193]. CXCR4 antagonism reduce cardiac fibrosis and improves cardiac performance in dilated cardiomyopathy [196].

2.3. CXCR4 in cancer therapy

CXCR4 was firstly found to target CD4-positive T-cells and function as a co-receptor for entry into T-tropic (X4) HIV virous. Then, CXCR4 has been confirmed expressed in many types of cancers. CXCR4 together with its ligand CXCL12, CXCL12/CXCR4 axis, controls and triggers downstream signaling pathway and variously involved in tumor cells proliferation, migration, and survival. Several studies suggested that the overexpression of CXCR4 has significantly role in cancer stem cells [206]. CXCR4 in promoting inflammatory colorectal cancer progression via recruiting immunocytes and enhancing cytoskeletal remodeling by lncRNA XIST/miR-133a-3p/RhoA signaling [207]. Another study suggested that cancer-associated fibroblasts (CAFs) derived from endometrial cancer (EC) tissue promoted EC progression via the CXCL12/CXCR4 axis in a paracrine- or autocrine-dependent manner [208]. The secreted CXCL12 drives the CXCR4+ cells migration and lead to the organ-specific metastasis, such as lungs, liver, and lymph nodes

show higher of CXCL12 expression which indicate the most common organs for the CXCR4+ receptor of cancer metastasis [209].

Blocking CXCR4 can alleviate cancer progression and metastasis. Various studies have been evaluated to inhibit CXCL12/CXCR4 axis for cancer treatment. In the past decades, several small molecules, CXCR4-binding peptides, siRNA, and polymer based on CXCR4 inhibition moiety have been evaluated to inhibit CXCR4-mediated processes in cancer treatment. Plerixafor (AMD3100), one of the small molecules CXCR4 specific antagonists, has been approved by US FDA for autologous transplantation in patients with Non-Hodgkin's Lymphoma and multiple myeloma in 2008 [210]. Blocking of CXCR4 with inhibitors exhibit high efficacy for cancer treatment via inhibiting metastasis, improving the tumor sensitivity to the chemotherapy, radiotherapy, and immunotherapy [211]. For examples, one of study proved that blocking CXCR4 attenuates desmoplasia and increases T-lymphocyte infiltration which improve immunotherapy in metastasis breast cancer [212]. Sison E.A *et al* developed Protein Epitope Mimetic POL5551, a novel and potent antagonist of CXCR4, has activity at nanomolar concentrations in decreasing CXCR4 antibody binding, blocking CXCL12 mediated ERK1/2 phosphorylation, inhibiting CXCL12-induced chemotaxis, and reversing stromal-mediated protection from chemotherapy [213]. Various of nanomedicine have been developed based on the CXCR4 inhibition for the effective cancer treatment. For example, CXCR4-targeted PEGylated PLGA NPs conjugated with CXCR4 inhibitor peptide (LFC131) codelivery of sorafenib

offer an effective strategy for enhancing the therapeutic efficacy on Hepatocellular carcinoma (HCC) [214].

3. Pancreatic cancer

Pancreatic ductal adenocarcinoma [PDAC, also referred to as pancreatic cancer (PC)] is the fourth leading cause of cancer-related deaths [215]. Unfortunately, PC is usually not diagnosed until late stage with the metastasis spread which led to the poor prognosis of PC. Clinically, even though the developments in detection and management of PC, only ~4% of patients will live 5 years after diagnosis [216]. Moreover, surgical tumors only improve 15~20% of patient's survival, and PC patients response poorly to most of chemotherapeutics [216]. Overall, it is unmet medical need to develop the better therapeutics.

3.1. Clinical challenges of therapeutic of PC

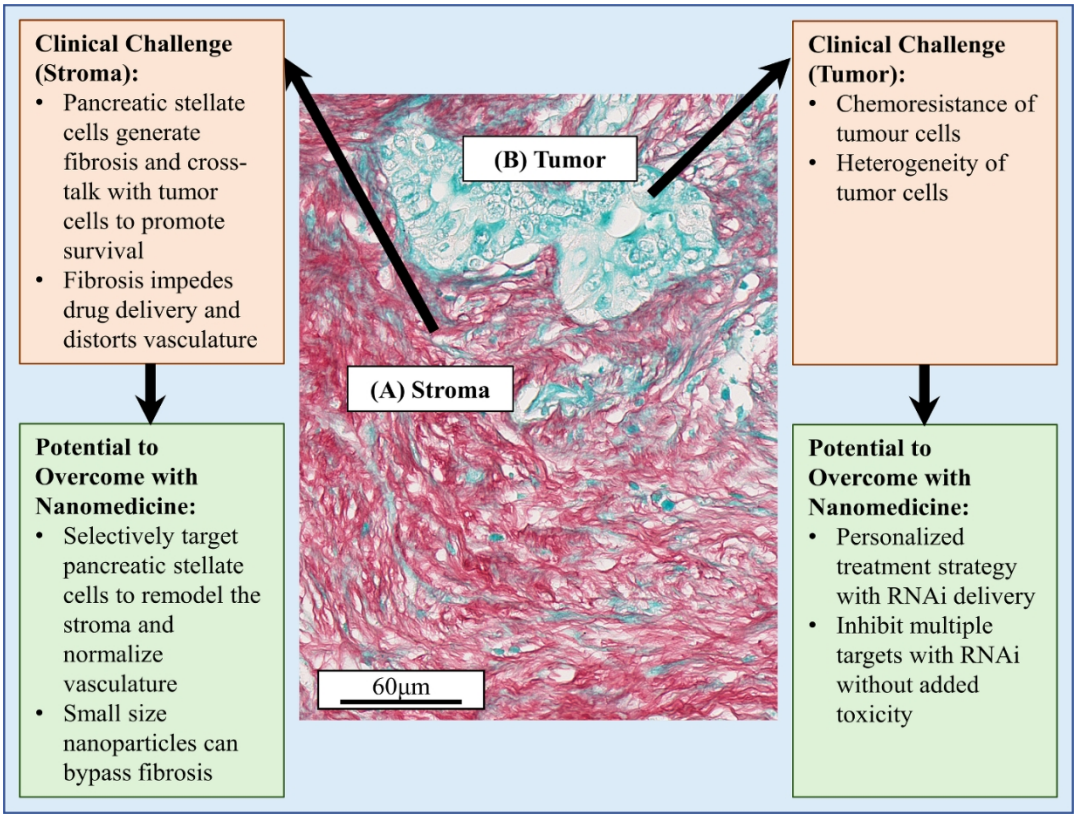

Figure 1.2 The unique clinical challenges of PC therapeutics [Adapted from [217].

The specific pathological challenges of PC therapeutics show rise to the development of PC treatment (Figure 1.2 [217]). For example, the pancreatic stellate cells (PSC) generate fibrotic foci surrounding with the tumor cells to promote the tumor cells survival and metastasis [218]. Moreover, the fibrotic area inhibits therapeutics delivery and penetration. Indeed, dense fibrotic stroma forms more than 80% of the PC tumor mass, which serve as one of the histopathological features of PC [217]. Moreover, the fibrotic dense stroma content in PC patients is related to the patient survival outcome [219]. Besides, this desmoplastic contributes to the hypoxia condition in PC solid tumors then

promotes the chemoresistance and heterogeneity of tumor cells, which play important roles to slow the PC treatment [220]. Herein, PSCs are considered as key cellular therapeutic targets to remodulate the fibrotic condition in PC. When designing the strategies for PC treatment, it is important to evaluate both the tumor cells and the surrounding PSCs.

3.2. siRNA delivery for treating PC

Researchers have identified various of novel cancer-related genes that involved in the PC tumor initiation, progression, and metastasis. Many important genetic alterations have been investigated to be involved in the PC, which contain KRAS and tumor suppression inactivators (TP53, SMAD4, CDKN2A) [221]. It shown highly promising to selectively knockdown these genes to impede the tumor progression and extended patient survival. RNA interference (RNAi) can be naturally occurred in mammalian cells, and this gene silence mechanism can be used to selectively inhibit the therapeutic gene targets. RNAi NPs not only can target the tumor cells that impeded the tumor progression but can selectively target PSCs that decrease the fibrotic foci which to normalize tumor vasculature and improve the tumor accumulation and penetration of therapeutics.

siRNA consists of double-stranded RNA with ~21-23 base pairs, which can selectively knockdown the expression of targeted gene and provide potential power to treat many of human disease including PC [222]. siRNA come up as potential and selectively targeted therapeutic approach. Moreover, some of clinical trials based on siRNA have been under evaluated now [223]. However, there are many challenges when researchers designing

siRNA-based therapeutics for treating PC, which including the poor stability, poor cellular uptake and endosome escape with low transfection ability, poor solid tumor penetration and off-target effects, *et al*. Consequently, it is urgent for the development of effective and safe therapeutics based on siRNA strategies for PC treatment. Here are some examples that demonstrating the potential of siRNA-based therapeutics for effectively treating PC. 1) Lipid and polymer-based NPs: Lipid-based NPs (LNPs) which contain pH-sensitive cationic lipid have been designed to effectively delivery siRNA for treating PC [224]. Cationic polymer shown great potential as siRNA delivery vehicles, such as PEI. 2) Inorganic-based NPs: Gold NPs and carbon nanotubes have been evaluated as highly effective siRNA delivery vehicles for cancer treatment [222]. 3) Hybrid-based NPs: One of the hybrid NPs have been designed which comprised of two cationic polymers, DOTAP and DOPE as well as cholesterol to self-assemble siRNA into a cationic nanocomplex for treating cancer [225].

3.3. Conclusion

Overall, the potential of siRNA strategies to selectively silence the tumor promoting exhibit great potential for PC treatment. Several of pre-clinical studies based on siRNA therapeutics shown promising anti-tumor and metastasis ability. However, there are various challenges to transfer these promising preclinical finding to clinic. It is crucial to establish the stronger collaborations between chemists, pathophysiologist, biologists, formulation scientist, and clinicians if we want to revolutionize the PC treatment.

Delivery system	siRNA	Disease	Delivery route	Key observations	Ref
Nano-embedded porous microparticles co-loaded with DOX and siRNA	MRP1	Lung cancer	Dry powder inhalation	Excellent aerodynamic performance and sustained drug release. Anticancer efficacy in chemoresistant lung cancer.	Xu PY, *et al.* 2018. [134]
Transferrin (Tf)-PEI	Fluorescently labeled siRNA	Asthma	Intratracheal	Optimal physicochemical properties and selective siRNA delivery to activated T cells.	Xie Y *et al.* 2016. [125]
Noncovalently PEGylated ternary complex	CTGF	IPF	Intratracheal	Significant reduction in target gene expression, collagen deposition, inflammatory cytokines production, attenuation of pulmonary fibrosis, increased survival rate.	Sung DK *et al.* 2013. [226]
Micelles	Amphiregulin and CTGF	PF	Intratracheal and intravenous delivery	Collagen accumulation in the lung of animal was effectively inhibited both in the intratracheal or intravenous delivery.	Yoon PO *et al.* 2016. [227]
Exosomes	ICAM-1	Human primary pulmonary microvas	*In vitro*	The Exo/siRNA compound efficiently delivered the target siRNA into HMVECs	Ju Z *et al.* 2017. [228]

		cular endotheli al cells (HMEVC s)		causing selective gene silencing, inhibiting the ICAM-1 protein expression, and PMN-EC adhesion induced by lipopolysaccharide (LPS).	
Exosomes	Myd88	ALI	Intratracheal	No lung immune response to exosomes. Delivery of siRNA into lung macrophages *in vivo*.	Zhang D *et al.* 2018. [45]
LHRH-NLC	EGFR	Lung cancer	Inhalation	Enhanced efficiency of lung cancer therapy.	Garbuze nko OB *et al.* 2019. [113]
Liposomes	Mcl1	Lung cancer	Intratracheal	High delivery efficiency and reduced formation of melanoma metastasis.	Shim G *et al.* 2013. [229]
Liposomes	αENaC	CF	Oropharynge al	Rapid translocation across mucus. Corrected aspects of the mucociliary defect in human CF cells. Effective delivery and silencing *in vivo*.	Tagalaki s AD *et al.* 2018. [114]
Targeted liposomes	αENaC	CF	Oropharynge al	Nebulized formulations retained biophysical properties and transfection activity. *In vivo*	Manunta , M. D. I *et al.* 2017. [230]

				silencing of the α-ENaC subunit gene expression.	
Targeted liposomes	αENaC	CF	Oropharyngeal	Rapid translocation across mucus. Transfections of primary CF epithelial cells.	Tagalakis AD *et al.* 2018. [114]
Hybrid lipid-polymer nanoparticles	αENaC	CF	Inhalation	Delivery to airway epithelial cells. No acute proinflammatory effect.	d'Angelo I *et al.* 2018. [117]
Targeted gold nanoparticles	c-myc	Lung cancer	Intratracheal	Tumor cell proliferation, tumor growth inhibition, prolonged survival.	Conde J *et al.* 2013. [157]
Surfactant-coated nanogels	CD45	Healthy mice	Intratracheal aerosolization	Safe and effective siRNA delivery to alveolar macrophages.	De Backer L *et al.* 2015. [44]
PEG-PEI polyplexes	EGFP	actin-EGFP mice	Intratracheal	Efficient *in vivo* gene silencing.	Merkel OM *et al.* 2009. [126]
PEI-cyclam polyplexes	PAI-1	IPF	Intratracheal	Decreased collagen deposition in the lungs.	Ding L *et al.* 2018. [129]
PEI polyplexes	Bcl2	Lung cancer	Intratracheal aerosolization	Co-delivery of siRNA and DOX improved the antitumor effect with low side effects on the normal tissues.	Xu C *et al.* 2015. [130]
Chitosan polyplexes	EGFP	Lung cancer	Intratracheal aerosolization	Deposition throughout the lungs. Silenced the	Capel V *et al.* 2018. [131]

				EGFP expression in lung tumors.	
G4-NH4 dendriplexes	EGFP	*In vitro*	pMDI	High respirable fractions (up to 77%) and fine particle fractions (~50%). Preserved biological activity of the siRNA after exposure to the pMDI propellant.	Conti DS *et al.* 2014. [137]
Dendrimer polyplexes	EGFP	*In vitro*	pMDI and DPI	Effective in producing aerosols suitable for deep lung deposition for both pMDI and DPI with no impact on the *in vitro* gene knockdown efficiency of the siRNA.	Bielski E *et al.* 2017. [138]
Dendrimer polyplexes	Fluc-TYE563	*In vitro*	Inhalation	Retained siRNA integrity and bioactivity after processing into dry powders. A binary mixture of trehalose and inulin showed optimal stabilization, enhanced cellular uptake and gene silencing efficiency.	Agnoletti M *et al.* 2017. [139]
VIPER polyplexes	GAPDH	Healthy mice	Intratracheal	Robust gene silencing (>75% knockdown) within the lungs.	Feldmann DP *et al.* 2018. [140]

Fluorinated polypeptide polyplexes	TNF-α	ALI	Intratracheal	siRNA delivery into macrophages. Fluorination enhanced the mucus permeation.	Ge C *et al.* 2020. [231]
Hybrid nanoparticles coated with SP-B	TNF-α	ALI	Tracheal aspiration	PS enhanced the siRNA delivery.	Merckx P *et al.* 2018. [30]
Hybrid fluorinated polymers	PDL-1	Lung cancer	Intratracheal	Decreased tumor fibrosis, increased T cell infiltration and relieved immunosuppression.	Li Z *et al.* 2020. [143]
PFC emulsion polyplexes	PAI-1	IPF and ALI	Intratracheal	Prolonged lung retention and widespread lung distribution. Promising therapeutic efficacy in ALI and in early fibrinogenic stage of IPF. Increased survival in IPF.	Wang Y *et al.* 2019. [148]
PFC emulsions stabilized with polycations	STAT3	Lung metastasis	Intratracheal	Improved anticancer effect.	Li Z *et al.* 2019. [147]
Targeted mesoporous silica nanoparticles	MRP1 and BCL2	Lung cancer	Inhalation	Enhanced cytotoxicity of anticancer drugs. Prevented systemic off-target organ exposure.	Taratula O *et al.* 2011. [155]
HMGB1A/R3V6 ternary complexes	S1PLyase	ALI	Intratracheal	Significantly reduced inflammatory response.	Oh B *et al.* 2014. [232]

				Reduced S1PLyase expression in ALI model.	
Multi-shell nanoparticles of CaP and PLGA with PEI	Mixture against pro-inflammatory mediators	Lung inflammation	Nasal	Decreased lung inflammation.	Frede A *et al.* 2017. [156]
Naked siRNA	TGF-β1	TB	Intratracheal	Increased expression of antimicrobial mediators (NO and iNOS). Reduced bacterial load in the lungs.	Rosas-Taraco AG *et al.* 2011. [82]
Naked siRNA	Interleukin 10	*In vitro*	Dry powder	First use of naked siRNA as inhalable dry powder using spray drying technology with integrity of siRNA retained.	Chow MYT *et al.* 2017. [163]
Naked siRNA	TGF-β1	IPF	Intratracheal	Inhibited pulmonary fibrosis, improved lung function, and prolonged survival.	D'Alessandro-Gabazza CN *et al.* 2012. [158]
Naked siRNA	TGF-β1 and miR-326	IPF	Intranasal	Attenuated fibrotic lung response.	Das S *et al.* 2014. [233]
Naked siRNA	VEGF	Lung cancer	Dry powder	Dry powder siRNA inhibited lung metastasis.	Miwata K *et al.* 2018. [132]
Naked siRNA	$SOCS_3$	Asthma	Intranasal	Decreased lung eosinophilia, improved mucus secretion, reduced	Zafra MP *et al.* 2014. [159]

				lung collagen content.	
Naked siRNA	IL-4 and anti-RSV	Asthma	Intranasal	Reduced total cell count and eosinophilia in bronchoalveolar lavage fluid.	Khaitov MR *et al.* 2014. [160]
Naked siRNA	Rip2	Asthma. COPD	Intratracheal	OVA-induced cytokine release, inflammatory cell infiltration and mucus hypersecretion inhibited in experimental allergic airway inflammation [161]. Rip2 siRNA suppressed CS-induced inflammatory and oxidative damage markers [234].	Goh FY *et al.* 2013. [161] Dong J *et al.* 2019. [234]
Naked siRNA	CD86	Asthma	Intratracheal	Inhibited OVA-induced airway eosinophilia and airway hyperresponsivenes	Asai-Tajiri Y *et al.* 2014. [235]
Naked siRNA	c-kit	Asthma	Intranasal	Inhibited expression of c-kit, reduced airway mucus secretion and infiltration of eosinophils in bronchoalveolar lavage fluid. Reduced production of SCF, IL-4, and IL-5.	Wu W *et al.* 2104. [236]

Table 1. Recent developments in the pulmonary siRNA delivery.

Chapter 2: Perfluorocarbon Nanoemulsions Enhance Therapeutic siRNA Delivery in the Treatment of Pulmonary Fibrosis

Please note that this part of the dissertation was published in the Advanced Science (Ling Ding et al, 2022). As the first author, I designed the experiments, collected, and analyzed the data, and wrote the paper. Prof. Oupicky guided me on this project. Siyuan Tang, et al, helped me with the experiments. Prof. Oupicky, Prof. Knoell, Prof. Wyatt, et al, helped with editing the manuscript. All the co-authors agree with including their work in this dissertation.

1. Introduction

Idiopathic pulmonary fibrosis (IPF) is the most common idiopathic interstitial lung disease. The progression of IPF is categorized by decline of lung function, progressive dyspnea, nonproductive cough, and decreased quality of life [237]. Increasing rates of hospital admissions and deaths due to IPF underlie the need for better therapies [237]. Development of pulmonary fibrosis is also implicated in severe COVID-19 infections, further underscoring the urgency [238, 239].

Current views of the pathogenesis of IPF rely on repeated subclinical epithelial injury combined with augmented epithelial aging that leads to abnormal repair and the formation of interstitial fibrosis by myofibroblasts [240]. The senescence of alveolar epithelial cells and activation and differentiation of myofibroblasts is a central phenotype that promotes IPF [241]. Fibroblastic foci, where disordered collections of type II alveolar epithelial cells

are present with fibroblasts, are considered a key pathological feature of IPF [242]. After decades of clinical trials, there are currently only two FDA approved anti-fibrotic medications that are considered safe and somewhat effective, nintedanib and pirfenidone [243]. The mechanism of pirfenidone is not fully understood, but it possesses both anti-inflammatory and antifibrotic effects, whereas nintedanib, a tyrosine kinase inhibitor, specifically blocks fibroblast proliferation, migration, differentiation, and the formation of extracellular matrix (ECM) [244].

With the recent regulatory approvals of the first siRNA therapeutics [15,18], the development of additional siRNA-based medicines for a broad range of diseases has become increasingly feasible. Direct delivery of siRNA into the lungs has beneficial characteristics, such as avoidance of undesired serum interactions and degradation. However, the anatomy of the respiratory tract is complex and creates obstacles for effective delivery. Several preclinical studies in pulmonary fibrosis demonstrated efficacy using siRNA formulations aimed at silencing the expression of collagen-specific chaperone heat shock protein 47 (HSP47) [115], Janus kinase type 2 (JAK 2) [245], E1A binding protein P300 (EP300) [246], plasminogen activator inhibitor-1 (PAI-1) [129, 148], and NLR family pyrin domain containing 3 (NLRP3) [247]. Related to this, two human clinical trials have utilized siRNA inhalation strategies to treat respiratory syncytial virus (RSV) (ALN-RSV01)[248] and asthma (ExcellairTM) via Syk silencing [249].

Perfluorocarbon (PFC) nanoemulsions are versatile soft nanomaterials with a unique set of properties suitable for multiple biomedical applications, including drug delivery and

bioimaging. Unlike self-assembled soft materials like micelles, PFC nanoemulsions are kinetically stable systems where the PFC oil phase is stabilized with amphiphilic surfactants [250, 251]. Nanoemulsions have a potentially large loading capacity for active molecules, with release properties controlled by the nature of the oil phase and choice of surfactant. PFC nanoemulsions also have high oxygen solubility, which prompted their first development as blood substitutes. Perfluorooctylbromide (PFOB) is among the most commonly used PFCs in biomedical applications [252, 253]. PFOB nanoemulsions have been studied in the treatment of cancer and atherosclerosis [254]. Pulmonary administration of PLGA-PEG/PFOB nanoemulsions have been shown to improve lung ventilation [150]. Photodynamic therapy has been another successful application of PFOB emulsions, which benefits from high oxygen solubility [252, 255].

Chronic dysfunctional inflammatory response and aberrant self-repair are critical factors in progressive IPF. This involves the recruitment of immune and mesenchymal cells by chemokines and chemokine receptors, which play a critical role in cell migration and also serve as potential therapeutic targets [256]. Invasion of fibroblasts into the alveolar region results in collagen deposition and fibroblast differentiation into myofibroblasts [257]. The G-protein coupled C-X-C chemokine receptor type 4 (CXCR4) is a candidate therapeutic target in IPF because of its role in the recruitment of CXCR4-positive fibrocytes to the lung that increase the extent of fibrosis [258]. Stromal cell-derived factor-1 (SDF-1) chemokine is a CXCR4 ligand generally secreted by bone marrow stroma cells. However, SDF-1 also can be secreted by pulmonary fibroblasts and alveolar

epithelial type II cells (AEC II), leading to activation and recruitment of CXCR4 positive cells [259]. CXCR4 is abundantly expressed in IPF patients, with prominent expression in honeycomb cysts and the distal airway epithelium [260]. CXCR4 inhibition attenuates the progression of bleomycin (BLM)-induced pulmonary fibrosis in mice [148].

Excessive phosphorylation of a signal transducer and activator of transcription 3 (STAT3) has been implicated as a driver of aberrant fibroblast activation [261]. STAT3 is a cytoplasmic transcription factor with important role in cell proliferation, migration, differentiation, and survival [262]. TGF-β signaling triggers phosphorylation of JAK2, which then interacts with and phosphorylates STAT3 to induce a fibrotic response [263]. STAT3 signaling is hyperactivated in systemic sclerosis in a TGF-β-dependent manner, suggesting that STAT3 may be a core mediator of fibrosis. In this study, we report on the development of PFC nanoemulsions, termed emulsion polyplexes (EPs), for pulmonary siRNA delivery that combine CXCR4 inhibition and STAT3 gene silencing. We present results demonstrating *in vitro* antifibrotic activity, favorable pulmonary biodistribution, and the potential to reduce the severity and prolong survival in BLM-induced lung fibrosis (Scheme 1).

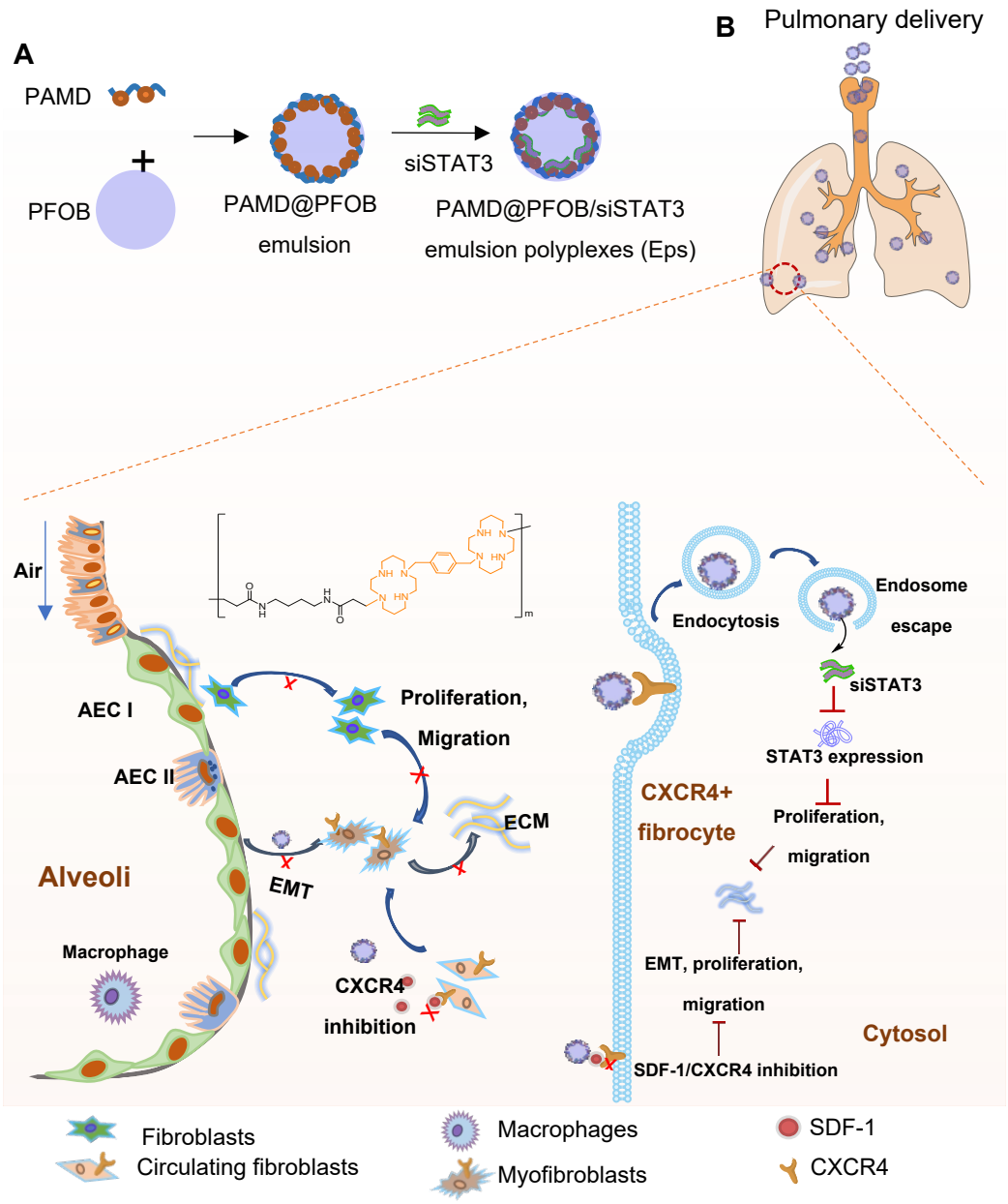

Scheme 1. Preparation (A) and proposed mechanism of action of PAMD@PFOB/siSTAT3 emulsion polyplexes (EPs) in inhibiting pulmonary fibrosis (B).

2. Materials and methods

2.1. Materials

Fetal bovine serum (FBS), Dulbecco's phosphate buffered saline (PBS), Dulbecco's modified Eagle medium (DMEM), Ham's F-12 medium, Amphotericin B, trypsin, penicillin, and streptomycin were brought from Thermo Scientific (Waltham, MA). Hexamethylenebisacrylamide (HMBA) and 1-bromoheptadecafluorooctane (PFOB) were purchased from Sigma-Aldrich. AMD3100 was from Biochempartner (Shanghai, China). All siRNA (siScr, sense strand, 5'-UUC UCC GAA CGU GUC ACG UTT-3'; siSTAT3, sense strand for mice, 5'-GGU CAA AUU UCC UGA GUU GUU-3'; siSTAT3, sense strand for human, 5'-GGA GAA GCA UCG UGA GUGA-3'; carboxyfluorescein (FAM)- and Cy3-labeled siRNA) and real-time (RT)-PCR primers were purchased from Sigma-Aldrich. Curosurf® (poractant alfa) was purchased from Chiesi, Inc. (USA). Unless otherwise stated, all other reagents were obtained from Fisher Scientific and used as received.

2.2. Methods

2.2.1. Cells and tissues

Deidentified human primary lung fibroblasts (HPLFs), which were isolated from patients with IPF and from non-disease control (NDC) patients, were provided through the University of Nebraska Medical Center lung tissue biobank with prior approval from the UNMC IRB. All HPLFs were cultured in DMEM with 10% FBS, 1% amphotericin B, 1% L-glutamine, penicillin (100 U/mL), and streptomycin (100 μg/mL) at 37 °C in a humidified

chamber with 5% CO_2. Mouse primary lung fibroblasts (MPLFs) were isolated from the lungs of mice with BLM-induced pulmonary fibrosis as described before [129] and cultured at 37 °C with 5% CO_2 in high-glucose DMEM with 10% FBS and Pen-Strep (100 U/mL, 100 μg/mL).

CXCR4, STAT3, col1a1, and col1a2 mRNA levels in the HPLFs and MPLFs were measured by RT-PCR. Cells were homogenized with TRIzol reagent to isolate total RNA following the protocol. Then the total RNA was converted into cDNA via a High-Capacity cDNA Transcription kit. The PCR reaction was run on the Rotor-Gene Q (QIAGEN) using iTaq Universal SYBR Green Supermix.

Deidentified human lung parenchyma slides from NDC and IPF patients were provided by the University of Nebraska Medical Center Lung Transplant Biobank, and the slides were sectioned and analyzed with H&E and Masson's trichrome staining. Immunofluorescence dual-staining for STAT3 and p-STAT3, collagen-1, and α-SMA (smooth muscle actin) was performed, and slides observed using a confocal microscope.

2.2.2. Preparation and characterization of PAMD@PFOB/siRNA EPs

PAMD was synthesized as described previously by Michael addition of reacting 1:1 molar ratio of HMBA and AMD3100 and stirred under nitrogen in the dark at 37 °C for 3 days [264]. Excess AMD3100 was added, and the reaction was stirred for another 6 h. The product was collected and dialyzed for 3 days against HCl acidified water (pH 3.0) followed by final dialysis against deionized water and lyophilization. ^{1}H-NMR in D_2O (Figure S1) using Varian INOVA (500 MHz) was used to confirm the polymer structure. To

prepare fluorescently labeled Cy5-PAMD, Cy5-NHS ester was conjugated to PAMD in Na_2CO_3/$NaHCO_3$ buffer (pH 8.2) and kept overnight to obtain Cy5-PAMD. To prepare the PAMD@PFOB nanoemulsion, 20 µL of PFOB was added to 2 mL PAMD (0, 0.25, 0.5, 1, 2 mg/mL) in water and ultrasonicated with a probe-type ultrasonic processor with a 2 mm diameter (Hielscher, UP200ST) with energy limited to 8000 W under 80% output amplitude setting.

Binding of siRNA to the PAMD@PFOB emulsion was evaluated by agarose gel electrophoresis with 2% agarose gel containing 0.5 µg/mL of ethidium bromide. PAMD@PFOB/siRNA EPs were formed by adding a different volume of emulsion to an siRNA solution to achieve the desired w/w ratio, incubated at room temperature for 30 min, and run in 0.5x Tris/borate/EDTA buffer for 15 min at 110 mV. The gels were imaged under UV with a KODAK Gel logic 100 imaging system. Hydrodynamic diameter and zeta potential of the EPs were measured by using NanoBrook Omni (Brookhaven Instruments, Holtsville, NY, USA). EPs morphology was analyzed using TEM (Tecnai G2 Spirit, FEI Company, USA) with NanoVan negative staining (Nanoprobes, USA). The colloidal stability of the emulsions in PBS was tested by measuring particle size after incubation at 4, 25, and 39 °C for 1-48 h.

2.2.3. Stability of EPs in mucus

A mucus stability assay with naked siRNA, PAMD/siRNA, and PAMD@PFOB/siRNA (w/w = 4) EPs was evaluated via agarose gel electrophoresis. Naked siRNA, PAMD/siRNA, and EPs (w/w = 4, 0.2 µg siRNA) were incubated at 37 °C with 10% mucus (diluted in

PBS) obtained from patients with chronic obstructive pulmonary disease (COPD). We collected the samples at predetermined time points. Heparin (80 μg/mL) was used to release siRNA, then analyzed by gel electrophoresis. FRET was also used to measure the mucus and pulmonary surfactant stability of EPs against disassembly. Cy5-PAMD@PFOB/Cy3-siRNA (w/w = 4) were prepared using the same methods as described above, and EPs containing 5 μg Cy3-siRNA were incubated with the 10% mucus obtained from COPD patients (2 mL) or 20% of Curosurf® (pulmonary surfactant) for 5 h, and 24 h at 37 °C. The fluorescence intensity at 667 and 568 nm upon excitation at 550 nm was measured by recording the fluorescence emission spectra according to an earlier report [231].

A heparin displacement assay was performed to analyze siRNA release from EPs. PAMD@PFOB/siRNA EPs (w/w = 4) were incubated with different concentrations of a heparin solution for 30 min, then assayed by gel electrophoresis. SYBR-Safe was used to evaluate the amount of released siRNA. EPs with 0.2 μg siRNA were prepared in HEPES buffer, and 100 μL of each EP solution was distributed in a white 96-well plate. 3 μL 40x SYBR safe was added to each well and incubated for 10 min in the dark. Fluorescence was measured by a SpectraMax iD3 plate reader microplate reader (Molecular Devices, CA) at 500 nm excitation and 555 nm emission wavelengths. An analogous procedure with free siRNA was used and set as 100%.

To evaluate the PAMD@PFOB/siRNA-mucus interactions, the EPs (w/w = 4, 5 μg siRNA) were mixed with mucus solution (0.3% or 0.5% mucus and diluted in PBS, 2 mL)

and incubated for 5 h at 37 °C. The mixture was centrifuged for 2 min. Then, the precipitates were washed with PBS and treated with NaOH (5 M, 200 μL) for 10 min, and the fluorescence intensity was measured by SpectraMax iD3 plate reader (Ex = 550 nm, Em = 565 nm) [231].

Multiple particle tracking was used to evaluate the trajectory of particles in the mucus. Briefly, PAMD@PFOB/siRNA or PAMD/siRNA were mixed with COPD mucus (1 mL) and transferred to 1 mL syringe. After equilibration for 1 h at room temperature, 20 s videos of particle movement and particle trajectories were captured using NanoSight (NS300). ImageJ software (Fuji) was used to convert particle movement into metric displacement in both the X and Y directions. The mean square displacement (MSD) was determined as $(X_{\Delta t})^2 + (Y_{\Delta t})^2$.

2.2.4. Cytotoxicity of PAMD@PFOB emulsion in HPLFs and MPFLs

Cytotoxicity of PAMD@PFOB emulsion was tested via a CellTiter-Blue Cell (CTB) Viability Assay (Promega, WI). Cells were seeded onto 96-well plates at 6,000 cells per well, then, after 12-18 h, the cells were treated with a 100 μL of emulsion with increasing concentrations in culture medium for 24 and 48 h. Then, cell viability was evaluated by the CTB reagent according to the manufacture recommendations. The half-inhibitory IC50 values were calculated from a dose-response analysis in GraphPad Prism.

2.2.5. Fibroblast proliferation and migration

The *in vitro* cell proliferation assay was evaluated by CTB assay. The HPLFs were seeded in a 96-well plate (6,000 cells per well). After 18 h, the cells were treated with EPs (w/w = 4, siRNA 100 nM) using serum free medium. The medium was replaced after 4 h with medium containing 10% FBS for another 48 h. Cell viability was then measured using CTB assay according to the manufacturer's recommendations. NDC HPLFs treated with PBS served as a negative control and IPF HPLFs treated with PBS served as a positive control.

The Transwell migration assay was conducted as previously described.[265] For comparison of migration between NDC and IPF HPLFs, the cells were detached and washed with PBS, then re-suspended in serum free medium ($1x10^4$, $2x10^4$, $4x10^4$, and $6x10^4$ cells in 300 µL medium per insert, 8.0 µm pores). 600 µL medium with 10% FBS was added into the lower transwell chamber. After 16 h of incubation, the non-migrated cells in the top chamber were removed. Migrated cells at the bottom were fixed and stained with 0.2% Crystal Violet. The migrated cells were observed and counted under EVOS xl microscope.

The effect of PAMD@PFOB/siSTAT3 EPs on the myofibroblast migration was evaluated with IPF HPLFs. Cells were detached and washed with PBS, then resuspended in serum free medium. Cells were pretreated with EPs or polyplexes (without emulsion) for 30 min, and 300 µL of serum-free medium ($4x10^4$ cells per insert) was added into the cell culture inserts. 600 µL medium with 10% FBS was added into the lower transwell

chamber. After 16 h incubation, the non-migrated cells in the top chamber were removed. Migrant cells were fixed and stained with 0.2% Crystal Violet. The migrated cells were observed and counted under EVOS xl imaging system. NDC HPLFs treated with PBS served as a negative control, and IPF HPLFs treated with PBS served as a positive control. Results were interpreted as the percentage of migrated cells relative to NDC HPLFs (n = 3).

2.2.6. Cellular uptake and intracellular tracking

HPLFs and MPLFs were seeded in 12-well plates and adhered overnight before treatment. Cells were then treated with PAMD/FAM-siRNA or PAMD@PFOB/FAM-siRNA (w/w = 4, 100 nM FAM-siRNA) for 4 h. Cells were washed with PBS, detached, and analyzed by flow cytometry. Subcellular distribution of nanoparticles was observed by confocal microscopy. Cells were seeded in confocal dishes 24 h before the treatment. Cells were then treated with PAMD@PFOB/Cy5.5-siRNA EPs. After 4 h, cells were washed with PBS, stained with Hoechst 33324, and visualized under confocal microscopy (LSM 710, Zeiss, Jena, Germany). To investigate the endosome siRNA escape, HPLFs (IPF) were treated by Cy3-PAMD@PFOB/Cy5.5-siRNA. After 4 h incubation, cells were washed with PBS, stained with LysoView (green) and Hoechst 33324, and visualized with confocal microscopy.

2.2.7. Pulmonary distribution of EPs in pulmonary fibrosis mice

All animal experiment protocols were approved by the University of Nebraska Medical Center Institutional Animal Care and Use Committee. Male C57BL/6 mice were injected intraperitoneally with BLM (twice per week, 4 weeks, 30 U/kg) to induce pulmonary fibrosis. On day 28, mice were intratracheally administered 40 μL of EPs prepared with Cy5-PAMD and FAM-siRNA (15 μg siRNA per mouse, w/w = 4). At different times post-treatment (1 h, 5 h, and 24 h after the treatment), whole body fluorescence imaging was conducted prior to ex vivo analysis of the fluorescence in individual organs using Xenogen IVIS 200. Lungs were collected, inflated with O.C.T compound to ensure embedded, cut into frozen sections (10 μm), nuclei stained with DAPI, and then imaged by confocal microscopy.

2.2.8. Ciliary beat frequency (CBF) [266]

After 4 weeks of treatment with BLM, C57BL/6J male mice were euthanized, the trachea was extracted and opened lengthwise, then placed in protease solution (1.5 mg/mL) for 18-24 h. The tracheas were then discarded, and the solutions were centrifuged (200 x g) to get the mouse tracheal epithelial cells (MTECs). Then cells were plated onto an uncoated polystyrene plastic culture dish in MTEC basic media with 10% FBS [MTEC basic media consists of a 1:1 solution of Ham's F-12 and DMEM supplemented with Pen/Strep (1%), amphotericin B (250 μg/mL), gentamicin (40 mg/mL), and glutamine (4 mM)]. Due to the differential adherence property of MTECs, after 4 h incubation, the adhered fibroblasts were removed, then washed and counted the MTECs. MTECs were seeded on inserts with Type I collagen-coated membrane and grown in MTEC

supplementary media [consists of basic media supplemented with 0.1% insulin, 0.1% transferrin, 0.1% Epidermal Growth Factor (EGF), 0.4% Bovine Pituitary Extract (BPE), 0.1% cholera toxin (CT), 0.001% retinoic acid (RA), and 5% FBS]. By the 6th day, the cells were cultured at air-liquid interface (ALI).[266] After 14-21 days at ALI, a baseline CBF reading was measured, and the cells were treated with 100 µL of EPs or polyplexes (w/w = 4, siRNA = 100 nM). After 48 h, the beating cilia were observed using an inverted phase-contrast microscopy, and CBF was calculated using the Sisson Ammons Video Analysis (SAVA) method [267].

2.2.9. Anti-fibrosis activity of EPs *in vivo*

Pulmonary fibrosis was induced in C57BL/6 mice as stated previously; however, on day 14, mice were randomly assigned to four intratracheal treatment groups: PBS, PAMD/siSTAT3, PAMD@PFOB/siScr, and PAMD@PFOB/siSTAT3 (w/w = 4, 40 µL, 15 µg siRNA/mouse). The mice were administered treatment on days 14, 17, 20, 23, and 26. Untreated C57BL/6 mice served as controls. Mouse body weight was recorded during the entire process. At day 30, bronchoalveolar lavage fluid (BALF) from three mice of each group was collected, centrifuged for 10 min at (300 x g) at 4 °C, the cell pellets were re-suspended in 200 µL PBS, and total cell number enumerated. All mice were euthanized at day 30 and lung tissues were inflated with 400-800 µL formalin and harvested for the histological and biomedical analyses. The pulmonary edema was evaluated by measuring the wet/dry (W/D) weight ratio. The lungs were excised, washed with PBS, and weighed to acquire the wet weight. Then, lung tissue was dried at 65 °C for 3 days to acquire the

dry weight and the W/D weight ratio was calculated. STAT3, CXCR4, and connective tissue growth factor (CTGF) mRNA levels in the lung were measured by RT-PCR. Lungs were homogenized with TRIzol reagent to isolate total RNA following the protocol. Then the total RNA was converted into cDNA via a High-Capacity cDNA Transcription kit. The PCR reaction was run on the Rotor-Gene Q (QIAGEN) using iTaq Universal SYBR Green Supermix. Hydroxyproline (HYP) levels in the lung tissues were measured according to the protocol of the Hydroxyproline Assay Kit (Abcam, US). A 60-day survival study was also performed with the same treatment regimens previously stated using 8 mice per group.

2.2.10. Immunohistochemical analysis

IPF HPLFs were seeded in an 8-well chambered for 24 h before treatment. The cells were then treated by PAMD@PFOB/siRNA EPs or polyplexes (w/w = 4, 100 nM siSTAT3) in serum-free medium. After 4 h incubation, replace with fresh medium containing 10% FBS for another 48 h. Cells were fixed for 15 min, blocked with 5% bovine serum albumin and 0.2% Triton X-100 for 1 h. The cells were incubated with α-SMA primary antibody (1:200) at 4 °C overnight. Then, the cells were rinsed three times in PBS for 5 min each and incubated with anti-rabbit IgG AlexaFluor 488 secondary antibody (Thermo Fisher) for 1 h at room temperature. Hoechst 33324 was used to stain nuclei for 15 min and imaged by confocal microscopy. NDC HPLFs treated with PBS served as negative controls and IPF HPLFs treated with PBS served as positive controls.

Mouse lung tissues obtained from the treatment groups were inflated and fixed in 4% paraformaldehyde and then stored in 75% ethanol. Then, the lung tissues were embedded in paraffin and sectioned for histochemical analysis with H&E and Masson's trichrome staining. Immunohistochemical (IHC) staining for CXCR4 was conducted in tandem with immunofluorescence (IF) dual-staining for STAT3 and p-STAT3, collagen-1 and α-SMA. Lung slides were deparaffinized and treated with endogenous peroxidase inhibitor, then block slides for 10 min with blocking solution, followed by incubating with primary antibodies at 37 °C for 32 min. The slides were rinsed in IF buffer 3 times for 5 min each, then incubated with the Discovery Cy5 or Cy3 Kit. Slides were also counterstained for 5 min with DAPI and then evaluated using confocal microscopy (LSM 710). IHC images were obtained by the EVOS xl microscope (Thermo, US).

2.2.11. Statistical analysis

Results are presented as mean ± SD. Total sample size (n) was given for each experiment as follows: *in vitro* study (n = 3-6); *in vivo* biodistribution study (n = 3); *in vivo* therapeutic study (n = 10); survival study (n = 8); H&E staining, Masson's trichrome staining, immunochemistry staining, and immunofluorescence staining (n = 3-6). One-way ANOVA test with Tukey's multiple comparisons test was used to analyze differences among multiple groups followed by a comparison test. Student's t-test was used to analyze the statistical significance between two groups, and differences were assessed to be significant. In all the case, P-value < 0.05 were considered statistically significant, and

significance was indicated as *p<0.05 or #p<0.05, **p<0.01 or ##p<0.01, and ***p<0.001 or ###p<0.001. All the statistical analysis was performed with GraphPad Prism 8.

3. Results and discussion

Our group previously demonstrated pulmonary administration of EPs with effective lung distribution and therapeutic efficiency [147, 148]. Here, we further optimized the EPs formulation by developing PFOB nanoemulsions to improve delivery of polycation/siRNA polyplexes to treat pulmonary fibrosis in a BLM-induced small animal model [268]. This novel approach relies upon creating positively charged PFOB nanoemulsions that can bind and deliver siRNA. When combined with stabilizing polycations that function as inhibitors of CXCR4, the resulting delivery system offers a unique two-pronged small molecule and siRNA strategy for inhalation therapy to reduce pulmonary fibrosis.

3.1. Physiochemical characterization of PAMD@PFOB/siRNA EPs

We have developed CXCR4-inhibiting polycations, named PAMD, that form nanosized polyplexes with nucleic acids, such as siRNA, miRNA, and DNA [264, 269-273]. In this study, we have used PAMD as a surfactant to stabilize PFOB nanoemulsions and to form EPs to improve the pulmonary siRNA delivery in mice with pulmonary fibrosis. We synthesized PAMD with a weight-average molecular weight of 10 kDa and its ^{1}H-NMR spectrum is shown in Figure 2.1. PAMD@PFOB (o/w) emulsions were prepared via a one-step ultrasonication method [252] using 1% v/v PFOB in the presence of different concentrations of PAMD (Figure 2.2A). The emulsion consisted of the PFOB core and the stabilizing PAMD shell (Figure 2.2B). The structure enabled exposure of the CXCR4-binding moieties in PAMD on the surface of the emulsion while providing the positive surface charge needed for siRNA binding. The PAMD@PFOB emulsions remained

relatively stable for at least three days at room temperature as indicated by a particle size increase of less than 20% (Figure 2.2C). As shown in Figure 2.2D, even the lowest tested concentration of PAMD (0.25 mg/mL) was sufficient to stabilize the PFOB emulsion and limit particle size growth. The particle size of the PAMD@PFOB emulsion prepared with 2 mg/mL PAMD was 175 ± 2 nm and the zeta potential was 20.5 ± 0.9 mV (Figure 2.2A&F). The ability of siRNA to bind to PAMD@PFOB emulsions was then evaluated by a gel retardation assay (Figure 2.2E). The EPs were prepared by mixing increasing amounts of PAMD@PFOB emulsion with siRNA solution. We found that siRNA bound completely to the emulsion at a w/w ratio of PAMD/siRNA (excluding PFOB) above 2. We used w/w=4 in subsequent *in vitro* and *in vivo* studies to maintain slight excess of CXCR4-binding moieties not engaged in electrostatic interactions with siRNA. The EPs that were prepared at w/w=4 had a size of ~190 nm and the zeta potential was ~19 mV (Figure 2.2E). The residual positive zeta potential confirmed that some CXCR4 binding moieties likely remained presented on the surface of the emulsion despite siRNA binding. CXCR4 antagonism of PAMD@PFOB emulsion was validated using a CXCR4 receptor redistribution assay (Figure 2.3). Both PAMD and PAMD@PFOB displayed dose dependent CXCR4 antagonism.

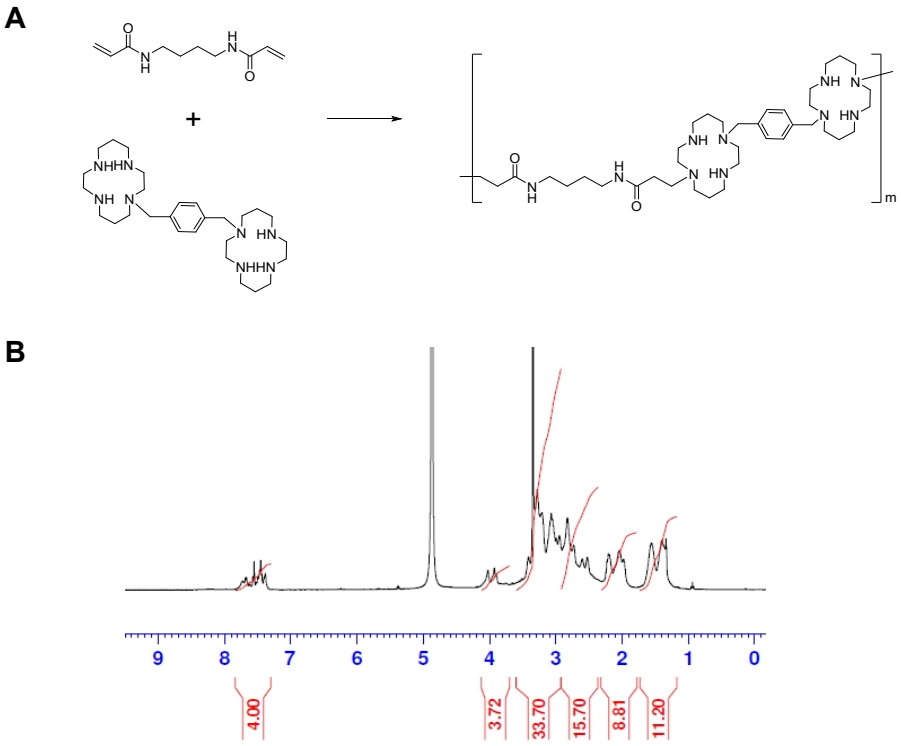

Figure 2.1 Synthesis and 1H-NMR of PAMD.

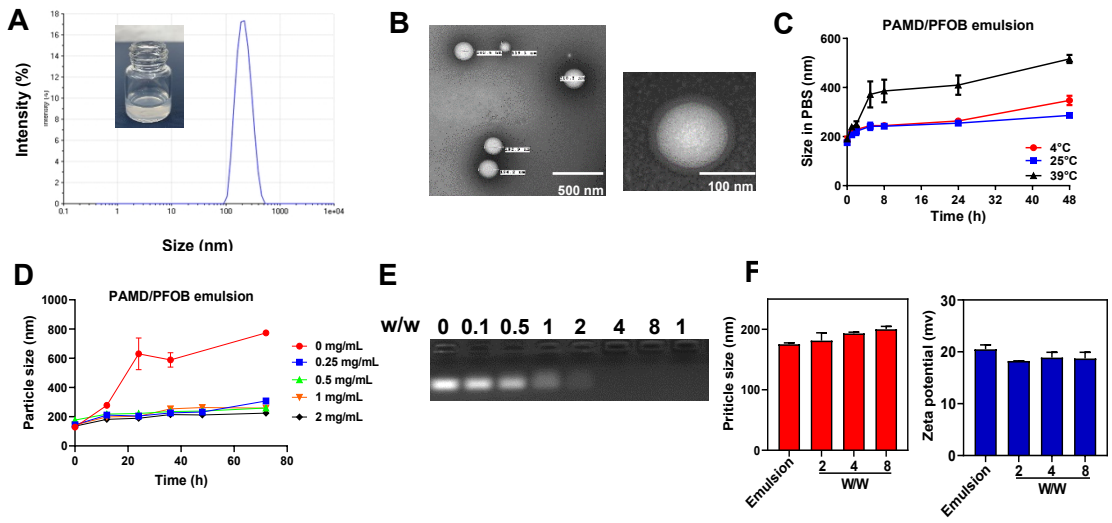

Figure 2.2 Characterization of PAMD@PFOB emulsion and PAMD@PFOB/siRNA emulsion polyplexes. (A) Particle size distribution of PAMD@PFOB emulsion. (B) Representative TEM image of the PAMD@PFOB emulsion. (C) Colloidal stability of the PAMD@PFOB emulsion in PBS. (D) The stability of the PAMD@PFOB emulsion at different used PAMD concentrations. (E) siRNA condensation ability of PAMD@PFOB emulsion by agarose gel retardation assay. (F) Hydrodynamic particle size and zeta potential of the EPs at different PAMD/siRNA w/w ratios.

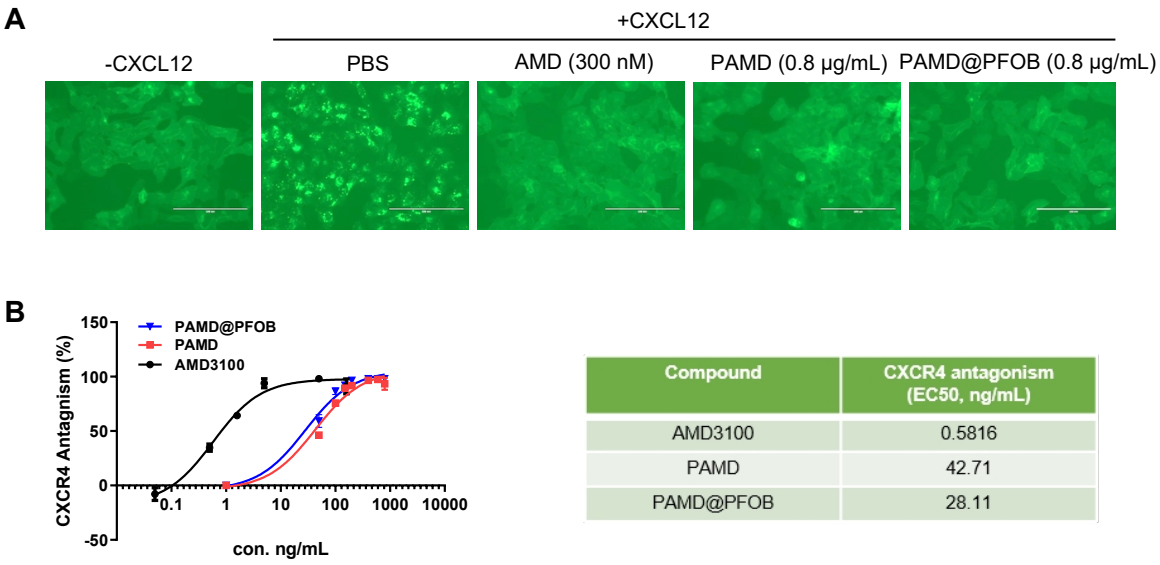

Compound	CXCR4 antagonism (EC50, ng/mL)
AMD3100	0.5816
PAMD	42.71
PAMD@PFOB	28.11

Figure 2.3. CXCR4 antagonism of PAMD@PFOB vs. PAMD. AMD3100 was used as the positive control. (A) CXCR4 receptor redistribution assay in U2OS cells expressing GFP-tagged CXCR4 (green). Scale bar = 100 μm. (B) EC50 values determined from receptor redistribution assay in U2OS cells (n = 3).

3.2. Cytosolic siRNA delivery and anti-fibrotic effect of EPs in primary mouse and human lung fibroblasts

We first assessed the toxicity of EPs in mouse primary lung fibroblasts (MPLFs) that were isolated from lungs with established fibrosis [MPLFs (IPF)], as well as human primary lung fibroblasts (HPLFs) isolated from IPF patients [HPLFs (IPF)] and non-disease control [HPLFs (NDC)] (Figure 2.4). MPLFs (IPF) exhibited less cytotoxicity in response to PAMD and EPs than both NDC and IPF HPLFs. No significant cytotoxicity was observed with the EPs formulations used at a w/w ratio of 4 and 100 nM siRNA, and these were thus used in subsequent studies. Based on prior studies, we hypothesized that the localization of the PAMD and siRNA on the surface of the PFOB nanoemulsions would improve siRNA cytosolic delivery. EPs were prepared with fluorescently labeled siRNA and cell internalization in the HPLFs (IPF, Figure 2.5A) and MPLFs (IPF, Figure 2.5B) was examined by confocal microscopy and flow cytometry. We found that PAMD@PFOB/siRNA EPs significantly improved siRNA cellular uptake when compared with the PAMD/siRNA in both the human primary and mouse primary fibroblasts obtained from fibrotic lungs. This result was also confirmed by flow cytometry. Endosomal escape of the PAMD@PFOB/siRNA EPs in HPLF (IPF) was evaluated using LysoView to stain lysosomes. After 4 h incubation, Cy5.5-siRNA was found mostly in the cytoplasm with only a small amount present in the lysosomes as suggested by the limited overlap with the LysoView signal (Figure 2.5C). These results suggested that PFOB nanoemulsion can enhance the cytosolic siRNA delivery. However, the mechanism governing this process is

poorly understood. The cellular uptake and endosome escape results showed that most siRNA could escape from the lysosomes and be transported to the cytosol, which suggested that the mechanism may involve the perturbation of intracellular phospholipid membranes.[274] Further studies need to be performed to gain better understanding.

Differentiated fibroblasts play a key role in the progression of IPF and strategies that modulate their function may have a significant impact on the treatment of IPF.[275] The characteristic differential expression of cytoskeletal proteins such as α smooth muscle actin (α-SMA) can be used as a marker of activated lung myofibroblasts. We evaluated expression of α-SMA in IPF and NDC HPLFs and determined the effect of treatment with EPs (Figure 2.5D). As expected, the IPF HPLFs showed higher expression of than HPLFs (NDC), and treatment with PAMD@PFOB/siSTAT3 EPs significantly decreased the α-SMA expression. Control treatment with EPs prepared with scrambled siRNA and polyplexes without the PFOB emulsion showed a less pronounced effect on α-SMA expression. Fibroblasts in IPF lungs represent a population of cells with diverse phenotypes and functions. The accumulation of fibroblasts and myofibroblasts is a hallmark of IPF, leading to the production of excessive ECM [276]. Activated myofibroblasts can induce apoptosis of epithelial cells, which contributes to the absence of re-epithelialization and thereby perpetuating IPF [277, 278]. Activated fibroblasts from IPF can be also distinguished by increased migration as confirmed in Figure 2.6A when compared with NDC HPLFs. CXCR4, STAT3, col1a1, and col1a2 expression were significantly elevated in IPF HPLFs when compared with NDC HPLFs (Figure 2.6B,C).

Importantly, when treating the IPF HPLFs with the PAMD@PFOB/siSTAT3 EPs, the expression of STAT3, col1a1, and col1a2 decreased and reached the levels similar to the control HPLF (NDC) (Figure 2.6C). We also examined the role of CXCR4 and STAT3 inhibition in fibroblast proliferation and migration (Figure 2.5E,F). IPF HPLFs were treated with PAMD/siSTAT3, PAMD@PFOB/siScr, and PAMD@PFOB/siSTAT3. All the used treatment were capable of CXCR4 inhibition and achieved nearly complete inhibition of cell migration, similar to NDC HPLFs. Moreover, treating the HPLFs (IPF) with PAMD@PFOB/siSTAT3 resulted in better migration inhibition than treatments with PAMD/siSTAT3 and PAMD@PFOB/siScr. Fibroblast proliferation experiments showed similar results in that the IPF HPLFs displayed significantly increased proliferation (Figure 2.5F). To further confirm that proliferation of fibroblasts requires CXCR4 and STAT3 activation, we treated cells with PAMD@PFOB/siSTAT3 EPs. As shown in Figure 3F, PAMD@PFOB/siSTAT3 EPs significantly suppressed fibroblasts proliferation. We also evaluated the STAT3 gene silencing efficacy in the HPLFs IPF, siRNA cell uptake was improved significantly by the EPs and resulted in improved STAT3 gene silencing efficacy (Figure 2.5G).

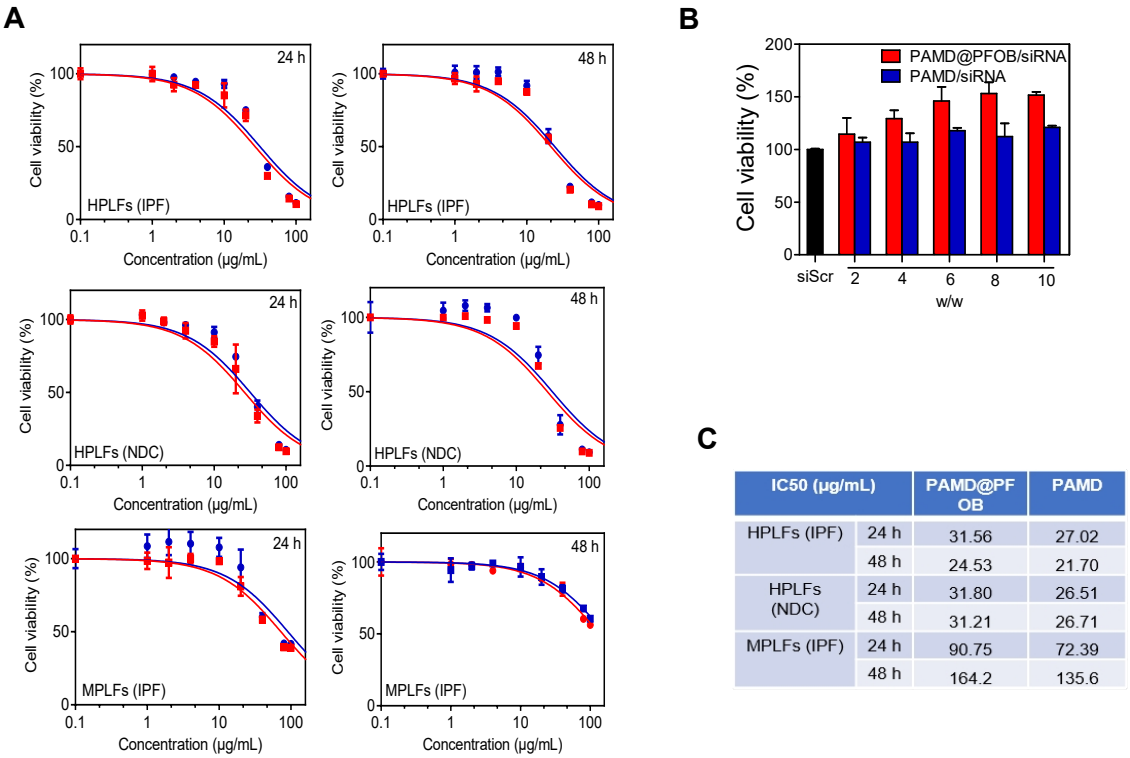

C

IC50 (μg/mL)		PAMD@PFOB	PAMD
HPLFs (IPF)	24 h	31.56	27.02
	48 h	24.53	21.70
HPLFs (NDC)	24 h	31.80	26.51
	48 h	31.21	26.71
MPLFs (IPF)	24 h	90.75	72.39
	48 h	164.2	135.6

Figure 2.4. Cell toxicity of the PAMD@PFOB in HPLFs which were isolated from the IPF patient or NDC and in the MPLFs which were isolated from IPF mice.

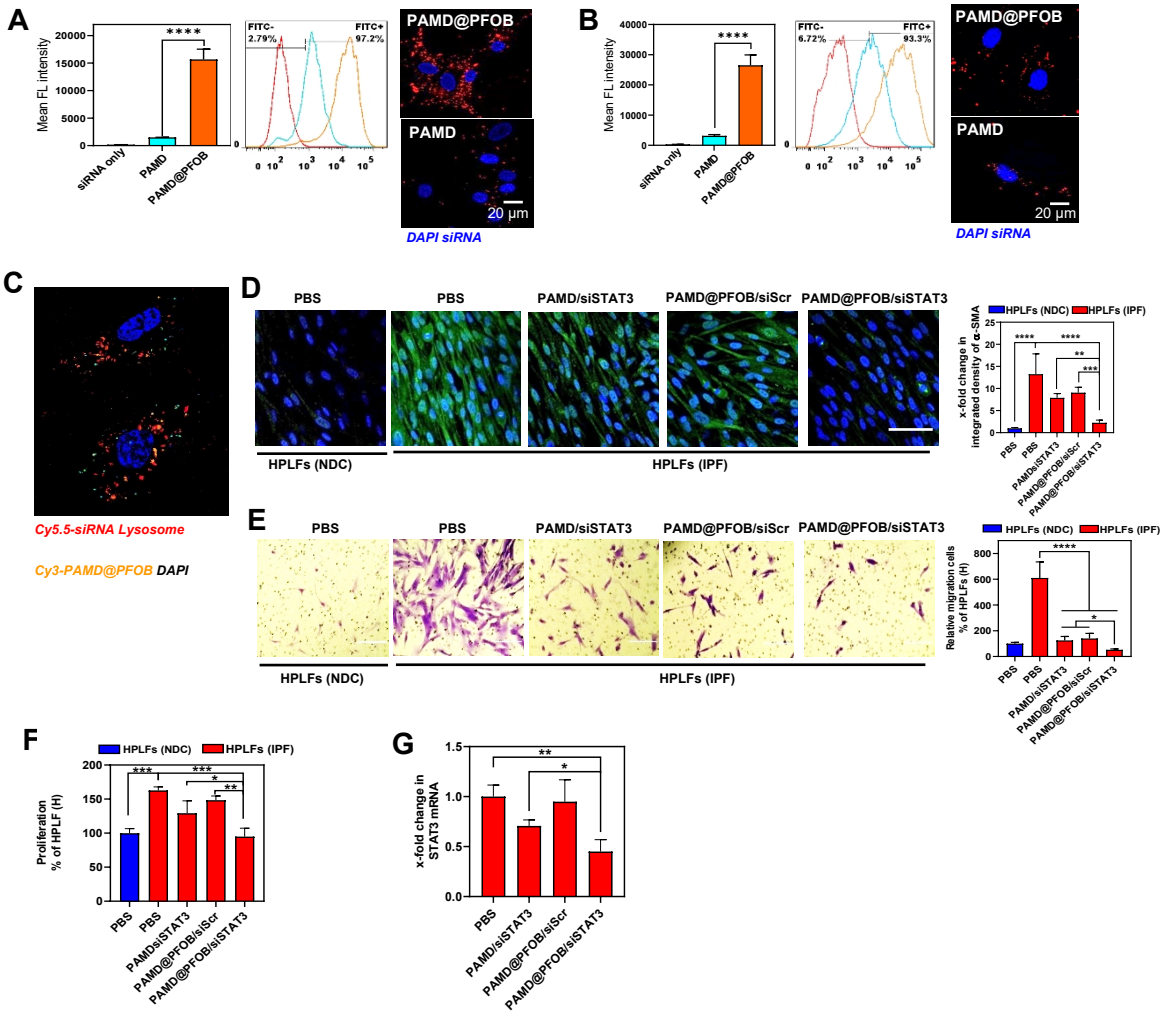

Figure 2.5 Effect of CXCR4 inhibition and STAT3 gene silencing on fibroblast proliferation and migration. Cytosolic siRNA delivery in (A) HPLFs (IPF), (B) MPLFs (IPF), scale bar = 20 μm. (C) Endosome escape of PAMD@PFOB/siRNA. (D) Immunofluorescence staining of α-SMA (green). Cell nuclei stained with DAPI (blue), scale bar = 100 μm. (E) Representative images of fibroblast migration with different treatments. (F) Fibroblast proliferation following different treatments. (G) STAT3 mRNA expression in the IPF HPLFs after treatment.

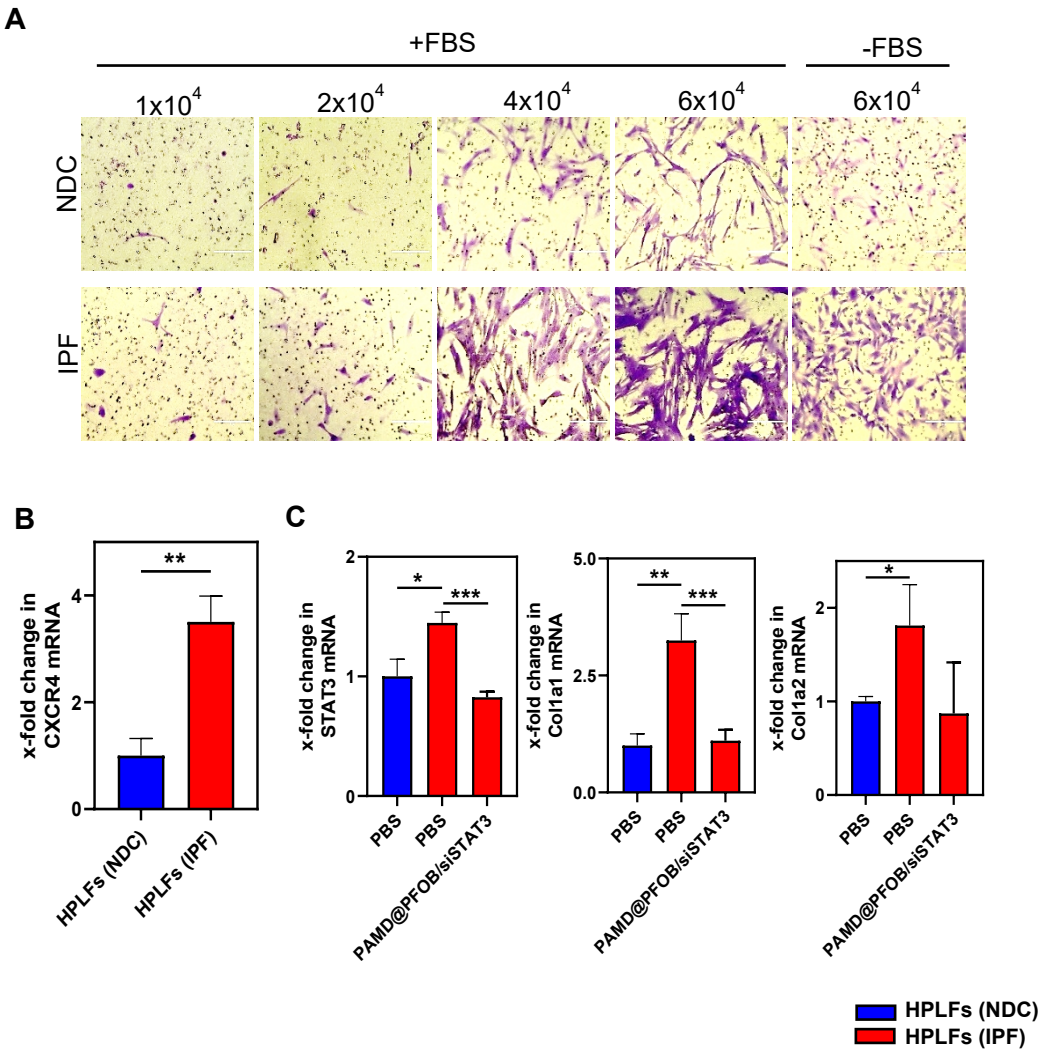

Figure 2.6 Analysis of HPLFs. (A) Migration assay of HPLFs (NDC&IPF). (B) x-fold changes in CXCR4 mRNA levels between NDC and IPF. (C) STAT3, col1a1 and col1a2 mRNA levels in HPLFs (NDC) and after treated with PAMD@PFOB/siSTAT3 in HPLFs (IPF).

3.3. Enhanced mucus stability and penetration and decreased CBF by EPs

Efficient pulmonary delivery of siRNA is a complex process that demands sufficient stability of the delivery system to reach the desired location in the lungs. The mucus that covers the airway epithelium is a major obstacle to pulmonary siRNA delivery in addition to other host defense factors that capture the particles and eliminate them from the lungs [279].

As part of comprehensive stability testing, a heparin displacement assay was first used to evaluate the resistance against polyelectrolyte exchange causing the release of siRNA from EPs. As shown in Figure 2.7, siRNA was completely released from the EPs when the heparin concentration was above 80 μg/mL indicative of good stability.

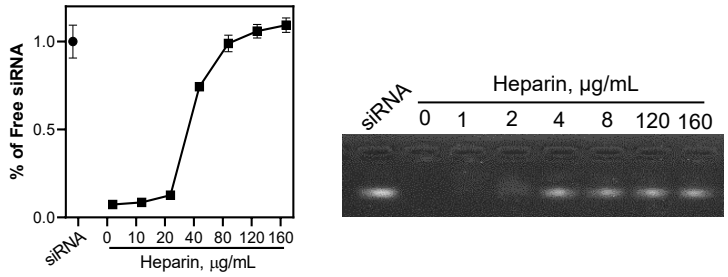

Figure 2.7 Physicochemical characterization of PAMD@PFOB/siRNA EPs. (A) Heparin induced siRNA release from PAMD@PFOB/siRNA emulsion polyplexes (w/w=4) with increasing heparin concentration.

Stability and penetration of the fluorescently labeled nanoemulsions (Cy5-PAMD/Cy3-siRNA) were probed in mucus obtained from patients with chronic obstructive pulmonary disease (COPD) using fluorescence resonance energy transfer (FRET) by labeling

separate batches of EPs with Cy3-siRNA and Cy5-PAMD (a known FRET couple).[280] As shown in Figure 2.8A, after 24 h of coincubation with mucus, a significant decrease in FRET signal (fluorescence intensity at 667 nm upon excitation at 550 nm) was exclusively observed for the PAMD-Cy5/Cy3-siRNA group, suggesting disassembly of the polyplexes. After 24 h in 10% mucus, the EPs were more stable, whereas the FRET changes in case of polyplexes (PAMD-Cy5/Cy3-siRNA) suggested that there were almost no remaining particles at 24 h. Thus, the PAMD@PFOB/siRNA EPs remained more stable in mucus and prevented undesired dissociation and siRNA release. Aggregation in mucus may also contribute to poor delivery and limit efficacy of the particles. Therefore, adsorption of mucin to EPs was investigated by quantitating the amount of EP/mucin aggregates (Figure 2.8B). In this assay, higher fluorescence intensity corresponds to increased formation of the particle/mucin aggregates. After 5 h in mucus, the fluorescence intensity of the PAMD/Cy3-siRNA group was higher than the PAMD@PFOB/Cy3-siRNA EPs group, suggesting more of the polyplex/mucin aggregation than the EPs/mucin, proving that the EPs aggregated significantly less than the control PAMD/siRNA polyplexes both in 0.3% and 0.5% mucus.

Mucus penetration properties of PAMD@PFOB/siRNA EPs were evaluated using NanoSight to track the trajectories of the nanoparticles in mucus. As shown in Figure 2.8C, the movement of PAMD/siRNA polyplexes in the mucus was severely impeded when compared with the movement in water. However, the movement of PAMD@PFOB/siRNA EPs in the mucus remained high. Importantly, the geometric averaged mean square

displacement (MSD) values for PAMD@PFOB/siRNA also remained relatively stable when compared with the MSD values for PAMD@PFOB/siRNA in water. In contrast, the MSD of PAMD/siRNA decreased significantly when compared with the water. Both mucus and pulmonary surfactant are important in defining the fate of the materials in the lung. We thus evaluated the effect of porcine pulmonary surfactant (Curosurf®) on the stability of PAMD@PFOB/siRNA EPs (Figure 2.9). Using FRET, agarose gel, and TEM showed that PAMD@PFOB/siRNA EPs retained their integrity and remained stable in the presence of pulmonary surfactant.

We evaluated the influence of EPs treatment on ciliary beat frequency (CBF). The cilia were assayed by measuring the average number of motile points in multiple whole field measurements of the mouse tracheal epithelial cells (MTEC) grown at an air-liquid interface (ALI) (Figure 2.8D). Treating the MTEC with PBS did not significantly change CBF. In contrast, there was a decrease in CBF compared to the PBS group when MTEC were treated with PAMD@PFOB/siSTAT3. Because particle stimulation of cilia is a well-established concept,[281] this result may point to benefits for the inhalation of EPs as it may decrease the extent of their clearance. The mechanism of PAMD@PFOB/siSTAT3 influence on the CBF in MTEC may involve silencing STAT3 expression but this requires further investigation.

The siRNA stability in the EPs in mucus was also evaluated via agarose gel electrophoresis (Figure 2.8E). Compared with free siRNA and PAMD/siRNA, PAMD@PFOB/siRNA EPs were better at protecting siRNA from mucus-induced

degradation. Moreover, in agreement with the above *in vitro* studies that demonstrated enhanced mucus and pulmonary surfactant stability and decreased CBFs by EPs, the histological results showed that the distribution of PAMD/siRNA polyplexes was confined to the mucus layer of the airways with extremely limited penetration to the deeper areas of the lung (Figure 4F). In contrast, the EPs could efficiently permeate through the mucus layer and penetrate into deeper regions of the lung. We contend that unlike most PFCs, PFOBs has less lipophilicity due to the bromine atom in its structure [282]. This may in turn decrease the interaction between EPs and negatively charged mucin glycoproteins, which may help with mucus penetration.

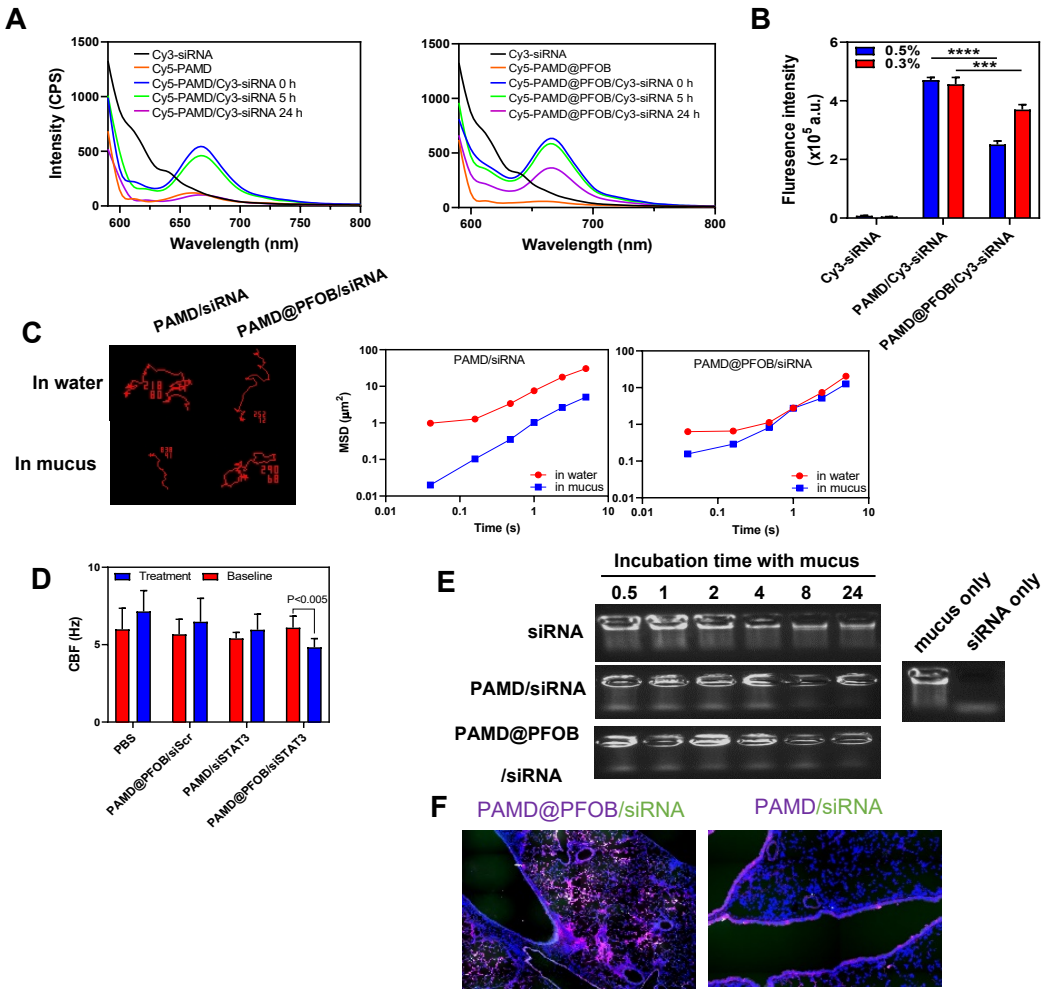

Figure 2.8 PFOB improved the mucus penetration of PAMD@PFOB/siRNA EPs and PAMD@PFOB/siSTAT3 EPs inhibited the ciliary beat frequency (CBF). (A) Fluorescence emission spectra after coincubation with 10% COPD mucus for 0 h, 5 h, 24 h. (B) The fluorescence intensity of the aggregates following 5 h coincubation. (C) Representative trajectories in the mucus and water during 20 s movies. MSD as a function of time. (D) PAMD@PFOB/siSTAT3 EPs inhibit the CBF. (E) Mucus stability assays of PAMD@PFOB/siRNA EPs compared with free siRNA and PAMD/siRNA. (F) Distribution of PAMD/siRNA and PAMD@PFOB/siRNA EPs in lung epithelial tissue following the intratracheal administration in mice with established pulmonary fibrosis.

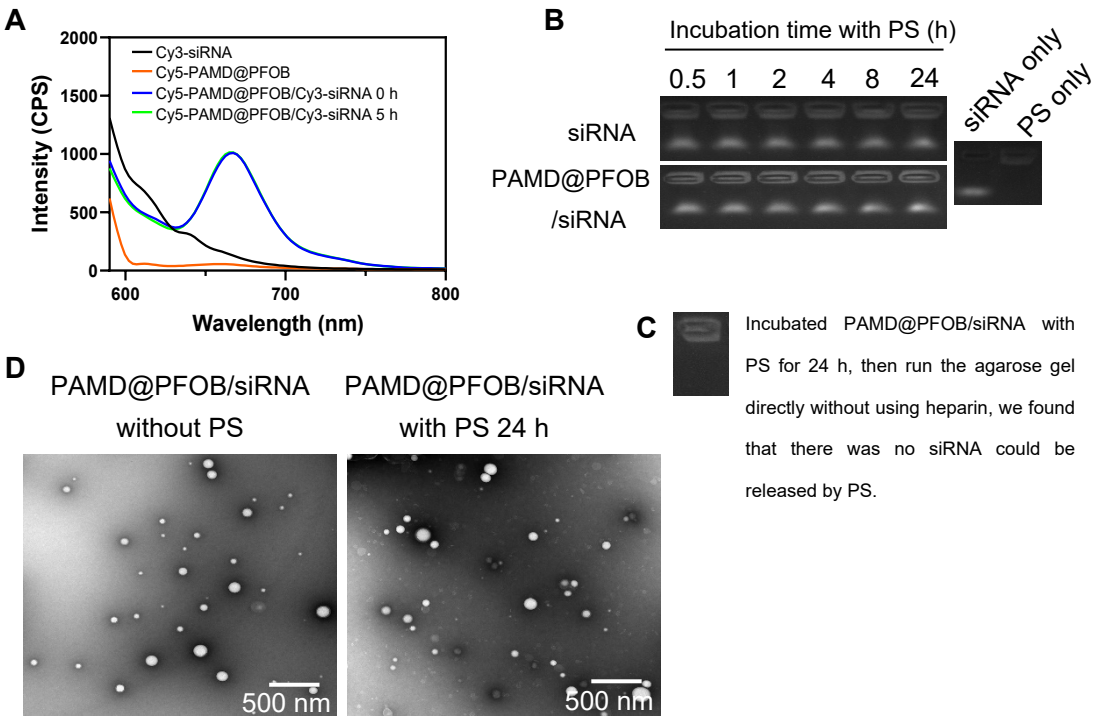

Figure 2.9 Stability of PAMD@PFOB/siRNA within pulmonary surfactant. (A) Fluorescence emission spectra of Cy5-PAMD/Cy3-siRNA, and Cy5-PAMD@PFOB/Cy3-siRNA EPs (excitation at 550 nm) after coincubation with 20% pulmonary surfactant for 0 h and 5 h. (B) Pulmonary surfactant stability assay of PAMD@PFOB/siRNA EPs compared with naked siRNA. (C) Pulmonary surfactant stability assay of PAMD@PFOB/siRNA EPs. Incubated PAMD@PFOB/siRNA with pulmonary surfactant for 24 h, then run the agarose gel directly without using heparin to release siRNA, we found that there was no siRNA could be released by pulmonary surfactant. (D) Integrity of PAMD@PFOB/siRNA coincubation with pulmonary surfactant.

3.4. Histology analysis of the lungs from IPF patients and mice with pulmonary fibrosis

Figure 2.10A&B shows H&E and Masson's trichrome stained slides from IPF patients and mice with BLM-induced pulmonary fibrosis together with healthy controls. As shown in Figure 2.10A, healthy lung (NDC) appeared normal with intact alveolar size and structure. As expected, IPF patient samples revealed dense thickening of the lung parenchyma, displacement and damage to the alveolar walls, and perivascular fibrosis was evident. Similar results were also found in the mice with BLM-induced pulmonary fibrosis, validating that the animal model mimics the human disease (Figure 2.9B). Masson's trichrome staining also revealed large amounts of collagen deposition in the IPF patient lungs compared to NDC, as confirmed by increased immunostaining of collagen I and α-SMA (Figure 2.10C-E). Collagen I (red) and α-SMA (green) staining was significantly more abundant in IPF than in NDC lung sections.

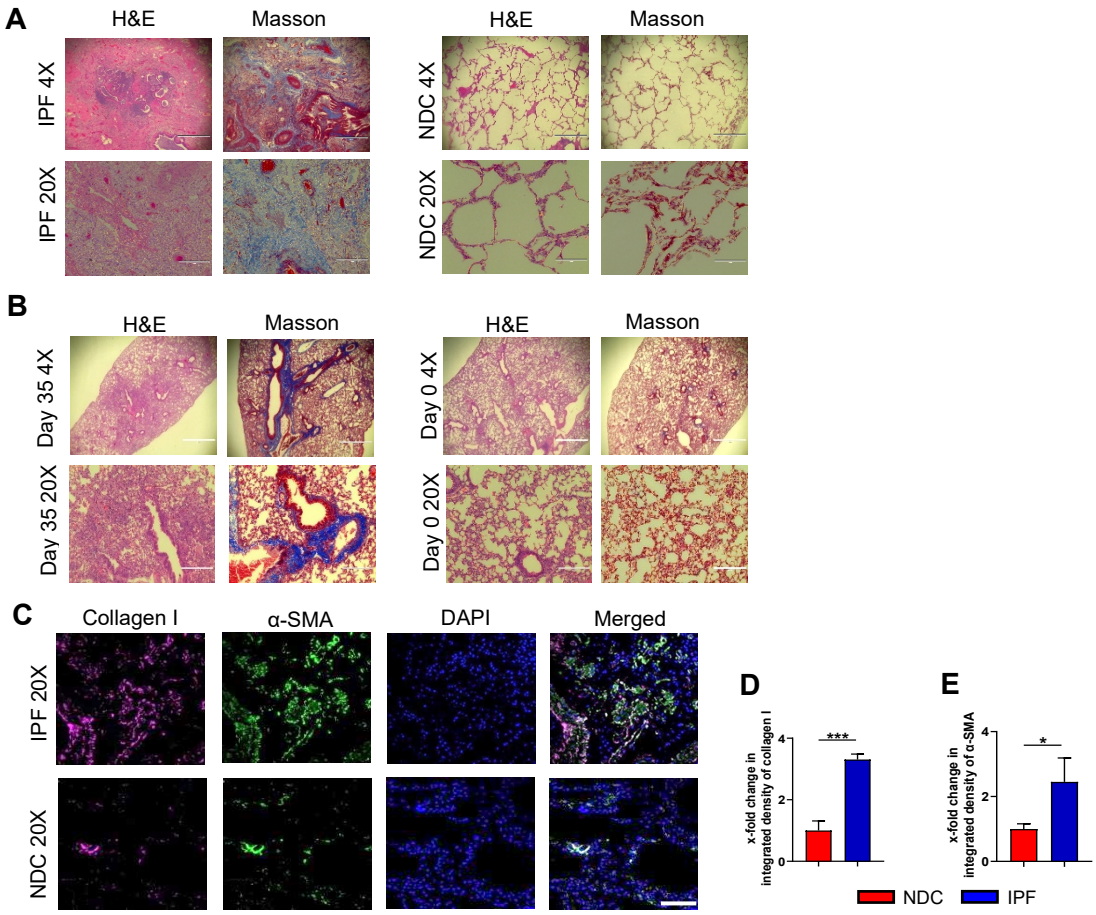

Figure 2.10 Histology analysis of the lungs from IPF patients compared with NDC, and BLM-induced pulmonary fibrosis mice (Day 35) compared with healthy (Day 0) control. (A) H&E and Masson staining of the human samples. (IPF patients compared with the NDC). (B) H&E and Masson staining of lungs from BLM-induced pulmonary fibrosis mice (Day 35) compared with healthy (Day 0) control. (C) Representative images of IF staining for collagen I (red) and α-SMA (green) co-stained with DAPI (blue). (D) Quantitative analysis of IF staining for collagen I. (E) Quantitative analysis of IF staining for α-SMA. 4X: Scale bar = 1000 μm. 20X: scale bar = 200 μm.

STAT3 expression and activation were analyzed by quantifying the extent of phosphorylation at tyrosine 705 (p-STAT3), a marker for STAT3 activation. Consistent with α-SMA and collagen I expression, increased p-STAT3 and total STAT3 were observed in the parenchyma of IPF patient samples ($P<0.0005$ vs NDC), whereas only a few cells were positive for p-STAT3 in healthy individuals (NDC, Figure 2.11A-C). The activation of STAT3 signaling in mice with pulmonary fibrosis was also evaluated in experimental models of BLM-induced pulmonary fibrosis in mice (Figure 2.11D-F). Establishing pulmonary fibrosis by repeated intraperitoneal injection of BLM (30 U/kg) into mice significantly increased p-STAT3 and total STAT3 as compared to control mice. Increased STAT3 signaling was detected after 4 injections of BLM (2 weeks after first injection) and persisted throughout the transition to established fibrosis.

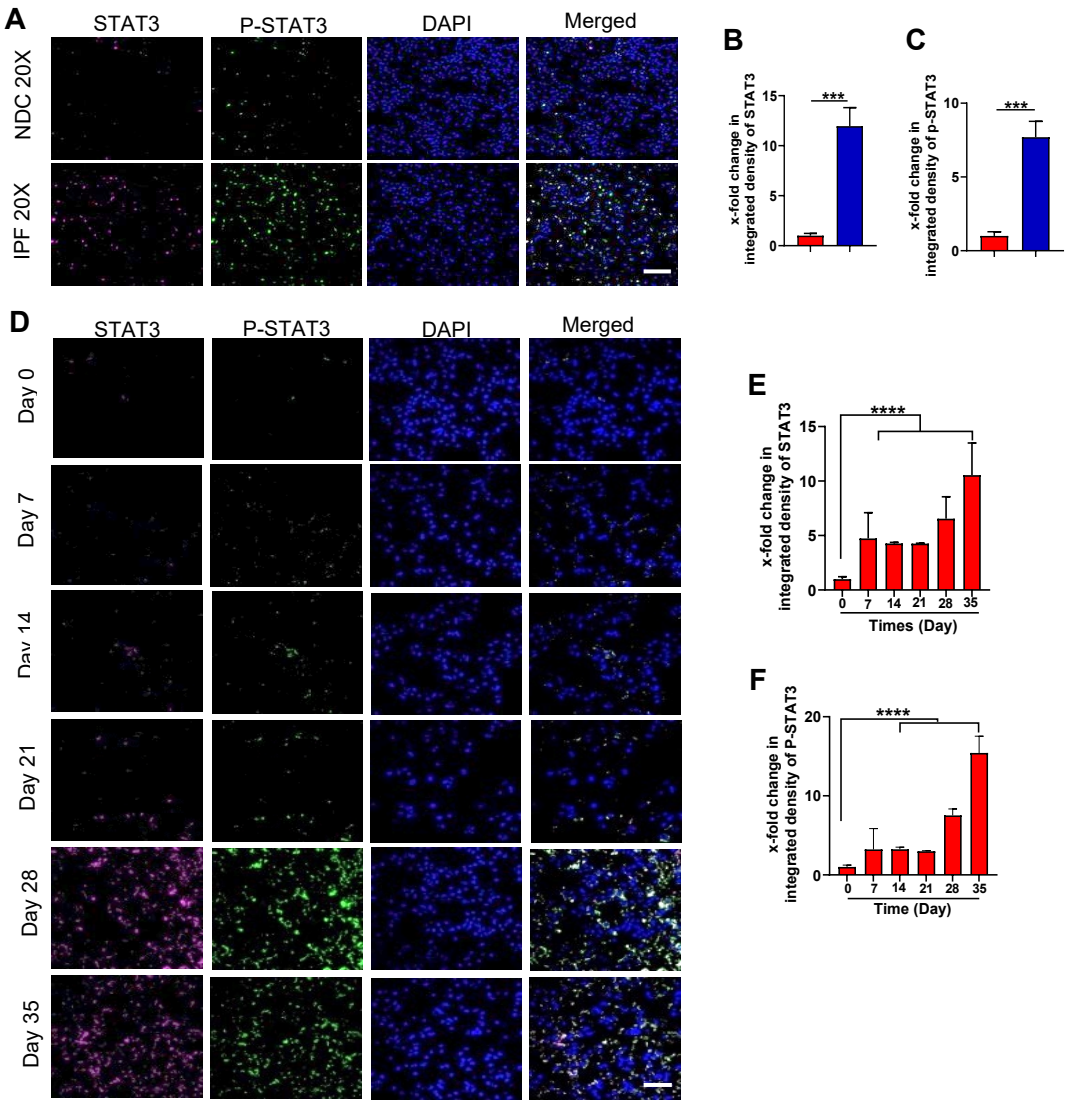

Figure 2.11 Activation of STAT3 signaling in IPF patients and BLM-induced pulmonary fibrosis mice. (A) Representative image of IF staining for P-STAT3 and total STAT3 co-stained with DAPI in IPF patient and NDC. Scale bar = 200 μm. Quantitative analysis of IF staining for STAT3 (B) and P-STAT3(C). (D) Representative image of IF staining for P-STAT3 and total STAT3 co-stained with DAPI in different stages of pulmonary fibrosis. Scale bar = 100 μm. Quantitative analysis of IF staining for STAT3 (E) and P-STAT3 (F).

3.5. Improved siRNA pulmonary delivery by EPs

We used a lung fibrosis model based on repeated intraperitoneal injection of BLM in C57BL/6 mice. This model mimics human disease with similar lung pathology, including injury and activation of epithelial cells and inflammatory cell infiltrates, the production of proliferation factors, collagen deposition, and parenchymal consolidation [283]. The model progresses through the following three stages: (1) acute injury and inflammation phase (day 1-12) that is characterized by an influx of inflammatory cells and upregulation of proinflammatory cytokines and chemokines; (2) the transition phase from inflammation to active fibrosis (day 12-24), which shows gradual subsiding of the inflammatory response with an accompanying increase in fibroproliferation, myofibroblast emergence, and increase in the expression of α-SMA, collagen I, CXCR4, STAT3, and p-STAT3 (Figure 2.12&2.13); and (3) the established chronic fibrosis stage (day 25-42), which is characterized by the expansion of the myofibroblast population and substantial deposition of ECM.

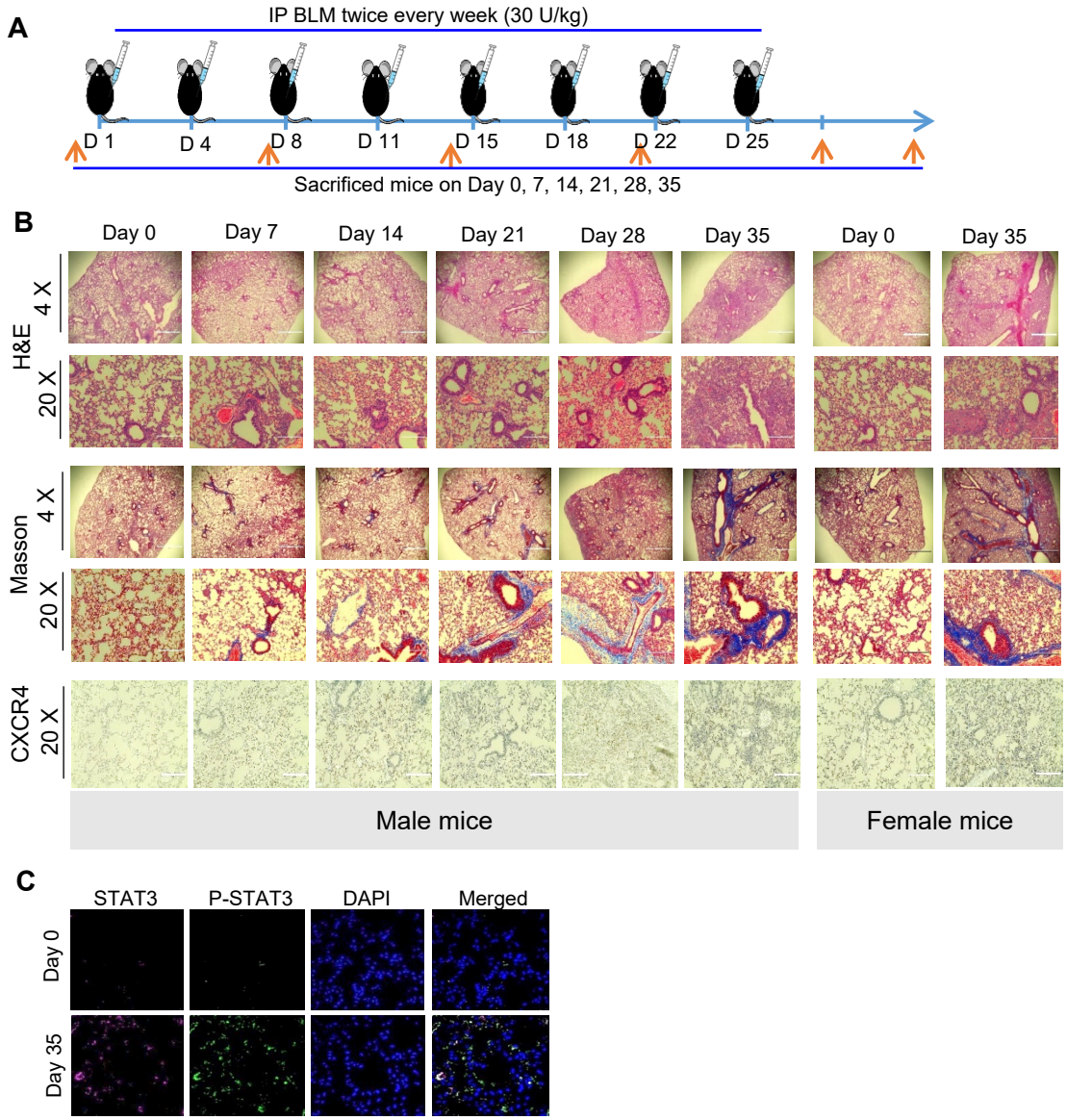

Figure 2.12 Representative image of BLM-induced pulmonary fibrosis mice. (A) Timeline. (B) Representative images of the histopathological examination of the lung sections with H&E, Masson's staining and IHC staining of the CXCR4 in BLM-induced pulmonary fibrosis mice. 4X: Scale bar = 1000 μm. 20X: scale bar = 200 μm. (C) Activation of the STAT3 signaling in BLM-induced pulmonary fibrosis mice (female).

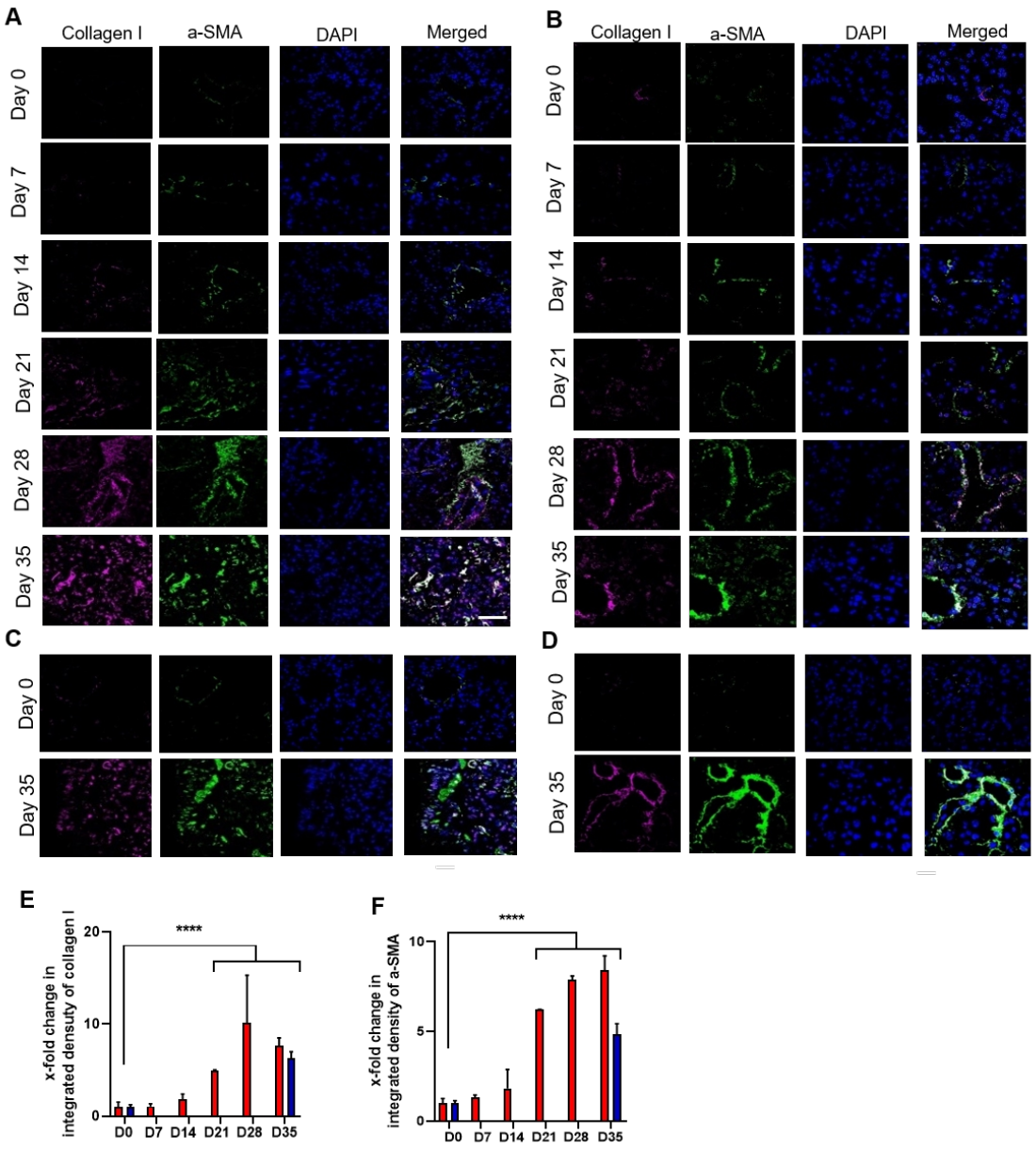

Figure 2.13 Accumulation of collagen I deposition and expression of α-SMA in BLM-induced IPF mice (male and female). Representative image of IF staining for collagen I (red) and α-SMA (green) co-stained with DAPI (staining of nuclei) (A&B: male mice. C&D: female mice. A&C: 40x, scale bar=100 μm. B&D: 63x, scale bar= 60 μm). Quantitative analysis of IF staining for α-SMA (E) and collagen I (F).

We first evaluated the biodistribution of EPs at the different stages of BLM-induced pulmonary fibrosis (Figure 2.14). Using dual labeled EPs (Cy5-PAMD@PFOB/FAM-siRNA) that were instilled intratracheally (40 µL, 15 µg siRNA per mouse), the biodistribution was determined 5 h post-administration using whole-body imaging and *ex vivo* imaging of lungs and other major organs. The results showed optimal EPs accumulation during the second stage of fibrosis when the transition from inflammation to active fibrosis occurs. The lung clearance in healthy mice was faster than in mice with established pulmonary fibrosis (Figure 2.14B,D). Importantly, EPs penetrated throughout the entire lung, even at stage 3 where extensive collagen and ECM deposition is present (Figure 2.14E). From these results, we conclude that PFOB enhances mucus penetration of polycationic vectors *in vivo*.

Lung deposition and penetration were further evaluated in detail at established fibrotic mice lungs. Cy5-PAMD@PFOB/FAM-siRNA (40 µL, w/w = 4, siRNA 15 µg per mice) or Cy5-PAMD/FAM-siRNA polyplexes were intratracheally instilled. Following this, the animals were sacrificed at 1 h, 5 h, and 24 h, and fluorescence imaging of the whole body and major organs was performed (Figure 2.15). At 5 h post treatment, the mice administered EPs had the highest lung accumulation, most likely due to better mucus stability and penetration of EPs than the simple polyplexes without PFOB emulsion. The Cy5-PAMD/FAM-siRNA polyplexes were largely trapped in the mucus layer and cleared; thus, unable to diffuse into deeper regions of the lung. The fluorescent signal was remained localized in the lung and not found in the other organs within 24 h post instillation.

To further explore the extent of penetration into the lung tissue, the intra-lung distribution of labeled EPs was evaluated via confocal microscopy. Lungs were collected, inflated with OCT, and embedded for frozen tissue sectioning (Figure 2.15D). Both Cy5-PAMD (red) and FAM-siRNA (green) fluorescence colocalized in the lungs, suggesting that the EP integrity was retained during the delivery phase. We were also able to demonstrate that EPs penetrated into lower lobes as early as 1 h post administration and spread to all lobes within 5 hours.

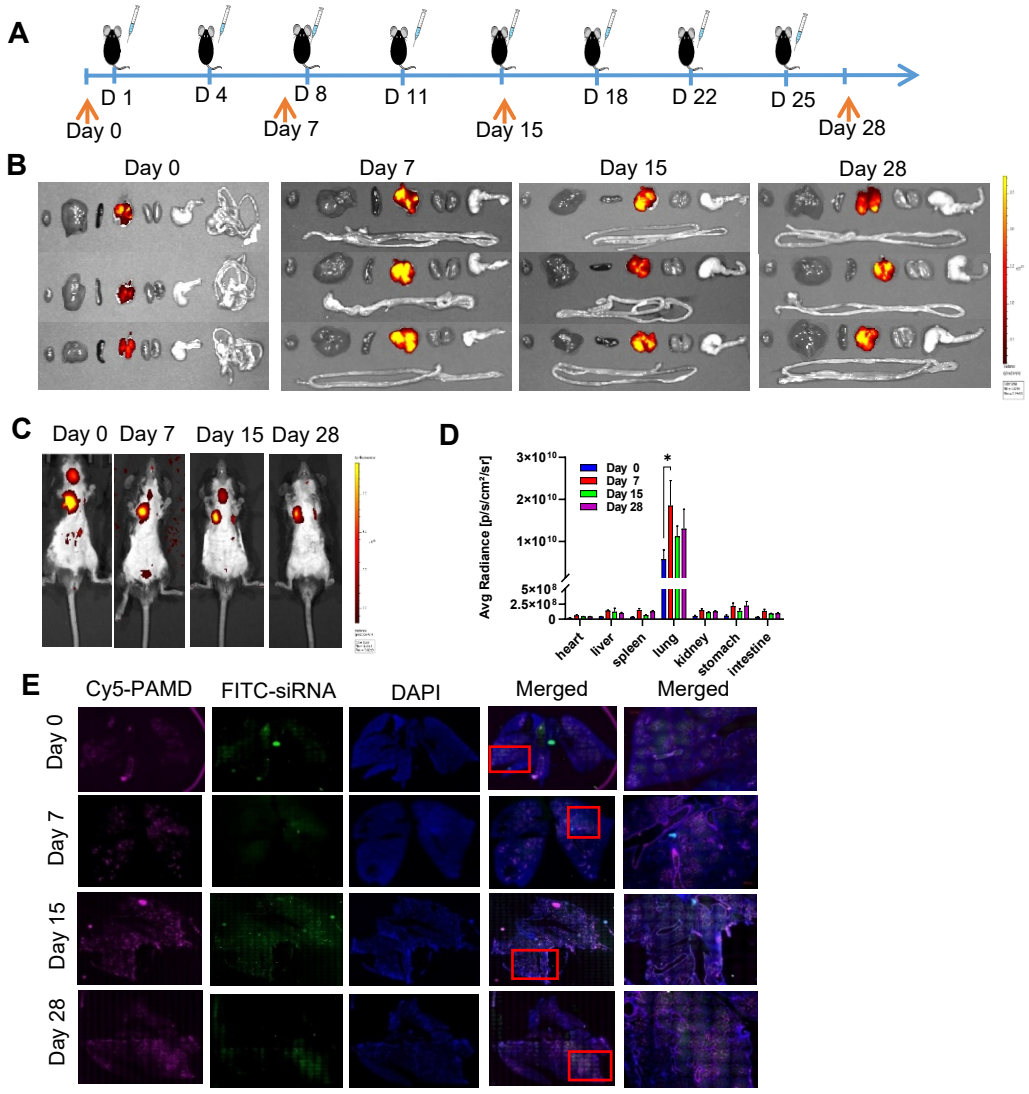

Figure 2.14 Biodistribution of the PAMD@PFOB/siRNA EPs at different stages of BLM-induced pulmonary fibrosis mice. (A) Timeline. (B) *Ex vivo* major organs. (C) Whole-body fluorescence images after intratracheal administration of EPs. (D) *Ex vivo* quantification of fluorescence distribution in major organs during different time points. (E) Intra-lung distribution.

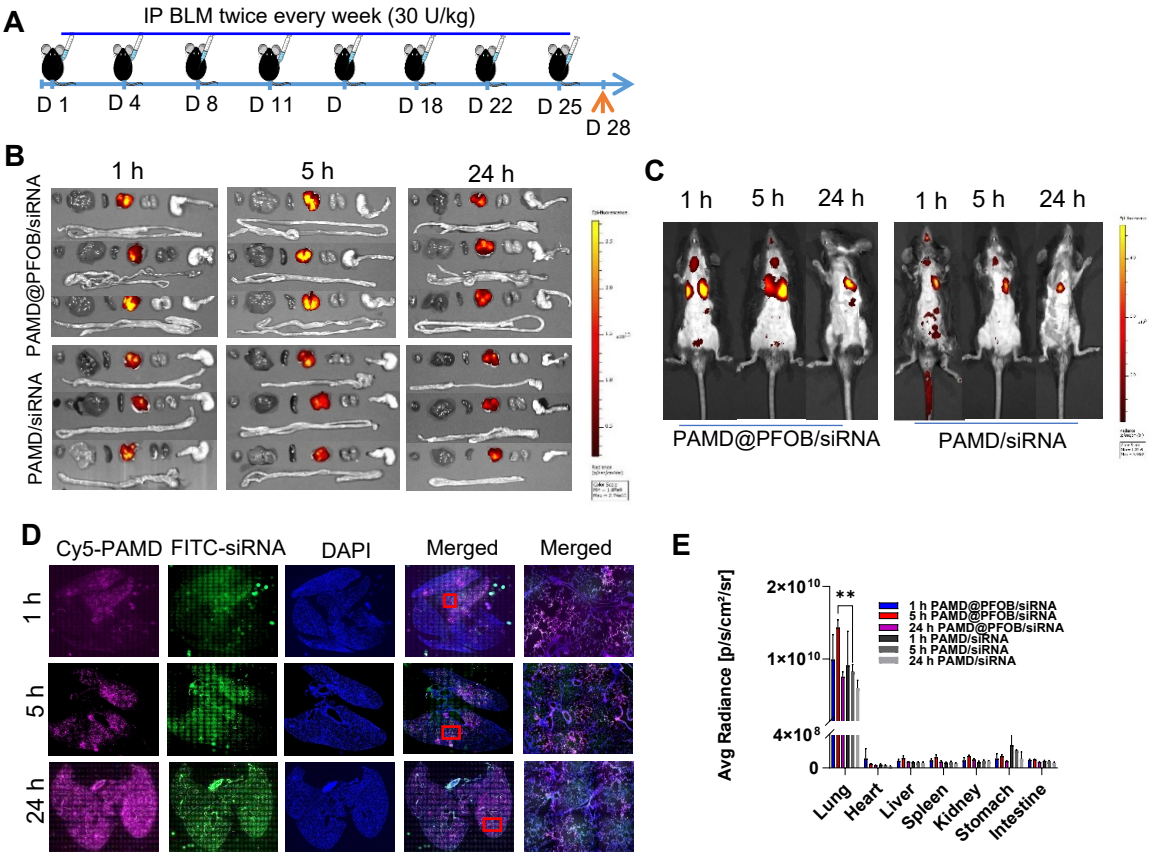

Figure 2.15 Biodistribution of EPs in BLM-induced pulmonary fibrosis. (A) Timeline. (B) *Ex vivo* fluorescence imaging of major organs at different times after intratracheal instillation of Cy5-PAMD@PFOB/FAM-siRNA EPs or Cy5-PAMD/FAM-siRNA. (C) Whole-body fluorescence imaging. (D) Intra-lung distribution of the PAMD@PFOB/siRNA EPs prepared with Cy5-labeled PAMD@PFOB (red) and FAM-siRNA (green), DAPI (blue). (E) *Ex vivo* quantification of fluorescence distribution in major organs at different time points.

3.6. Therapeutic efficacy of EPs in BLM-Induced pulmonary fibrosis mice

Next, we evaluated the anti-fibrotic efficiency of PAMD@PFOB/siSTAT3 *in vivo*. EPs (15 μg siRNA per mouse) were intratracheally instilled on day 14 and continued every 3 days for a total 5 doses (Figure 2.16A). Histopathological analysis of isolated lungs from the untreated fibrosis group showed loss of normal alveolar appearance and thickening of the alveolar wall (Figure 2.16B). Increased airway exudate (edema) was also observed. Treatment with PAMD@PFOB/siSTAT3 notably alleviated tissue damage, including interstitial edema and thickening of the alveolar wall (Figure 2.16B). Histopathological scores were assigned to the lung tissue sections in a blinded manner by a pathologist (Figure 2.16C) using the following scale: 1 = normal lung, 2 = mild inflammation, 3 = moderate inflammation, 4 = obvious inflammation, 5 = severe inflammation. As expected, the untreated (BLM+PBS) group showed severe inflammation and the treatment with PAMD@PFOB/siSTAT3 decreased the pathology score significantly.

Pulmonary collagen deposition was evaluated by Masson's trichrome staining (Figure 2.16B, blue area) and a HYP assay (Figure 2.16D). The untreated fibrosis group showed 5.7 times more collagen deposition than healthy mice. Treatment with PAMD@PFOB/siSTAT3 EPs decreased collagen content by ~50% when compared to untreated controls. This result is consistent with the inhibition of activation and migration of HPLFs and suggests that PAMD@PFOB/siSTAT3 EPs reduce activation and proliferation of fibroblasts and decrease ECM production via combined CXCR4 inhibition and STAT3 silencing. Therefore, combined inhibition of CXCR4 and STAT3 gene silencing

is protective in BLM-induced pulmonary fibrosis as shown by the reduced alveolar wall thickening, fibroblast proliferation and migration, myofibroblast differentiation, and HYP content.

Immunohistochemical staining of lung sections and RT-PCR were performed to measure CXCR4 lung expression (Figure 2.16B,E). The lungs of animals treated with the PAMD@PFOB/siSTAT3 showed the lowest levels of CXCR4 expression because of the inhibition of fibroblast differentiating into myofibroblast as well as inhibition of CXCR4+ fibrocyte recruitment from the bone marrow to fibrotic lung tissue. We contend that due to improved mucus penetration, EPs had superior ability to inhibit CXCR4 expression *in vivo* when compared to control polyplexes. Pulmonary edema is also an indicator of lung fibrosis [284] and can be estimated by the W/D ratio (Figure 2.16F). The lungs of untreated fibrotic mice had an increased W/D ratio compared to healthy mice. Strikingly, W/D ratios decreased as a result of EPs treatment in comparison to control polyplexes. Consistent with this the total number of cells in BALF, an indicator of inflammatory cell infiltration was significantly decreased following PAMD@PFOB/siSTAT3 treatment (Figure 2.16G). Severe loss of body weight was observed in the untreated fibrosis group (BLM+PBS) (Figure 2.16H), while weight loss in the PAMD@PFOB/siSTAT3 treatment group was less severe.

We next determined whether PAMD@PFOB/siSTAT3 treatment improved survival. PAMD@PFOB/siSTAT3 treatment extended mean survival to 52 days when compared to animals that received no treatment (Figure 2.16I). H&E and Masson’s staining of the lungs

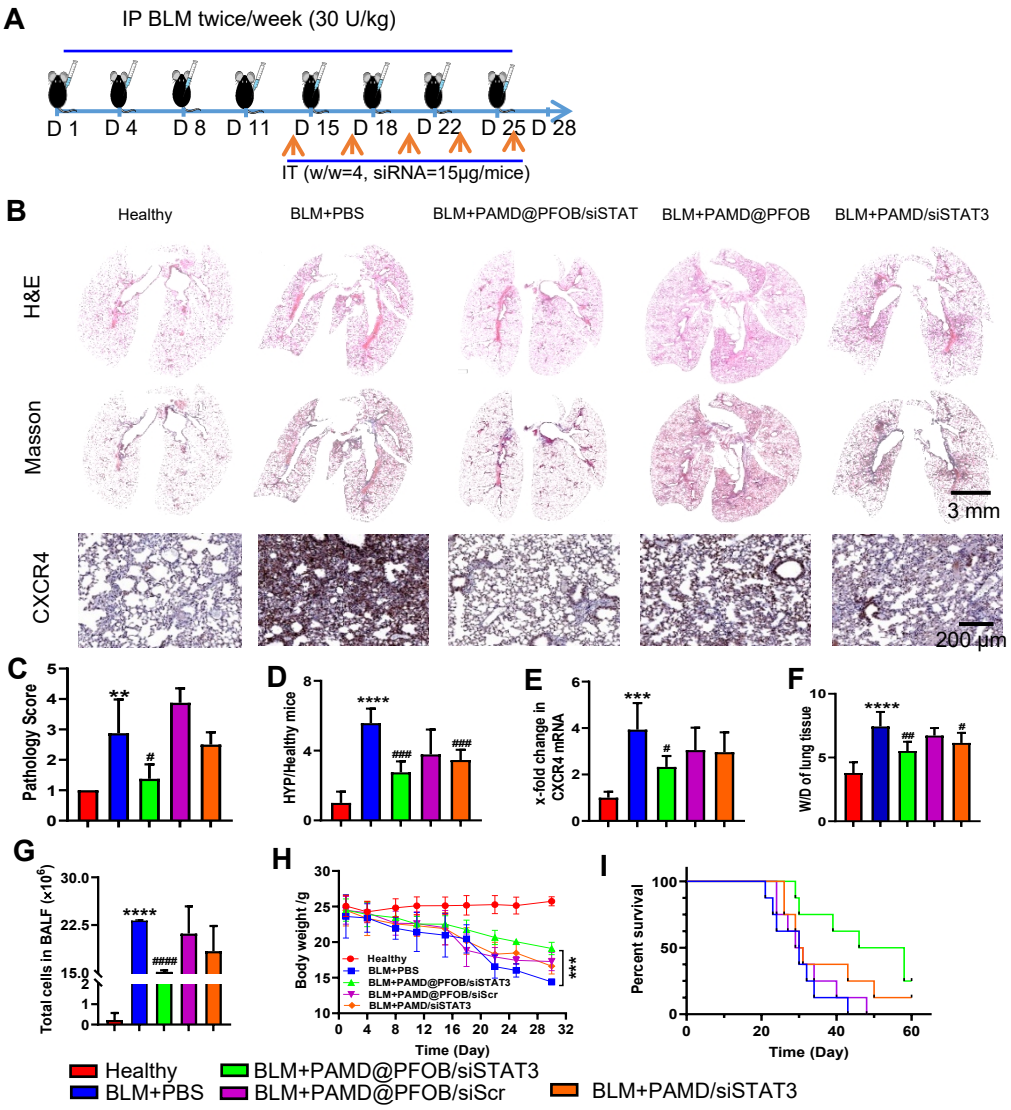

Figure 2.16 Therapeutic activity of EPs in BLM-induced pulmonary fibrosis. (A) Timeline. (B) Representative images from histopathological examination of lung sections with H&E, Masson's trichrome staining, and IHC staining of CXCR4. (C) Pathology scores. (D) Hydroxyproline levels. (E) CXCR4 mRNA level. (F) W/D ratios. (G) Total cell count in BALF. (H) Body weight. (I) Survival (n=8). * vs healthy group. # vs BLM+PBS group (untreated group).

from two mice that survived out to 60 days show that EPs treatment prolonged survival

and attenuated fibrotic progression (Figure 2.17).

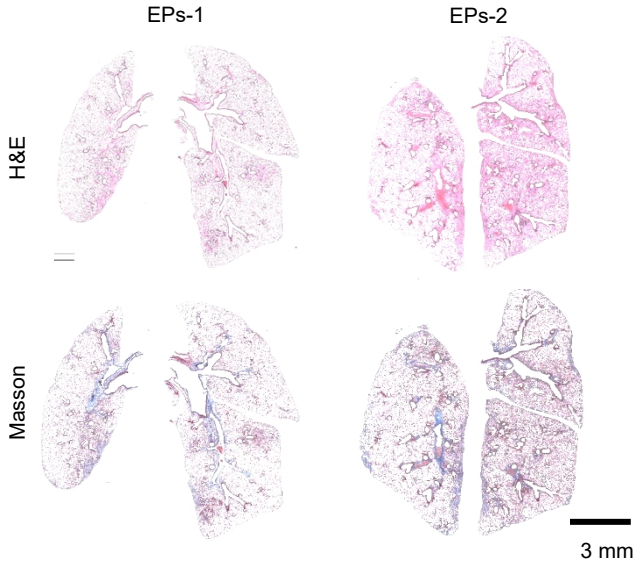

Figure 2.17. Representative images of the histopathological examination of the lung sections with H&E, Masson's staining of 2 mice who survived at day 60 at PAMD@PFOB/siSTAT3 EPs group.

The extent of p-STAT3 and total STAT3 expression was also assessed by IF staining and RT-PCR and images were further analyzed by ImageJ (Figure 2.18A-D). The untreated group had significantly increased expression of all markers whereas, PAMD@PFOB/siSTAT3 EPs treatment silenced STAT3 expression and reduced activation. The representative images of IF staining of collagen I and a-SMA, co-stained with DAPI, are shown in Figure 2.18E with quantification in Figure 2.18F (a-SMA) and Figure 2.18G (collagen I). Collectively, PAMD@PFOB/siSTAT3 treatment decreased ECM production. Moreover, Evaluation of the CTGF mRNA levels in the lung showed significantly elevated CTGF expression in the untreated mice (Figure 2.18H). Treatment with PAMD@PFOB/siSTAT3 EPs attenuated the CTGF expression.

Previously, studies proved that control of STAT3 signaling by pharmacological methods inhibited TGF-β-dependent fibroblast activation and ameliorated experimental fibrosis in murine models. Mice with conditional deletion of STAT3 in fibroblasts are protected from skin fibrosis [285]. As a result of epithelial damage in IPF, alveolar epithelial cells undergo apoptosis and epithelial-mesenchymal transition to provide mesenchymal cells for the initial repair process [286]. Residual lung fibroblasts in the interstitium start to proliferate and migrate to the site of injury, leading to excessive fibroblast proliferation, migration, and transformation to myofibroblast, as well as synthesis and deposition of ECM [244]. Moreover, CXCR4/SDF-1 and STAT3 signaling interferes with fibroblasts to myofibroblast proliferation and migration. Here, we developed PFOB EPs, combining the properties of CXCR4 attenuation and STAT3 silencing, that could potentially inhibit the

progress of pulmonary fibrosis pathology, and the synthesis and deposition of ECM were reduced by inhibiting the number of fibroblasts/myofibroblasts.

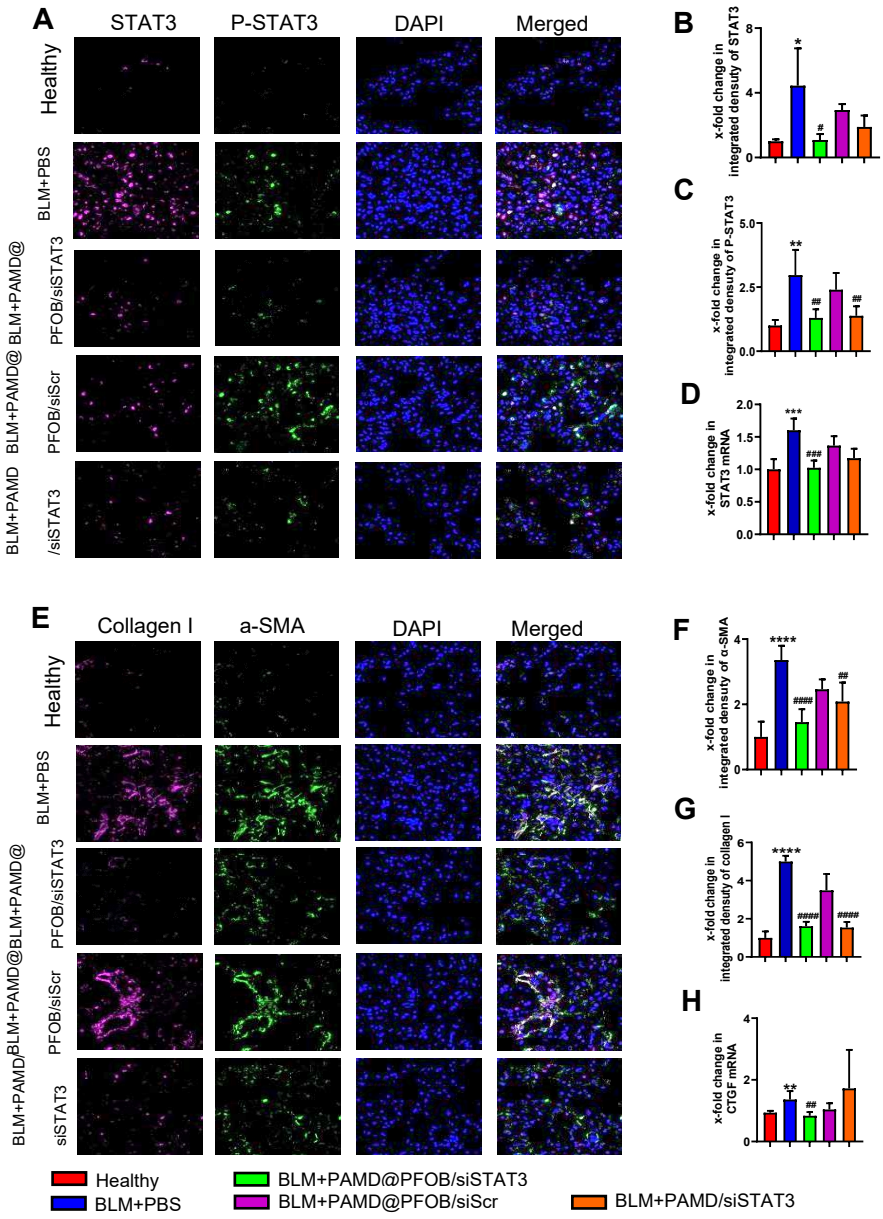

Figure 2.18 Therapeutic activity of EPs in BLM-induced pulmonary fibrosis mice. (A) IF staining for P-STAT3 and total STAT3. (B&C) Quantitative analysis for total STAT3 expression (B) and P-STAT3 expression (C). (D) STAT3 mRNA expression. (E) IF staining for collagen I and α-SMA. Quantitative analysis for α-SMA (F) and collagen I (G). (H) CTGF mRNA expression. Scale bar = 100 μm.

4. Conclusion

In summary, we report EPs capable of safe and effective siRNA delivery to the lungs, which have high mucus penetration and cellular uptake to mediate highly effective pulmonary STAT3 silencing and CXCR4 attenuation against BLM-induced pulmonary fibrosis upon intratracheal administration. PFOB EPs with SDF-1 targeting and STAT3 silencing remarkably potentiated the mucus penetration, which happened largely because of the stabilization of siRNA in the presence of mucus and decreased adsorption of mucus glycoproteins onto the surface of EPs. Therefore, the emulsion that we developed in this study can: 1) bind siRNA into EPs, 2) improve the intracellular uptake, 3) penetrate the mucus layer, and 4) improve pulmonary siRNA delivery and gene silencing efficiency. Taken together, this may lead to a promising treatment of pulmonary fibrosis via noninvasive, localized delivery.

Chapter 3. Nanoemulsion-assisted siRNA delivery to modulate the nervous tumor microenvironment in the treatment of pancreatic cancer

Please note that this part of the dissertation was published in the ACS Appl Mater Interfaces (Ling Ding et al, 2022). As the first author, I designed the experiments, collected, and analyzed the data, and wrote the manuscript. Prof. Oupicky guided me on this project. Siyuan Tang, et al, helped me with the experiments. All the co-authors agree with including their work in this dissertation.

1. Introduction

Pancreatic cancer (PC) is one of the most lethal forms of human cancer, with a dismal five-year survival rate of 8%. PC is also one of the few cancers for which patient survival rates have remained relatively unchanged since the 1960s [287]. The current best approach is to effectively diagnose and treat the cancer at an early stage. Unfortunately, PC is often diagnosed at an advanced stage with metastatic spread observed at diagnosis. Advanced stages of PC have proven difficult to treat using conventional methods like surgery and chemotherapy. The available treatment regimens typically only increase patient medium survival from 5 to 7.2 months [288]. Therefore, there is an urgent need to develop more effective treatments.

PC is characterized by a complex tumor microenvironment (TME) that plays a key role in the progression and dissemination. The TME in pancreatic tumors is nutrient-poor, desmoplastic, and highly innervated. Nervous TME has been suggested to have a crucial

impact on PC progression and metastasis [289]. Neurons can release stimulatory factors, such as nerve growth factor (NGF), to accelerate PC tumorigenesis and promote tumor innervation [290]. In the PC microenvironment, NGF binds tyrosine kinase A (TrkA) receptors, which leads to the activation of multiple downstream signaling cascades [291], including the mitogen-activated protein kinase (MAPK)-RAS pathway, then contributes to the survival, proliferation, and invasion of cancer cells [292]. Another activated pathway in the PC tumors is the phosphaphatidylinositol 3-kinase (PI3K)-Akt pathway, which supports survival of both cancer and neuronal cells in the tumors [293]. The expression of NGF in established PC cell lines and in human pancreatic tumors was reported previously [294, 295]. NGF and its receptors contribute to the survival, proliferation, invasion, and metastasis of pancreatic cancer cells.[294] Blockade of compensatory neuronal innervation by LOXO-101, a Trk-NGF inhibitor decreased the PC tumor growth and suggested that the axonal-cancer metabolic crosstalk is a critical adaptation mechanism to support PC growth [296]. Moreover, perineural invasion is considered as one of the factors responsible for the high rate of post-surgical PC recurrence and the pain associated with PC.

Small interfering RNA (siRNA) is a short double-stranded RNA that can selectively silence the target gene expression with many advantages over traditional chemotherapeutics. siRNA-based nanoformulations are a promising strategy for treating various diseases. Tumor accumulation of nanoformulations is associated with its' physicochemical properties, such as particle size, zeta potential, and surface modification

[297]. We have developed perfluorocarbon (PFC) nanoemulsions based on perfluorooctylbromide (PFOB) for combined delivery of siRNA and simultaneous inhibition of C-X-C chemokine receptor type 4 (CXCR4). Polymeric CXCR4 antagonists (PCX) developed in our lab have been used as stabilizers of the PFOB nanoemulsions and combined with siRNA to form emulsion polyplexes (EPs) as a new type of multifunctional soft materials. CXCR4 overexpression is strongly corelated with the poor clinical outcomes in PC [297, 298]. C-X-C motif chemokine 12 (CXCL12) binds to CXCR4 expressed on the cancer cells and triggers multiple biological effects, including remodeling of the TME and promotion of the proliferation, metastasis, and chemoresistance [299]. Blocking of the CXCL12/CXCR4 axis has been shown promising for treating PC [300].

Due to the immature, compressed tumor blood vessels and the dense extracellular matrix, conventional intravenous (IV) injection provides limited utility in the treatment of PC as it leads to the accumulation of low amounts of even small molecule drugs, let alone nanoparticles, in the tumors. Intraperitoneal (IP) administration emerged as more effective approach to nanoparticle delivery to PC tumors and peritoneal metastases [297, 301]. Local delivery methods like IP injection can enhance the local drug concentration and enhance the therapeutic effect [302].

The goal of current study was to investigate the potential of PFOB nanoemulsions as IP siRNA delivery vectors capable of favorable modulation of the nervous TME (Figure 1). We selected CXCR4 and NGF as the therapeutic targets because they are both actively involved in the progression and metastasis of PC. We hypothesized that combining

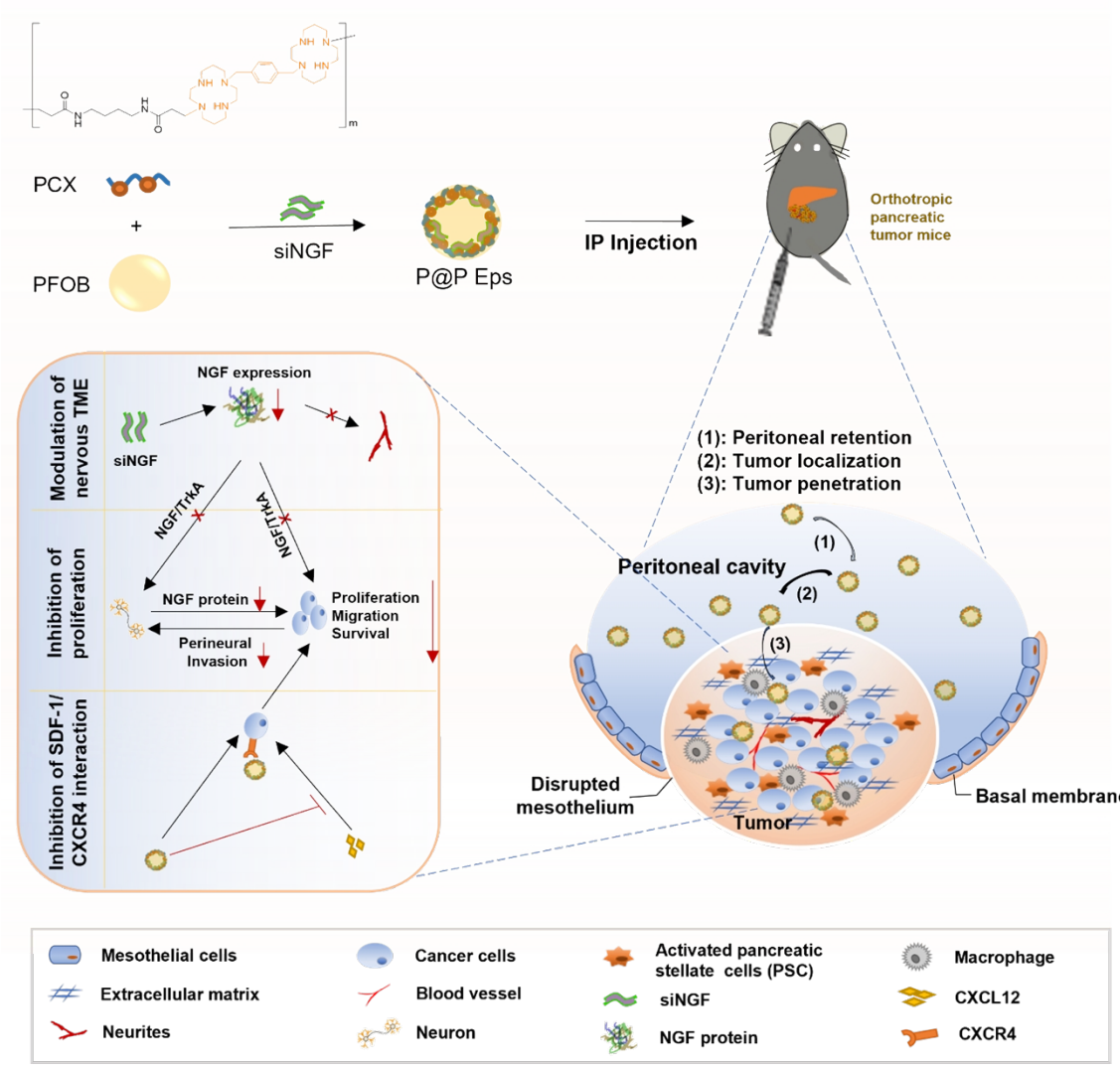

Scheme 2. Delivery mechanism of P@P EPs (PCX@PFOB/siNGF) for NGF silencing and PC therapy. The P@P EPs protects the NGF siRNA from the ascites' degradation after the IP injection and enhance the siRNA accumulation to the primary tumors and metastasis sites. Moreover, the P@P EPs also has the tumor penetration ability, which will allow the efficient NGF silencing in the tumors. The downregulation of NGF expression inhibits the PC progression and PNI in pancreatic TME.

knockdown NGF expression with CXCR4 inhibition would enhance the PC therapy via

high of the tumor penetration and modulation the tumor microenvironments (Figure 1). To test our hypothesis, the nanoemulsions stabilized with PCX was prepared and complexed them with siRNA to prepare EPs. We investigated the efficacy of local IP tumor delivery compared with IV administration and the effect on the therapeutic outcomes in orthotopic PC model.

2. Materials and Methods

2.1. Materials

All chemicals were commercially available and used without further purification. Dulbecco's modified Eagle medium (DMEM), phosphate buffered saline (PBS), fetal bovine serum (FBS), trypsin, penicillin and streptomycin were purchased from Thermo Scientific (Waltham, MA). 1-bromoheptadecafluorooctane (PFOB) were purchased from Sigma-Aldrich. NGF siRNA (siNGF target human, sense sequence 5'-CCACAGACAUCAAGGGCAA[91]-3'. siNGF target mice, sense sequence: 5'-CAGUGUGUGGGUUGGAGAU-3'), negative control siRNA (siNC, sense sequence, 5'-UCACAACCUCCUAGAAAGAGUAGA-3'), and Cy5.5 labeled siRNA (Cy5.5-siRNA) were obtained from Sigma-Aldrich. Average Mw of siRNA is 13300 g/mol. AMD3100 was brought by Biochempartner (Shanghai, China). Real-time (RT)-PCR primers were obtained from Sigma-Aldrich. Unless otherwise stated, all other reagents were provided by Fisher Scientific and used without further purification.

2.2. Methods

2.2.1. Preparation of PCX@PFOB emulsion polyplexes (P@P EPs)

PCX and Cy3-PCX were synthesized as described previously [271]. PCX@PFOB emulsion (P@P emulsion) were prepared as follows. Twenty μL of PFOB was added to 2 mL PCX (2 mg/mL, in water) and ultrasonicated with a probe-type ultrasonic processor with a 2 mm diameter (Hielscher, UP200ST) with energy limited to 8000 W under 80% output amplitude setting. P@P EPs was prepared via mixing positively charged P@P emulsion with siRNA solution in HEPES (pH 7.4) buffer and incubated at room temperature for 30 min to complete the binding of siRNA onto the P@P emulsion via electrostatic interaction. siRNA binding to the P@P emulsion was confirmed by agarose gel electrophoresis. P@P EPs morphology was evaluated using TEM (Tecnai G2 Spirit, FEI Company, USA) with NanoVan negative staining (Nanoprobes, USA).

P@P E formulated with siNGF are abbreviated as P@P EPs (siNGF), PCX/siNGF polyplexes are abbreviated as PLX. P@P E formulated with siNC are abbreviated as P@P EPs (siNC) and served as control.

2.2.2. Cell culture

Mouse PC tumor cell line KPC8060 was kindly provided by Dr. Hollingsworth at UNMC. The human PC cell lines COLO357 and PANC-1 was kindly provided by Dr. Batra at UNMC. All three cell lines were cultured at 37 °C with 5% CO_2 in high-glucose DMEM with 10% FBS and penicillin-streptomycin (100 U/mL, 100 μg/mL) in a humidified chamber.

2.2.3. Cell viability assay

Cell viability of P@P EPs was evaluated via CellTiter-Blue (CTB) viability assay. Briefly, cells were seeded onto 96-well plates, after 18-24 h, cells were treated with 100 μL of

P@P EPs (w/w = 4, siRNA = 100 nM) in serum-free medium for 4 h. Then, replace with culture medium and culture for another 48 h. After that, the cell viability was evaluated by CTB according to the manufacture recommendations. The relative cell viability (%) was expressed as $[F]_{treated}/[F]_{untreated} \times 100\%$. The PBS treated cells were used as 100 % control.

2.2.4. CXCR4 cell surface expression

Cells were cultured under normoxia or hypoxia (0.2% oxygen) for 24 h before incubation with APC labeled CXCR4 antibody (BD, Bioscience, CA) at 4 °C for 1 h. The background fluorescence was assessed by isotype-matched antibody. After washing and centrifugation, cells were analyzed by a flow cytometry and acquired data were analyzed by FlowJo.

2.2.5. Transwell migration

COLO357 and KPC8060 cells were detached, washed with PBS. The cells were suspended in 300 μL of serum-free medium, treated with PBS, PCX, P@P E, AMD3100, and PEI for 15 min before their addition to the cell culture inserts (8.0 μm pores). 600 μL of serum-free medium containing 20 nM CXCL12 was added into the lower transwell chamber. After 20 h of incubation, cotton swabs were used to remove the non-migrated cells in the top chamber. PANC-1 cells were incubated for 24 h in hypoxia before being subjected to the same transwell migration protocol as COLO357 and KPC8060 cells above, with the exception of using 40 nM CXCL12 and incubating in hypoxia for 48 h. The migrated cells at the bottom were fixed and stained with 0.2% Crystal Violet. Migrated cells were observed under EVOS xl microscope. PEI was used as the negative control.

2.2.6. Cellular uptake and intracellular trafficking

KPC8060, COLO357, and PANC-1 cells were seeded in 12-well plates. After 18-24 h of incubation, cells were treated by P@P EPs labeled with FAM-siRNA (w/w = 4, 100 nM FAM-siRNA). 4 h later, cells were washed with PBS, detached with trypsin, and analyzed by flow cytometry. Confocal microscopy was used to observe the subcellular distribution of P@P EPs. Cells were seeded on 8-well chamber, incubated in incubator overnight. The cells were treated by P@P EPs prepared with Cy3-PCX and Cy5.5-siRNA. After 4 h incubation, nucleus was stained by Hoechst 33258, and visualized under confocal microscopy (LSM 800, Zeiss, Germany). To investigate the lysosomal escape, cells were treated by P@P EPs prepared with Cy3-PCX and Cy5.5-siRNA for 4 h. Then cells were washed with PBS, stained with LysoView (green), and visualized with confocal microscopy. To investigate the endocytic uptake mechanism, KPC8060 cells were pretreated with three inhibitors to inhibit different endocytosis pathways, including Chlopromazine {Cpz, 10 Mm, inhibit clathrin mediated endocytosis (CME) pathway}, Cytochalasin D {CyD, 4 μM, inhibit macropinoctytosis (MP) pathway}, and Nystatin {Nys, 50 μM, inhibit caveolae/lipid raft dependent endocytosis (C/LR) pathway}. P@P EPs prepared with FAM-siRNA were used to treat the cells and after 4 h incubation, cells were washed with PBS, detached with trypsin, and analyzed by flow cytometry and results analyzed by FlowJo software.

2.2.7. Nanoemulsion penetration in multicellular tumor spheroids

3D tumor spheroids prepared from KPC8060 cells were used to evaluate the

penetration ability of P@P EPs *in vitro*. KPC8060 tumor spheroids were prepared by seeding in 2% agarose attachment 48-well plates (Corning, US) at a density of $1x10^4$ cells per well and cultured 7 days to allow the spheroids diameter about 300 μm. Then, KPC8060 spheroids were treated by P@P EPs or PLX prepared with Cy3-PCX and FAM-siRNA for 12 h. After that, the spheroids were washed with PBS and observed under confocal microscope (z-stack with 10 μm intervals). To investigate the penetration mechanism of P@P EPs, the spheroids were pretreated by 2-[(4-Fluorobenzoyl)amino]-benzoic acid methyl ester (EXO-1) for 1 h, and then incubated with P@P EPs for another 12 h. ImageJ software were used to transform the fluorescence images to surface plots. Flow cytometry was also used to analyze the penetration ability of P@P EPs by trypsinzing the spheroids into single cell suspension.

2.2.8. Colony formation

Cells were washed with PBS, detached, and seeded in 12 well plates (KPC8060 200/well, COLO357 600/well, PANC-1 600/well). 24 h later, cells were treated by PLX, P@P EPs (siNC), and P@P EPs (siNGF) for another 7-10 days. Cells were fixed and stained with 0.2% Crystal Violet, then washed with PBS three times and photographed.

2.2.9. Apoptosis assay

Cells were seeded in 6 well plates (flow cytometry assay) or 96 well plates (nuclear staining assay). 24 h later, cells were treated by PLX, P@P EPs (siNC), or P@P EPs for another 48 h. Cells were trypsinized and stained by fluorescently labeled Annexin V FITC and propidium iodide (PI) and analysis by FACS. For the nuclear staining assay, cells

were stained with Hoechst 33258 (2 μg/mL) and photographed under EVOS xl fluorescence microscopy.

2.2.10. Orthotopic PC model

Animals. C57BL/6 mice (7 weeks old, male) and athymic nude mice (8 weeks old, male) were obtained from Charles River Laboratories. All animal studies were approved by the University of Nebraska Medical Center Institutional Animal Care and Use Committee.

We established orthotopic tumors in athymic nude mice using PANC-1 cells and in C57BL/6 mice using KPC8060 cells. Mice were anaesthetized before the surgery. Iodine and alcohol pad were used to get the sterilization of the surgical site. Then, incision at the left center abdomen region was made, and the pancreas was exposed. 40 μL Matrigel/PBS (1:1) contained one million of PANC-1 cells or 2.5 x 10^4 of KPC8060 cells were injected into the tail of the pancreas. The incision was closed with soft staples. 10 days after surgery, the soft staples were removed.

2.2.11. Blood circulation time

Mice with the KPC8060 orthotopic tumors were given 200 μL of P@P EPs prepared by Cy3-PCX and Cy5.5-siRNA (w/w = 4, 2.5 mg/kg Cy5.5-siRNA) by IV or IP injection 28 days after tumor implantation. 2 min, 10 min, 1 h, 4 h, and 24 h post-injection, ~80 μL of blood was collected into heparin-pretreated tubes. 50 μL of blood from each sample was transferred into plastic tubes and imaged by Xenogen IVIS 200 (Cy3: Ex = 535 nm, Em =

580 nm, Cy5.5: Ex = 675 nm, Em = 720 nm). The fluorescence intensity was analyzed by the supplied IVIS software.

2.2.12. Biodistribution of P@P EPs

To study the tumor-targeting ability of P@P EPs, orthotopic KPC8060-derived (28 days after cells implantation) and PANC-1-derived (35 days after cells implantation) PC models were injected with 200 μL of P@P EPs prepared with Cy3-PCX and Cy5.5-siRNA (w/w = 4, 2.5 mg/kg Cy5.5-siRNA) by IV or IP. Control animals were given IP injection of PLX prepared with Cy3-PCX and Cy5.5-siRNA. After 24 h, mice were sacrificed and imaged with Xenogen IVIS 200. Tumors and major organs were harvested for *ex vivo* fluorescence imaging. To investigate the tumor penetration mechanism of the P@P EPs, mice were pre-injected with EXO-1 (120 μg/mouse) via IP. 1 h later, mice were IP injected by P@P EPs. After 24 h, tumors were harvested and processed as above. Tumors were embedded into O.C.T compound, cut into frozen sections (10 μm), and observed by confocal microscopy.

2.2.13. Antitumor effect *in vivo*

Twelve days after KPC8060 cell implantation, mice were randomly divided into 4 different groups (n = 5) and IP injected with PBS, PLX (PCX/siNGF), P@P EPs (siNC), and P@P EPs (siNGF) (w/w = 4, 2.5 mg/kg siNGF). The animals were treated on day 12, 14, 16, 18, 20, 22, 24, and 26. Body weight was monitored during the experiment periods. Tumor growth was measured by Vevo 3100 ultrasound imaging system (Fujifilm, VisualSonics, Toronto, ON) in B-mode with an MX550D transducer. Tumor shape and

volume was analyzed by Vevo Lab software. On day 28, all the mice were sacrificed, and blood was harvested for analysis. Primary tumors were weighted and metastasis in each organ was evaluated.

2.2.14. Histological analysis

Tumor tissues were cryo-sectioned and permeabilized with endogenous peroxidase inhibitor. Tumor slides were incubated with primary antibody at 37 °C for 32 min, including NGF antibody (Abcam, Ab52918, 1:100), and neurofilament antibody (Abcam, Ab223343, 1:100). After that, the samples were incubated with secondary antibody labeled with FITC. Tumor slides were also counterstained with DAPI for 10 min at room temperature to assess the nuclei. The IF staining slides were mounted with antifade reagent and observed with confocal microscopy (LSM 800). Immunohistochemical staining of PGP 9.5 was performed to evaluate PGP 9.5 tumor expression after treated with P@P EPs.

2.2.15. *In vivo* toxicity

Histology analysis was used to assess the *in vivo* toxicity. Major organs, including heart, liver, spleen, lungs, and kidney, were sectioned, and stained with H&E staining, then, the slides were observed by EVOS xl microscope.

2.2.16. Statistical analysis.

All results were presented as mean ± SD. One-way ANOVA test with Tukey's multiple comparisons test was used to analyze the differences among multiple groups. Student's t-test was used to analyze the statistical significance between two groups, and P-value

<0.05 was considered statistically significant. All statistical analysis was performed with GraphPad Prism v8.

3. Results and Discussion

The nervous TME plays an important role during PC progression and metastasis but remains under-investigated as a target for therapeutic approaches. Here, we set to explore the possibility of targeting the nervous TME with siRNA therapeutic using novel dually functioning PFOB nanoemulsions. We have synthesized PCX and formulated P@P emulsion that maintained the CXCR4 inhibition ability while being able to condense siRNA.

3.1. Inhibition of cell migration

We have synthesized PCX and formulated PCX@PFOB (P@P) nanoemulsion that maintain the CXCR4 inhibition ability while being able to condense siRNA. CXCR4 antagonism of P@P emulsion was evaluated by CXCR4 receptor redistribution assay. Compared with the PCX, the EC50 of the P@P emulsion decreased from 42.7 ng/mL to 28.1 ng/mL.

Considering the improved CXCR4 antagonism of the nanoemulsion, we evaluated its ability to inhibit migration of murine (KPC8060) and human (COLO357) pancreatic cancer cells that both express high levels of CXCR4 receptor [297]. Non-cytotoxic concentrations of P@P emulsion and PCX were used to evaluate the anti-migration activity (Figure 3.1A). Incubation of the cells with CXCL12 induced their migration, which could be inhibited by the treatment with P@P emulsions and PCX. There was no difference in anti-migration activity of P@P and commercial CXCR4 antagonist AMD3100 at the used concentrations. All the used cell lines, negative control PEI failed to inhibit migration.

We also evaluated the CXCR4 surface expression in another human PC cell line PANC-1 cells (Figure 3.1B), but it showed negligible CXCR4 expression in normoxia condition. However, the expression of CXCR4 in PANC-1 cells greatly increased when incubating the cells under hypoxia condition (0.2 % oxygen) and we found that 28.9% of the cells strongly express the receptor (Figure 3.1B). The hypoxia effect on CXCR4 overexpression and the fact that the microenvironment of the solid pancreatic tumors is highly hypoxic is well established [303]. When we evaluated the ability of the P@P emulsion to inhibit migration of PANC-1 cells under hypoxia, we observed comparable results to KPC8060 and COLO357 cells (Figure 3.1A).

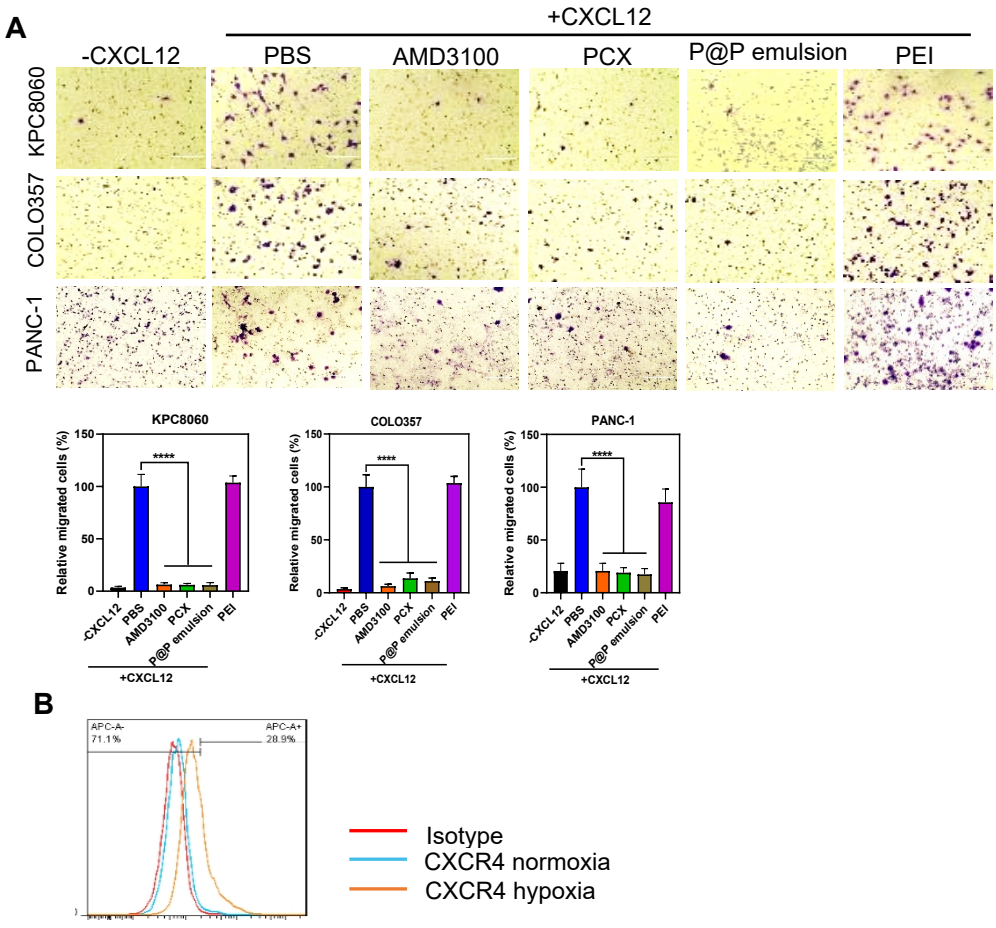

Figure 3.1 (A) Inhibition of CXCL12-induced PC cells migration. KPC8060, COLO357 and PANC-1 cells were treated with AMD3100 (300 nm), PCX (2 μg/mL), P@P (PCX 2 μg/mL), PEI (2 μg/mL) and cultured in a transwell membrane insert with CXCL12. Migrated cells were observed. (B) CXCR4 surface expression in PANC-1 cell surface.

3.2. Cell uptake and penetration in multicellular spheroids

We used fluorescently labeled P@P/siRNA EPs (P@P EPs, w/w = 4, particle size ~190 nm and zeta potential ~19 mV) to investigate the uptake, intracellular distribution in KPC8060, COLO357 and PANC-1 cells. As shown in Figure 3.2A, compared with the

control PEI/siRNA (M_W=10k, w/w=2, particle size ~ 145 nm and zeta potential ~ 24 mV) and PCX/siRNA polyplexes (PLX, w/w = 4, particle size ~ 160 nm and zeta potential ~ 25 mV) without the PFOB emulsion, the uptake of P@P EPs as determined from the mean fluorescence intensity (MFI) increased 3-fold and 4.8-fold, respectively. The enhanced siRNA cellular uptake by P@P EPs was also confirmed in the PANC-1 and COLO357 cell line (Figure 3.2A). the flow cytometry results were corroborated by confocal microscopy (Figure 3.2B). Both siRNA (yellow) and PCX (red) were observed in the cytoplasm of the cells, which confirmed effective cellular uptake mediated by the P@P EPs. Endosomal escape of the P@P EPs in KPC8060 was evaluated by using LysoView (green) to stain lysosomes. After 4 h incubation, as shown in Figure 3.2C, PCX (red) and siRNA (yellow) were found mostly in the cytoplasm with only a limited extent of colocalization with the lysosomes.

In the past decades, various studies have been conducted on the mechanism of cellular uptake of siRNA therapeutics, however there is no understanding of the internalization mechanism of systems based on PFC nanoemulsions. Understating of the siRNA delivery mechanism may help in designing more effective therapeutic strategies. In this study, the endocytic pathways involved in the uptake of P@P EPs were analyzed by flow cytometry using a panel of inhibitors that included Cpz, CyD, and Nys [304]. As shown in Figure 3.2D, the uptake of the P@P EPs was decreased by all three inhibitors with the strongest effect demonstrated by Nys, where 65% reduction on the uptake was

observed. This suggested that the endocytosis mechanism of P@P EPs was mostly depended on the caveolae pathway.

The intracellular distribution results of P@P EPs in cell monolayers showed that the cellular uptake of siRNA was improved significantly when compared with PLX. In addition to cell uptake, poor penetration of siRNA delivery systems into solid tumors is a significant impediment to their anticancer efficacy. Thus, we moved into the 3D *in vitro* tumor models to further determine the penetration ability of the P@P EPs. Penetration of fluorescently labeled P@P EPs into 3D tumor spheroids was evaluated with confocal microscopy and flow cytometry. As shown in Figure 3.3B, the P@P EPs exhibited effective tumor-penetrating ability as suggested by the observed internalization in ~66.3% of the cells in the tumor spheroids. In contrast, only ~15.9% of the cells internalized by PLX. Exocytosis inhibitor EXO-1 was used to evaluate the penetration mechanism of P@P EPs in the spheroids. EXO-1 is a reversible inhibitor of exocytosis that induces a rapid collapse of the Golgi to the endoplasmic reticulum thus inhibiting the traffic emanating from the endoplasmic reticulum [305]. Only ~16.4% of the positive cells in the tumor spheroids taken up the EPs when we pretreated them with EXO-1. This result suggested that the mechanism of the penetration of the P@P EPs was cell-based and dependent on the exocytosis via the Golgi to endoplasmic reticulum, not on a passive interstitial diffusion. These results were also confirmed by the confocal microscopy (Figure 3.3A).

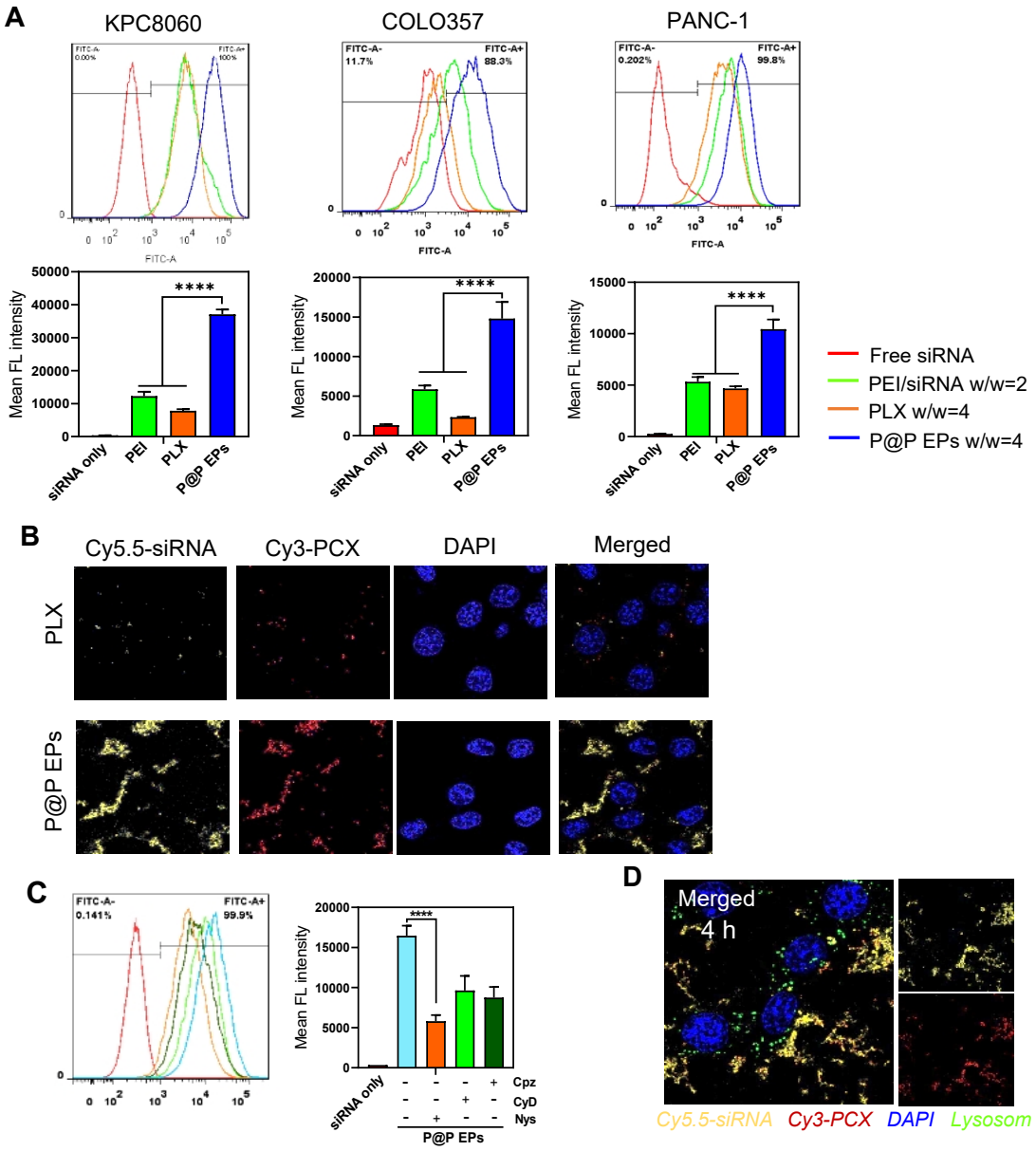

Figure 3.2 (A) The cellular uptake of P@P EPs in KPC8060, COLO357, and PANC-1 cells by flow cytometry for 4 h. (B) Confocal microscopy observation of KPC8060 cells after treated with P@P EPs for 4 h, PLX and PEI were used as control group. (C) Flow cytometry to evaluate the endocytosis mechanism of P@P EPs. (D) Confocal microscopy observation of intracellular tracking of P@P EPs in KPC800 cells after coincubation 4 h. Lysosome was stained via LysoView (green).

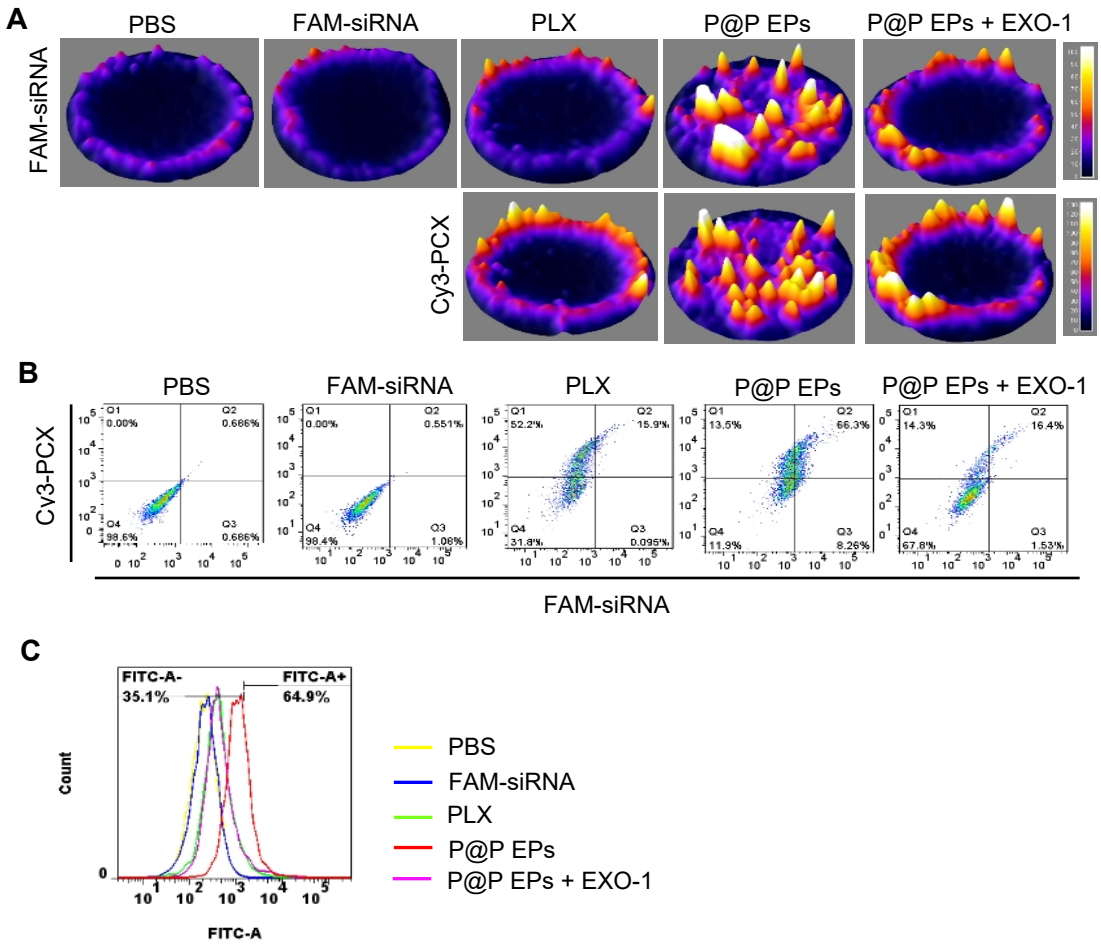

Figure 3.3 Penetration ability of P@P EPs into 3D tumor spheroids prepared from KPC8060 cells. The penetration was evaluated by measure the FAM-siRNA and Cy3-PCX using confocal microscopy and flow cytometry of single cells suspension prepared from the spheroids. (A) Surface plot of KPC8060 multicellular spheroids after treated with different of treatment group for 12 h. EXO-1: inhibitor of the exocytic pathway. (B&C) Flow cytometry analysis of KPC8060 cells digested from multicellular spheroids.

3.3. Anticancer effect of NGF silencing and CXCR4 inhibition *in vitro*

The anticancer efficacy of the P@P EPs combining the CXCR4 inhibition with silencing the NGF gene expression was evaluated in the three PC cell lines (KPC8060, PANC-1, and COLO357, Figure 3.4A). The cells were treated with P@P EPs, and the expression of the NGF mRNA was measured by RT-PCR. Treatment with P@P EPs significantly downregulated the NGF expression in KPC8060 cells (~60% reduction), PANC-1 cells (~45% reduction) and COLO357 cells (~80% reduction). Then, we evaluated the anti-cancer activity of the P@P EPs. The P@P EPs prepared with negative control siRNA (siNC) and PLX (PCX/siNGF) were used as controls. The anti-cancer activity was evaluated from the inhibition of the colony formation (Figure 3.4B,C) and the cell viability data (Figure 3.4D). In all three cell lines, the treatment with P@P EPs (siNGF) showed the highest cell killing activity. We observed 36.9% cell killing in KPC8060, 44.7% in COLO357, and 36.4% in PANC-1 cells. Moreover, the P@P EPs (siNGF) treatment strongly inhibited colony formation and growth, with the control groups showing only a modest inhibitory effect. The cell viability assay evaluates metabolic activity within 2 days, while the colony formation assay measures tumorigenicity as the capability of a single cells to form a colony (clonogenicity) lasting ~10 days. NGF is overexpressed in PC tumor and contribute to the cancer cells survival, proliferation, invasion, and metastasis. As shown in Figure 3.4B,C, silencing of NGF expression in the PC cells decreased their clonogenic potential.

The anticancer results were further validated in PANC-1 cells by measuring apoptosis (Figure 3.4E,F). More than 60% of the PANC-1 cells were apoptotic after treatment with the P@P EPs (siNGF). In contrast, P@P EPs (siNC) and PLX groups only showed negligible induction of apoptosis. We also stained the cells with DAPI and evaluated the nuclear morphology to count the number of apoptotic cells (Figure 3.4G,H).

NGF/TrkA/p75NTR signaling pathway contributes to the PC cell survival [306, 307]. On the downstream of NGF/TrkA signaling, the NGF-TrkA pathway also triggers the activation of RAS-MAPK pathway that promotes cancer cell survival and proliferation [306]. Moreover, the binding of SDF-1/CXCR4 can trigger downstream of ligand binding, which result in many responses, including chemotaxis, cell survival and proliferation. One of the important functions of chemokine is lymphocyte trafficking. CXCR4 mediated chemotaxis is mediated by PI3 kinase, which can lead to the activation of the serine-threonine kinase AKT, which have been evaluated to play a key role in tumor cell survival and possible proliferation [190]. CXCR4 antagonist can also induces apoptosis by decreasing the expression levels of the anti-apoptotic protein Bcl-2 and ERK [308]. As shown by our data, the NGF gene silencing significantly decreased the cancer cell proliferation and enhanced apoptosis. Overall, P@P EPs that delivered siNGF downregulated the expression of NGF in both human and murine PC cells, resulting in significant inhibition of the colony formation and inducing more of the cancer cell apoptosis *in vitro*. These results confirmed that combined NGF gene silencing and CXCR4 inhibition by P@P EPs has promising

anticancer activity even in PC cells alone without the expected effects on the tumor microenvironment.

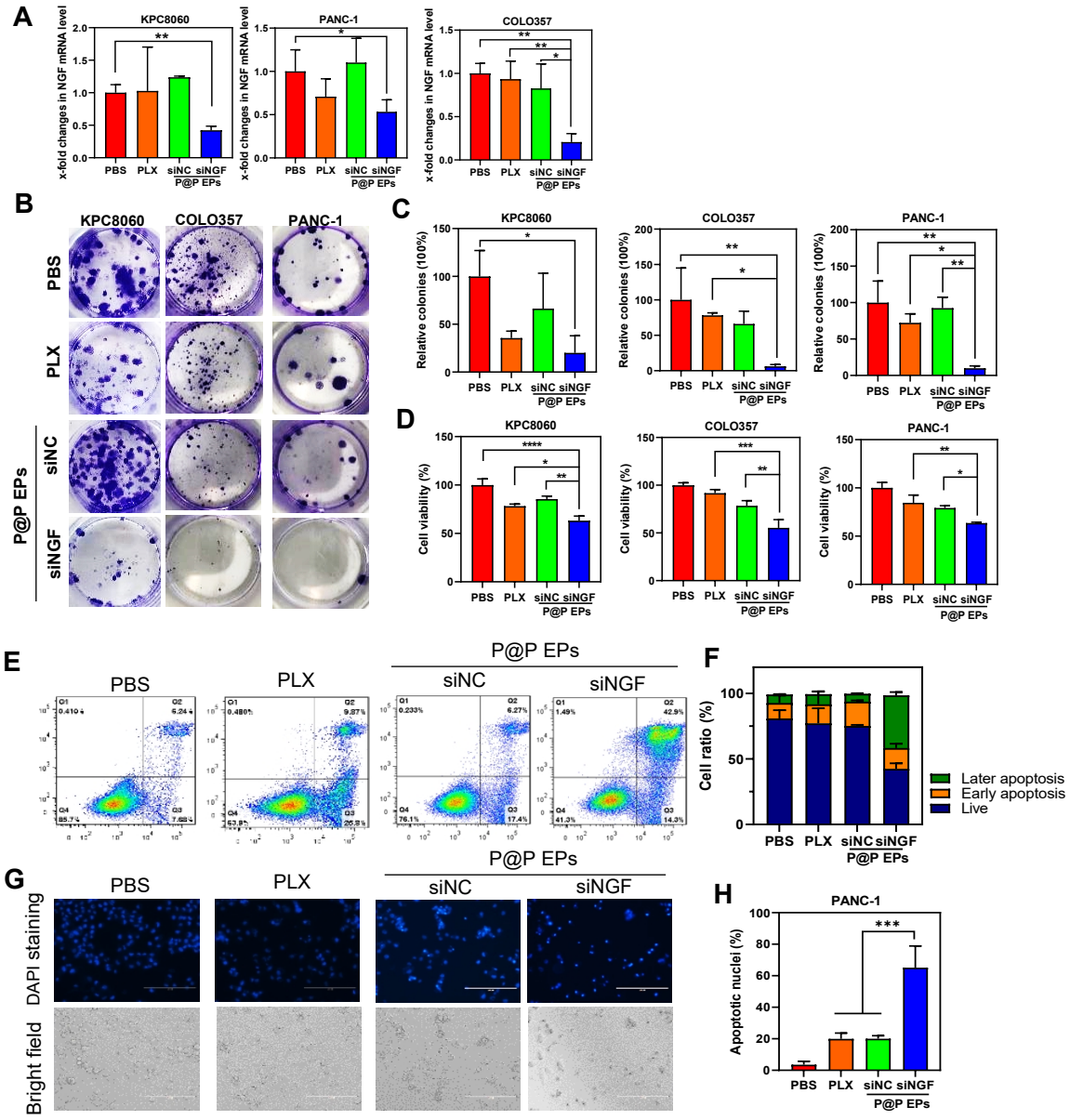

Figure 3.4 P@P EPs inhibited the pancreatic cancer cells *in vitro*. (A) Transfection study. (B&C) Colony formation assay. (D) Cell viability assay. (E&F) Apoptosis study in PANC-1 cells assayed by flow cytometry for 48 h using Annexin V-FITC/PI staining. (G&H) Apoptosis study in PANC-1 cells assayed by nuclei staining.

3.4. IP delivery of P@P EPs to orthotopic PC tumors

We established orthotopic PC tumors by injecting the murine KPC8060 and human PANC-1 cells into the pancreas. These orthotopic PC models mimic the human PC with similar tumor growth characteristics and oncogene expression, early metastasis, and strong desmoplastic stroma reaction [309, 310]. Large primary tumors and extensive metastasis were exhibited in both modes as soon as 4 weeks after cell injection [297].

We first studied how the route of administration affects the pharmacokinetics and biodistribution of P@P EPs prepared with fluorescently labeled PCX (Cy3) and siRNA (Cy5.5). The same dose of P@P EPs was given either by IP or IV injection and blood was collected at selected time points. The fluorescence intensity of Cy5.5-siRNA in the blood was measured and normalized to fluorescence intensity found 2 min after IV injection (Figure 3.5A). The siRNA fluorescence intensity in blood was decreased rapidly to ~5.6% within the first hour after injection, confirming the anticipated rapid clearance of the positively charged nanoemulsions. When given by IP injection, the blood siRNA fluorescence intensity reached maximum of ~7.3% at 1 h post-injection, suggesting limited absorption of the P@P EPs from the peritoneum into blood circulation [311]. This also suggested that a large portion of the P@P EPs was retained in the peritoneal cavity.

Biodistribution of the P@P EPs was determined 24 h after IP and IV injection. The fluorescence of whole body and major isolated organs was measured. When given by IV injection, the P@P EPs mostly accumulated in the liver, spleen, and kidney with negligible signal seen in the tumor (Figure 3.5). In contrast, the IP injection resulted in strong

accumulation both in the primary orthotopic tumors and peritoneal metastasis sites. Importantly, the IP administration significantly decreased the siRNA hepatic and splenic accumulation. IP injection of nanoformulations involves in different metabolic routes with faster biliary excretion, have different protein adsorption profiles when compared with IV injection [312]. To show the role of the PFOB emulsion in the observed biodistribution, we also determined the biodistribution of the PLX given by IP injection. Although the PLX showed strong accumulation in the primary tumors, the tumor/liver ratio was significantly decreased compared with P@P EPs (Figure 3.5F), indicating less effective tumor targeting, and increased potential for off-target effects.

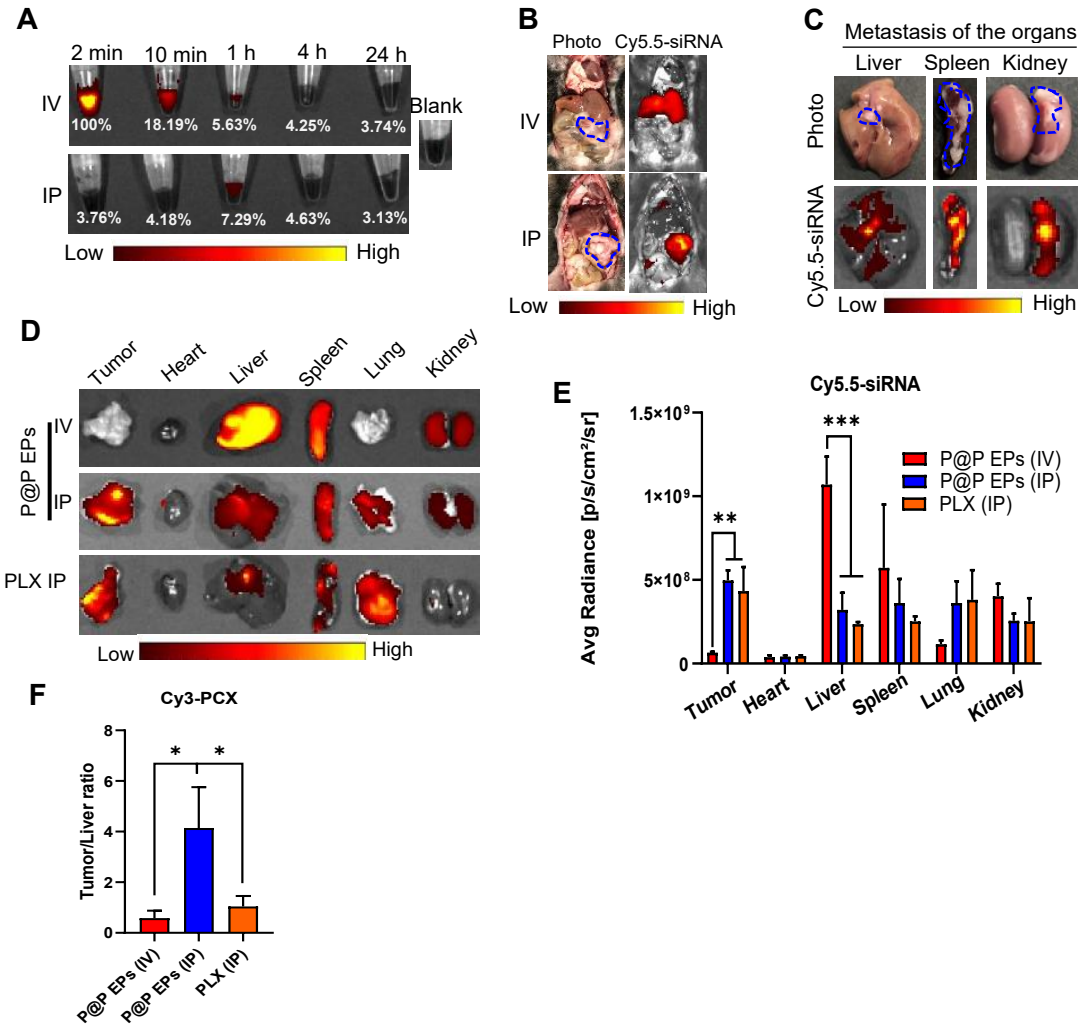

Figure 3.5 P@P EPs improve the siRNA delivery to orthotopic pancreatic tumor and metastasis sites through IP administration. (A) Blood fluorescence of P@P EPs. (B) Mice whole-body biodistribution. (C) Distribution in the metastasis of the organs after IP injection of P@P EPs. (D) Ex vivo fluorescence imaged of the tumors and tissues. (E) Semiquantitative analysis of Cy5.5-siRNA fluorescence intensity in the tumor and tissue site. (F) Semiquantitative analysis of Cy3-PCX in the tumor/liver ratio.

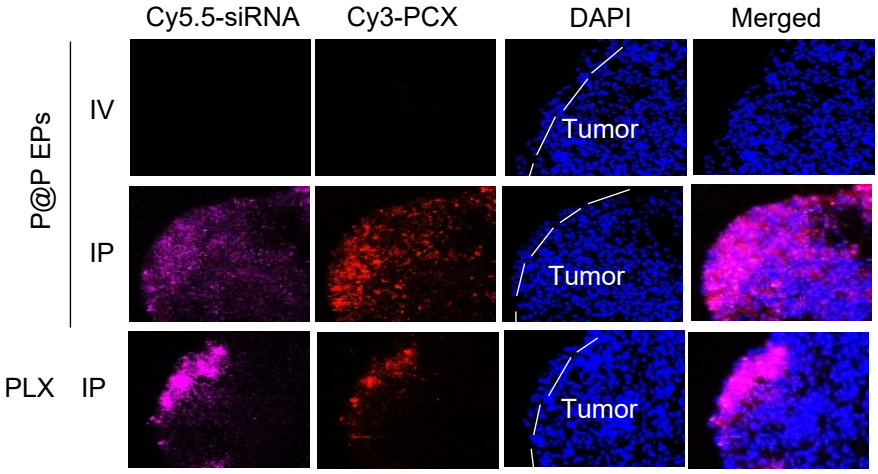

Figure 3.6 Confocal microscopy images of frozen tumor sections.

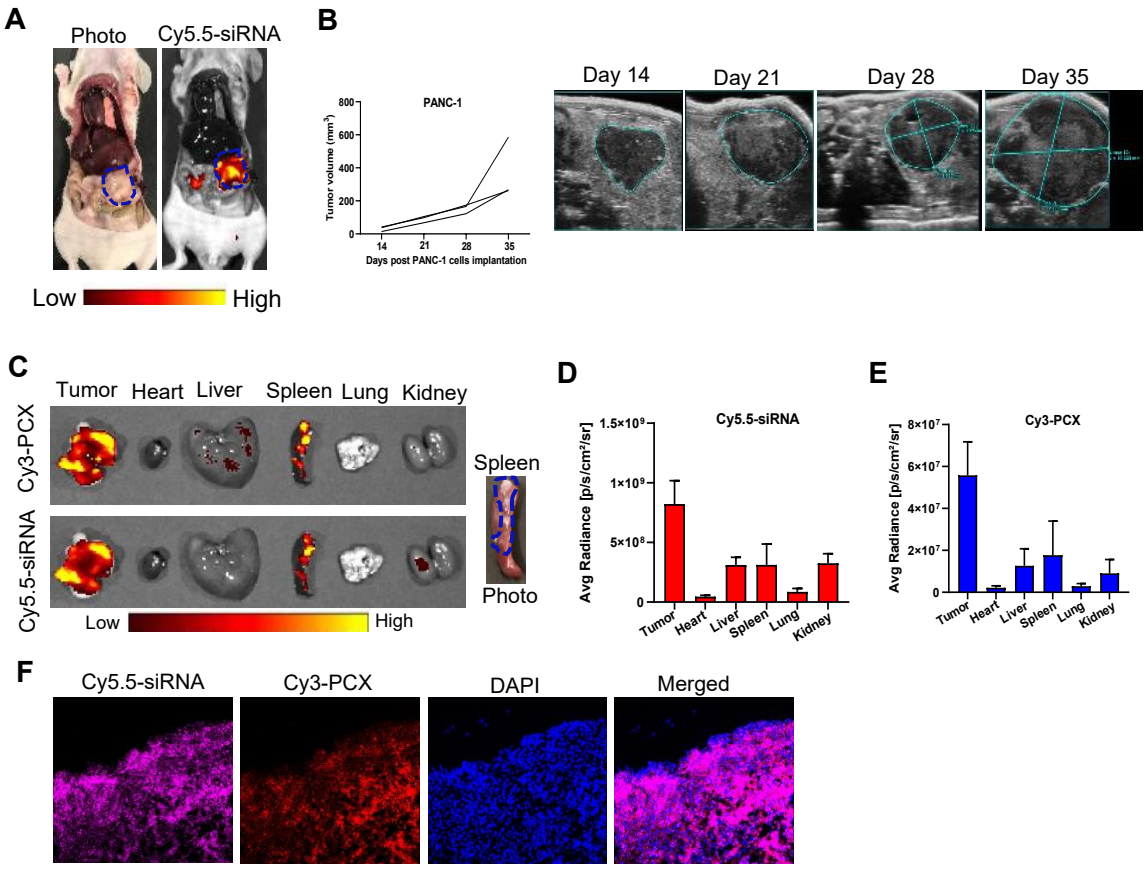

Figure 3.7 Biodistribution in orthotopic pancreatic tumor-bearing mouse-derived from PANC-1 cells were administrated with P@P EPs via IP injection. (A) Biodistribution of P@P EPs in whole body mice at 24 h after IP injection. (B) Primary tumor growth curves analysis by ultrasound imaging. (C) Ex vivo fluorescence imaged of the tumors and tissues at 24 h after injection. (D) Semiquantitative analysis of Cy5.5-siRNA fluorescence intensity in the tumor and other major organs. (E) Semiquantitative analysis of Cy3-PCX fluorescence intensity in the tumor and other major organs. (F) Confocal microscopy images of frozen tumor sections ad 24 h after injection. Cy5.5-siRNA is shown pink, Cy3-PCX is shown in red.

3.5. Intratumoral distribution of P@P EPs

To understand the intratumoral distribution and penetration ability of the P@P EPs, frozen tumor sections were analyzed by confocal microscopy. Both Cy5.5-siRNA (pink) and Cy3-PCX (red) fluorescence was observed in the tumors following IP injection (Figure 3.6). Importantly, the fluorescence signal of both active components of the formulation was found not only on the surface of the tumors facing the peritoneum but also in the inner regions of the tumors, validating the penetration ability of P@P EPs observed *in vitro* (Figure 3.3). Certain PC cell lines can secret factors that recruitment of the fibrogenic cells to the tumor sites, then generate the fibrotic pancreatic tumor [313]. The orthotopic KPC8060 tumors have highly fibrotic stroma [297]. A higher stomal content in PC patients is associated with poor survival outcomes [217]. Interestingly, P@P EPs exhibited effective tumor penetration even in the presence of the dense fibrotic stroma. In contrast, the PLX control group showed distribution predominantly on the tumor surface with limited interior penetration, suggesting a role of the PFOB emulsion in improving the penetration. As our previously published paper, the cholesterol modification of PCX also could improve the penetration of PLX. PFOB emulsion are relatively novel kind of soft nanomaterial, which show great promising in biological application [268, 314]. In contrast to the IP administration, only very weak Cy5.5-siRNA and Cy3-PCX signals were observed in the tumors of the mice treated with IV administration. We validated the tumor accumulation and penetration also in orthotopic PC model using human PANC-1 cells (Figure 3.7).

Similar to the murine KPC8060 model, effective accumulation and penetration into the primary tumors and metastatic lesions were observed.

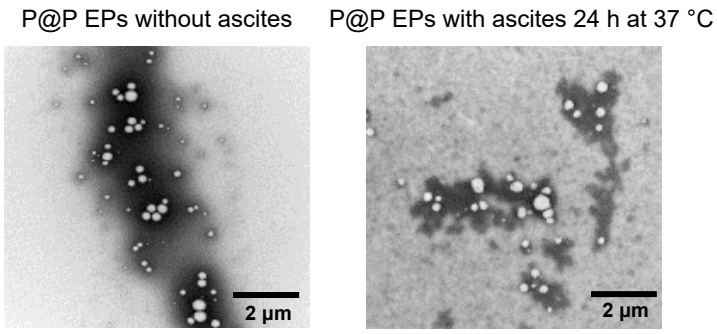

Figure 3.8 Stability of P@P EPs in ascites. TEM observation of nanoparticles after incubation with ascites 24 h at 37 °C (50% v/v).

Even though there are likely multiple factors involved, the mechanism of high tumor delivery efficacy of P@P EPs by IP injection is not fully understanding. In the peritoneal cavity, there are many types of cells and fluids which might be involved in the accumulation and penetration of the P@P EPs. For the PC delivery, one of the major physical barriers is the dense stromal desmoplasia [315]. In this study, we demonstrated high tumor and metastasis accumulation and penetration and limited normal tissue distribution. The peritoneal retention and protection improve the exposure of the tumors to the higher concentration as shown by the siRNA protection ability in the ascites (Figure 3.8). Previous studies showed that the lack of mesothelium on the tumor surfaces contributes to the tumor localization in peritoneal tumors [297, 311, 316, 317]. In our previous study, we confirmed that the primary pancreatic tumors and metastasis foci lacked the visceral

peritoneum composed of the flat mesothelial cells (mesothelium/mesothelial lining) [297]. Compared to the normal tissue, the primary pancreatic tumors and metastasis organs exhibited the broken mesothelial lining, and lack of the compact mesothelial cells

Even with higher tumor accumulation, successful treatment of solid tumors requires deep tumor penetration to access all cancer cells. The surface chemical properties of nanoparticles influence the cellular internalization, endocytosis, and penetration ability [318]. The core-shell structure of the P@P EPs exhibits unique properties arising from the combination of PFOB core and PCX shell and geometry. Overall, the IP administration of P@P emulsion in delivery siRNA is advantageous as it increases the stability of the siRNA in ascites, avoids the blood circulation of the nanoparticles, and enhances cellular uptake, tumor penetration and accumulation.

3.6. Mechanism of tumor penetration of P@P EPs

As hypothesized above, we believe that the observed tumor penetration of the nanoemulsions is a cell-mediated process. The interactions between P@P EPs and the tumor cells or other cells like infiltrating macrophages are complex and likely to all contribute to the delivery efficacy [301]. To evaluate if the penetration mechanism of P@P EPs *in vivo* is the same as the one proposed in our *in vitro* study, we have treated the tumor-bearing mice with IP injection of EXO-1 prior to administration of the P@P EPs. The siRNA intensity of the IP injected P@P EPs in the mice pretreated with EXO-1 was compared with that in mice without EXO-1 (Figure 3.9). We found that pretreatment with EXO-1 significantly reduced the total siRNA accumulation in the tumor ($P = 0.028$) and

most of the siRNA was found in the kidneys. We also found that the siRNA and PCX fluorescent signals were mostly localized at the tumor periphery in the EXO-1 treated animals (Figure 3.9C). The tumor accumulation and penetration of P@P EPs was decreased significantly when we pretreated them with EXO-1, suggesting that exocytosis-mediated secretion was related to mechanical stimulus (via mechanical stimulus-induced exocytosis) [319]. However, full understanding of the mechanism of tumor penetration and potential involvement of other cell types is not completely clear and needs further studies.

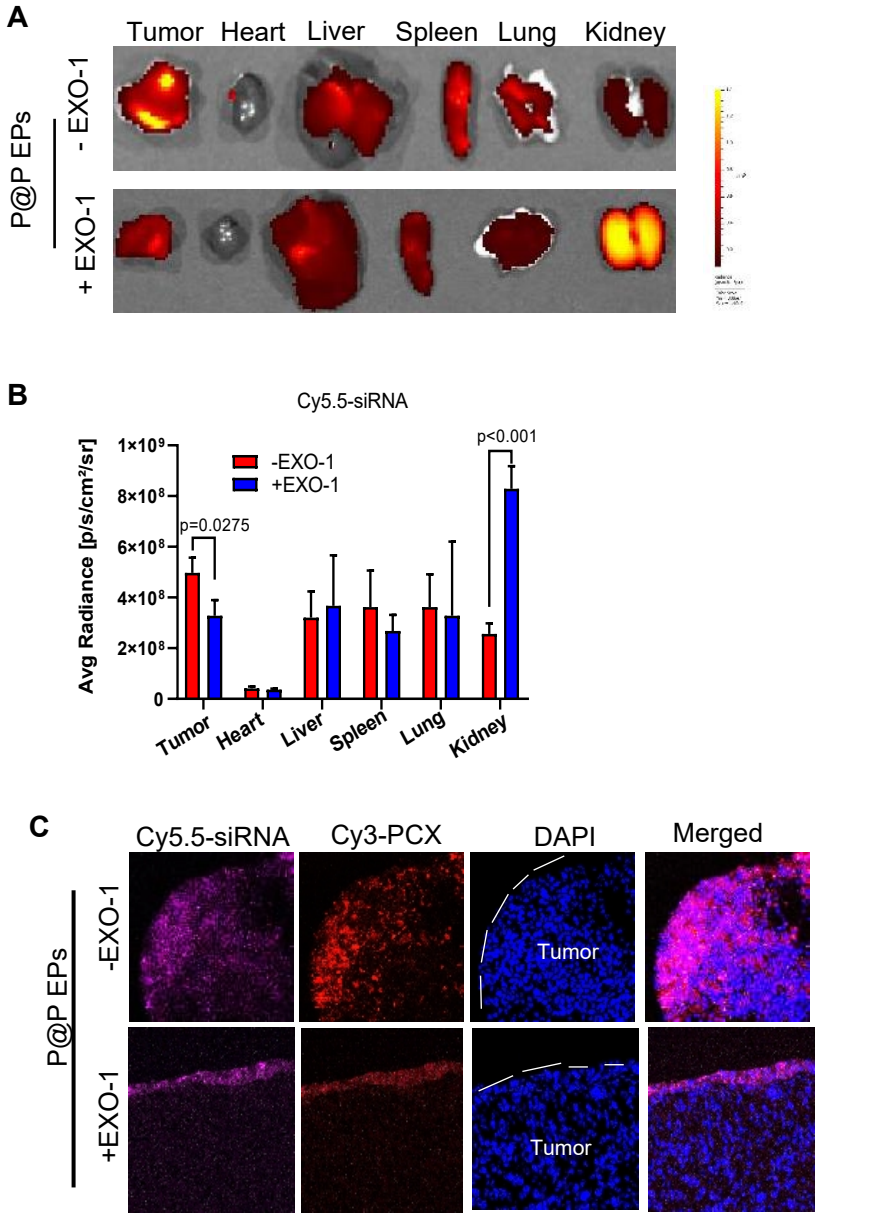

Figure 3.9 EXO-1 inhibited the P@P EPs tumor penetration *in vivo*. (A) Comparison of the P@P EPs distribution in the tumor at 24 h in mice with or without pretreated with the EXO-1. (B) Ex vivo fluorescence imaged of the tumors and tissues at 24 h after injection. (C) Confocal microscopy images of frozen tumor sections ad 24 h after injection. Cy5.5-siRNA is shown pink, Cy3-PCX is shown in red.

3.7. Antitumor efficiency and inhibition of PC metastasis by P@P EPs

We evaluated the antitumor effect of the P@P EPs (siNGF) in the orthotopic KPC8060 tumor model (Figure 3.10A). Tumor growth was followed using ultrasound (Figure 3.10B). The IP injection of P@P EPs (siNGF) remarkably inhibited tumor growth compared with the P@P EPs (siNC) and PLX according to the ultrasound imaging analysis. Compared with the untreated group (PBS), treatment with P@P EPs (siNC) exhibited wreaker effect on the primary tumor growth, suggesting that CXCR4 inhibition alone does not affect tumor cell proliferation significantly. Treatment with the PLX showed only a small decrease in the tumor size, likely due to poor tumor penetration ability. Then, the primary pancreatic tumors were collected for analysis on Day 28 (Figure 3.11A). P@P EPs (siNGF) treated mice showed the best activity with ~70% inhibition of the primary tumor growth, which corresponded with ultrasound imaging analysis (Figure 3.10B). The PLX and P@P EPs control groups only showed ~30% inhibition and 25% inhibition. The antitumor effect of the CXCR4 inhibition and NGF silencing by the P@P EPs have been improved significantly, which was due to the higher of the cellular uptake, siRNA transfection and better tumor penetration. There was no apparent toxicity caused by the different treatments as demonstrated by the unchanged body weight during the treatment period (Figure 3.11B).

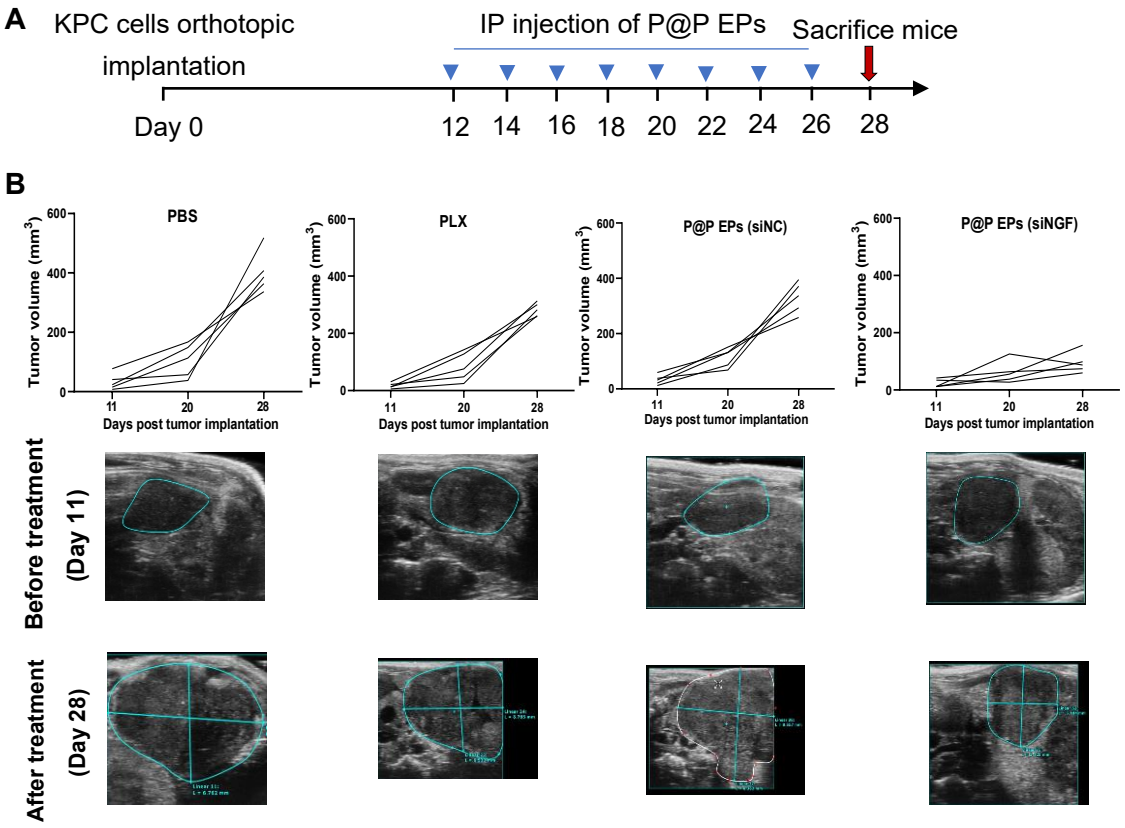

Figure 3.10 The antitumor effects of emulsion polyplexes via IP delivery in orthotopic tumors. (A) Scheme of IP delivery of nanoparticles treatment. KPC8060 cells were injected into the pancreas C57BL/16 mice to form orthotopic tumors. At day 12, mice were randomly divided into 4 groups and treated by different nanoparticles via IP injection for 8 times, the tumor volume were measured using ultrasound imaging during the treatment. All the mice were scarified at day 28. (B) Primary tumor growth curves analyzed by ultrasound imaging. Representative ultrasound images of tumor volume before and after treatment.

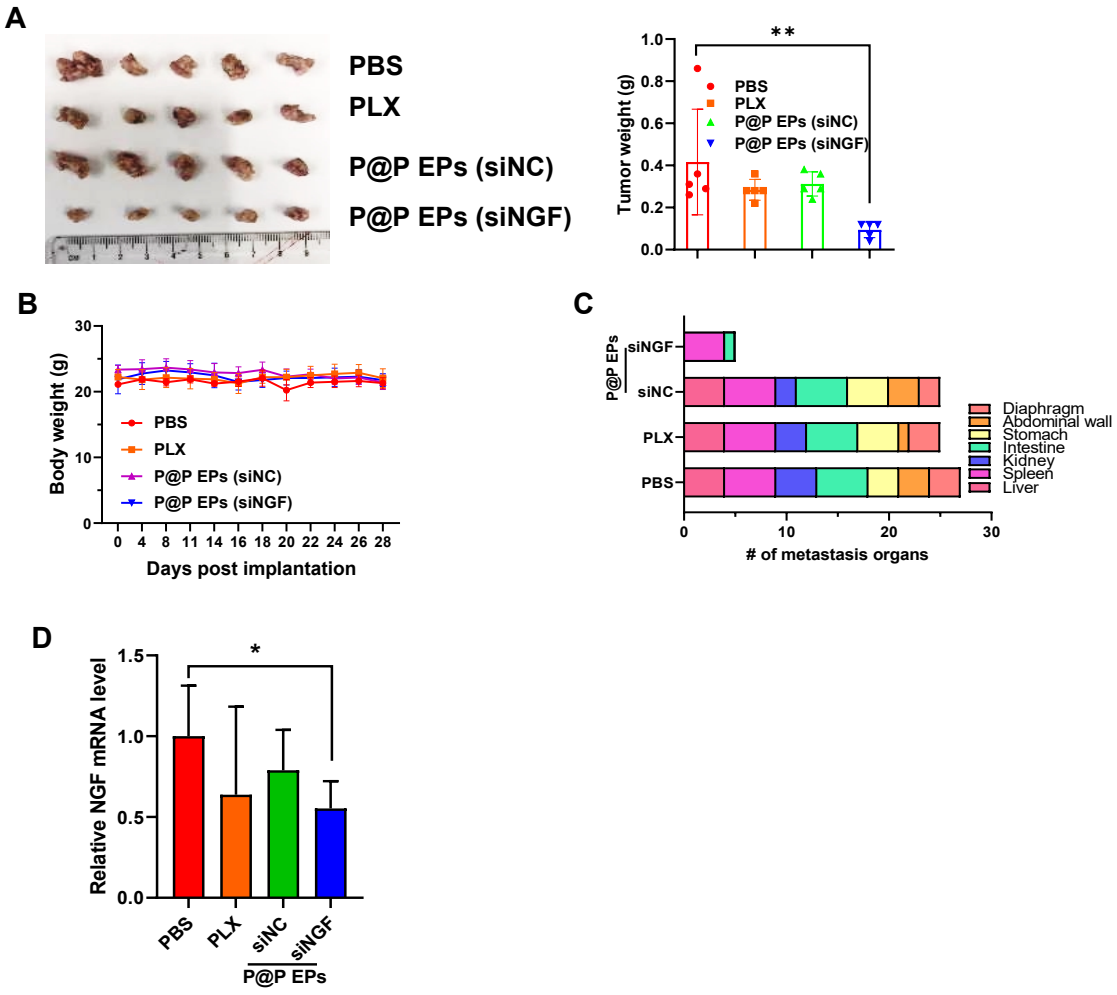

Figure 3.11 The antitumor effects of emulsion polyplexes via IP delivery in orthotopic tumors. (A) Weight and photo picture of primary tumor after the different treatment. Data were shown as mean ± SD (n = 5). (B) The changes of the mouse body weight during the treatment. (C) Tumor metastasis frequency in major organs and tissues. (D) NGF mRNA levels in the isolated tumors.

The metastasis is a common occurrence in PC patients and is a main cause of the morbidity and mortality of the disease [320]. After we showed the promising efficacy of the P@P EPs (siNGF) on the primary tumor growth inhibition, anti-metastasis activity was evaluated (Figure 3.11C). The metastasis in major organs, including liver, spleen, kidney, intestine, stomach, abdominal wall, and diaphragm were observed in untreated control (PBS). Treatment with PLX showed slight anti-metastatic effect as indicated by the reduced number of metastases in the kidney and abdominal wall. The mice treated by P@P EPs (siNGF) improved the antimetastatic activity even further, displaying complete inhibition of metastasis to all observed organs and tissues, except for splenic invasion (Figure 3.11C). Most important is that P@P EPs (siNGF) completely inhibited metastasis to the liver, which is the main metastasis site in PC. Treatment with P@P EPs (siNC) showed a weaker effect on the inhibition of PC metastasis. According to our previously paper, the CXCR4 inhibition by the PCX (PAMD-chol)/siNC exhibited the PC metastasis inhibition [269]. However, the PCX that we used wasn't conjugate with cholesterol, this might be the reason that our result shown that treatment with P@P EPs (siNC) showed a weaker effect on the inhibition of PC metastasis.

The P@P EPs (siNGF) treated mice showed a significant 45% silencing of the NGF mRNA expression in the treated tumors (Figure 3.11D). PLX treated mice showed minor inhibition of the NGF mRNA expression. We also used immunofluorescence staining to evaluate the effect of the treatment on tumor expression of NGF. The results showed that P@P EPs (siNGF) treatment induced the greatest inhibition of the expression of NGF

protein (Figure 3.12A). The enhanced NGF silencing of P@P EPs compared with PLX was mostly dependent on the enhanced cellular uptake and transfection of nanoparticles, and the better tumor penetration. Moreover, the P@P EPs induced efficient NGF silencing without any apparent off-target effects (Figure 3.13), which showed the feasibility of using P@P emulsion as siRNA carrier for selective siRNA delivery and anti-neurogenic cancer therapy via IP injection.

To better understand the effect of our treatment on the nervous tumor microenvironment, we stained neurofilaments (Figure 3.12B). The P@P EPs (siNGF) treatment significantly reduced the density of intra-tumoral neurites. The quantification showed that the P@P EPs (siNGF) group reduced ~75% neurite formation in the tumors compared with PBS group. PLX and P@P EPs (siNC) treatment reduced the intra-tumoral neurogenesis to a negligible degree. Neurofilament-specific staining of the human pancreatic tumors suggested that plentiful of neurites within pancreatic tumor tissue compared with the non-disease pancreas tissues [222]. One of the *in vitro* studies suggested that NGF knockdown in the co-culture of PANC-1 cells and dorsal root ganglion (DRG) neurons induced less DRG neurite sprouting. The NGF depletion with P@P EPs not only inhibited the primary tumor growth and metastasis but inhibited the intra-tumoral neurite growth in the PC tumors (Figure 3.10-3.12). The reduced neurogenesis may inhibit metastasis by the process of perineural invasion. As shown in Figure 8B, the density of neurites was significantly decreased when treated with the P@P EPs (siNGF). Moreover, previous study showed that the intratumoral neurogenesis contributed to the progression

of the pancreatic tumors. Thus, the density of the neurites in the tumor was significantly decreased where the tumor growth was significantly inhibited.

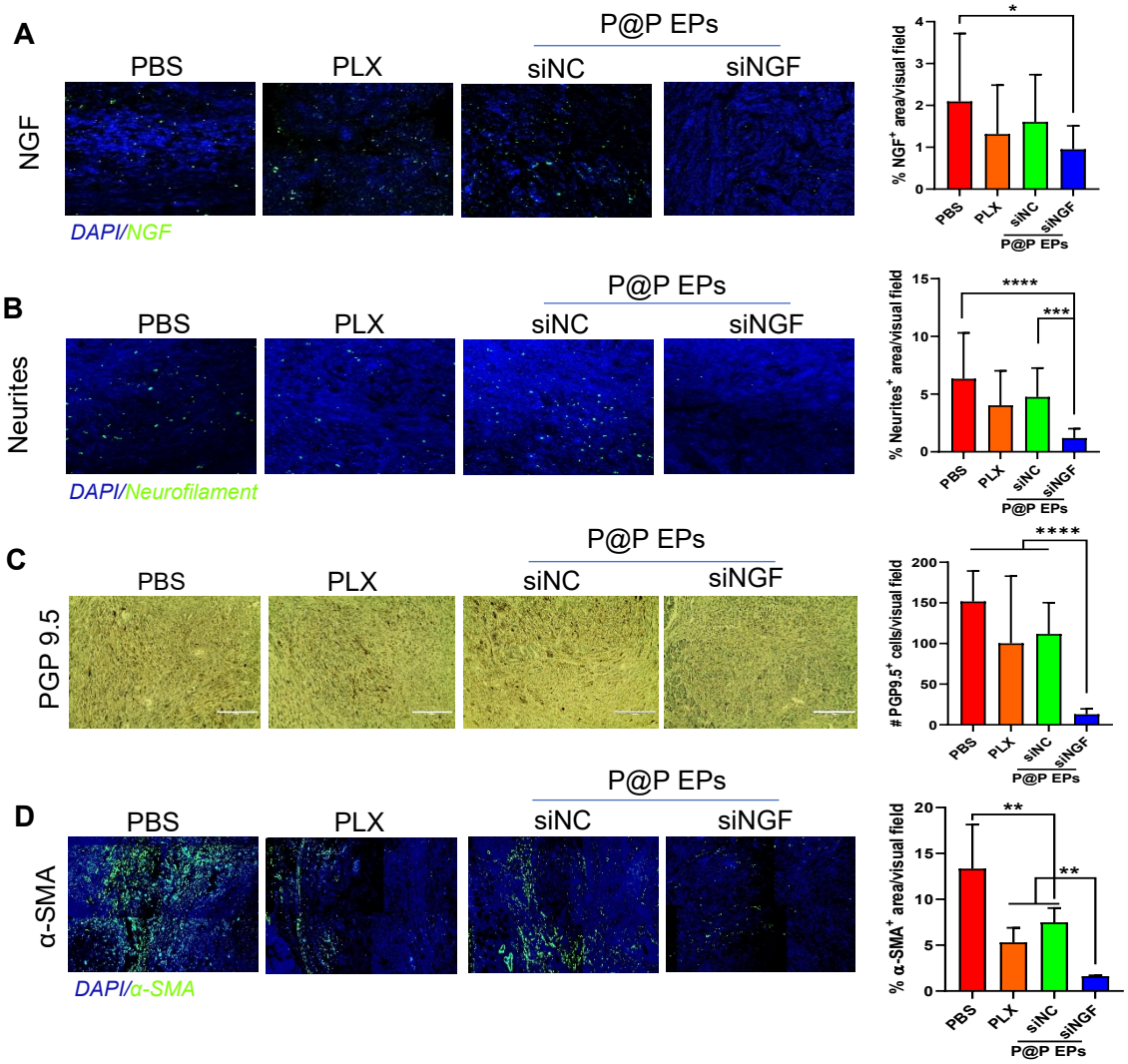

Figure 3.12 (A,B) Immunofluorescence analysis of NGF (green) and Neurites (green) in tumors after treatment. (C) Immunohistochemistry analysis of PGP9.5 in tumors after treatment. (D) Tumor associated fibrosis analysis in tumors after treatment. Scare bar = 200 μm.

Protein Gene Product 9.5 (PGP 9.5), also known as ubiquitin C-terminal hydrolase 1 (UCHL-1), is a nerve fiber marker which has been suggested as a useful prognostic marker in PC patients due to its relationship to tumor progression [321]. Immunohistochemical staining showed significant decrease of PGP 9.5 expression following treatment with P@P EPs (siNGF) (Figure 3.12C), indicating efficient inhibition of tumor nerve fiber formation that may contribute to the observed inhibition of the tumor growth. Increased content of intratumoral nerve fibers is related to higher metastatic potential and poorer prognosis [322, 323]. CXCL12/CXCR4 chemotactic pathway also involved in promoting perineural invasion in PC [324]. CXCL12 promotes the neurite outgrowth of DRG cells and the stimulating effect can be inhibited by treatment with a CXCR4 antagonist [325]. When treated by P@P EPs (siNC), the PGP9.5 expression was also decreased. In the future, we plan to validate these results in additional PC models.

α-SMA is a marker of activated pancreatic stellate cells (PSCs) and fibrosis useful for evaluating the effect of treatments on PC desmoplasia (Figure 3.12D). Both P@P EPs (siNC) and PLX reduced the number of activated PSCs in comparison with PBS group. P@P EPs (siNGF) nanoparticles further inhibited the activation of PSCs significantly. The activated PSCs can generate the collagen, which is the major component of the tumor microenvironment. This result confirmed that P@P EPs (siNGF) could inhibit activation of PSCs and tumor desmoplasia via the combined effect of CXCR4 blockade and NGF silencing.

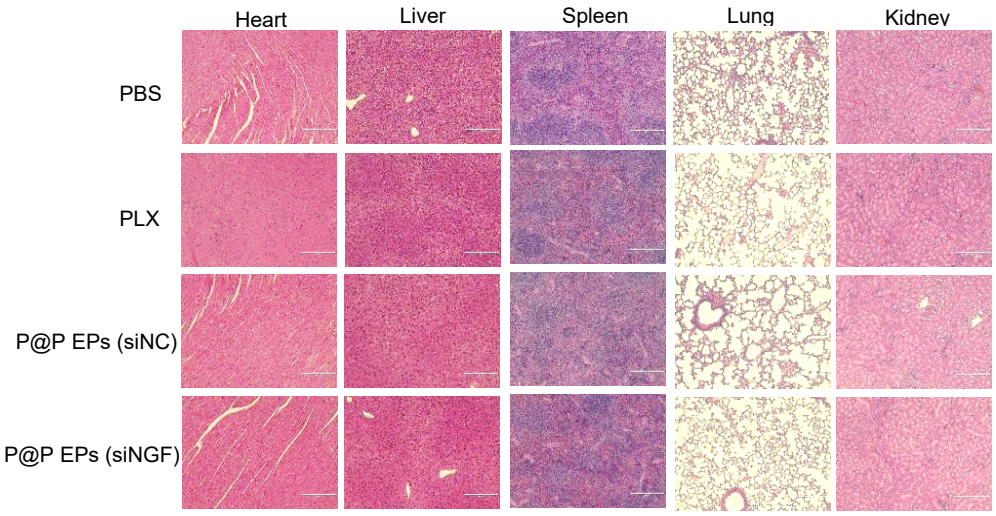

Figure 3.13 H&E staining of tissue to access treatment toxicity. Scale bar= 200 μm.

4. Conclusion

In summary, we have demonstrated P@P emulsion as a delivery platform for siRNA to target the tumor-neuron interaction for pancreatic cancer treatment via NGF silencing through EPR-independent delivery of nanomedicine using IP administration. P@P EPs show promising cellular uptake and tumor penetration ability, whereby cellular uptake depends on the caveolar/lipid raft endocytosis and the tumor penetration depends on the Golgi/endoplasmic reticulum/exocytosis pathway. P@P EPs provide not only a protective structure against the ascites in the peritoneal cavity, but also an opportunity for effective penetration to the tumor sites due to the lack of the mesothelium. P@P EPs exhibited the best tumor penetration and enhanced NGF gene knockdown *in vitro* and *in vivo*, which led to effective suppression of tumor growth in KPC8060 cells-bearing orthotopic pancreatic cancer in mice models without adverse effects. All together, P@P emulsion-assisted delivery of siNGF points to a promising treatment strategy of pancreatic cancer by improving the tumor penetration and targeting the interactions between the tumor cells and tumor microenvironment.

Chapter 4 - Summary and Future Directions

1. Summary

Pulmonary fibrosis is a chronic, progressive-fibrosing interstitial disease where there is scaring of the lungs, which makes it difficult to breath. It affects ~3 million people worldwide with incidence increasing dramatically with age. It is a fatal disease and needs urgent new treatments. PC is one of the most highly malignant tumors and the 5-year overall survival rate in patients with PC is lower than 5%, even when treated by the first-line chemotherapeutic drug, gemcitabine. It is necessary to develop methods to treating pulmonary fibrosis and PC. The CXCR4/CXCL12 axis has significant role in the fibroblasts-to-myofibroblasts transformation and the fibrosis progression, tumor progression, angiogenesis, metastasis, and cancer cell-microenvironment interaction. Studies suggested that inhibition of CXCR4 served as an effective strategy for the metastasis cancer treatment and pulmonary fibrosis. Various nanomedicines have been designed based on siRNA. The siRNA nanomedicines gained more attention in regulating gene expression for treating multiple diseases, including cancer and fibrosis. PFC nanoemulsion are disperse systems that consisting of nanoscale liquid PFC droplets and stabilized by an emulsify agent. It is a soft material which can be prepared by high-pressure homogenization or microfluidization. PFOB is a linear PFC which is well known for the biocompatibility and good tolerance for human being. PFOB NPs are multifunctional nanotechnology. We have synthesized PCX based on AMD3100, a CXCR4 antagonism. PCX is a dual function polycation which capable of CXCR4 inhibition

and nucleic acid delivery. In this study, PCX was emulsified with PFOB to form PCX@PFOB emulsion. Due to the cationic property of this emulsion, it can be used as the siRNA delivery system to form EPs. Then, we evaluated the therapeutic efficacy of the EPs for combined therapy in metastasis PC and pulmonary fibrosis. The PCX@PFOB emulsion can serve as nucleic acid delivery systems. Compared with the commonly used polyplexes, EPs showed improvement of siRNA cellular uptake and transfection. Moreover, EPs have better lung penetration, which might be due to the specific properties of PFOB that can reduce CBF and improve lung penetration. The delivery of siSTAT3 to the HPLFs resulted in inhibition of the proliferation and migration of fibroblasts, and then reduced the α-SMA expression and ECM production. The intratracheal delivery of Eps, combined with CXCR4 inhibition and STAT3 silencing, is a promising strategy for a combination therapy in pulmonary fibrosis treatment.On the other hand, P@P emulsion can inhibit the cancer cells migration mediated by CXCL12 due to the CXCR4 antagonism ability. P@P EPs showed promising cellular uptake and tumor penetration ability, where the mechanism of cellular uptake was mostly dependent on the C/LR, and the tumor penetration mechanism was dependent on the Golgi/endoplasmic reticulum/exocytosis pathway. The NGF depletion with P@P EPs not only inhibited primary tumor growth and metastasis, but also inhibited the intra-tumoral neurite growth and stromal density in KPC8060 cell-bearing PC tumor models *in vivo*. Taken together, P@P emulsion-assisted delivery of siNGF is a promising treatment approach for PC treatment by targeting the interaction between the tumor cells and nervous microenvironment.

2. Future directions

Nanoemulsions dosage form serves as a promising multimodal platform for the delivery pharmaceutical ingredients and have attracted great attention in pharmacotherapy. In this study, the capacity of the P@P nanoemulsion to delivery therapeutic nucleic acid and their ability to protect the siRNA mucin and ascites degradation with good penetration ability. However, there are still many challenges before we can consider translating the P@P EPs nanoemulsions to the clinic, even with the promising potential in mouse models of pulmonary fibrosis and PC, especially due to poorly controlled colloidal stability. It is necessary that the remaining of the size distribution after administration. Stability of nanoemulsion should be performed to evaluate the integrity of the nanoemulsion delivery system, the excipients and the loaded therapeutic nucleic acid. Hence, clinical translation needs to develop very stable EPs over a long storage time. Future directions will focus on the development of better of colloidal stability emulsion by combing with Generally Recognized as Safe (GRAS)-grade excipients, such as glycerol, soybean oil, disodium edetate and egg lecithin. Even though it is available that nanoemulsions are easily produced in the industry by using mechanical extrusion process or high shear stress in large scale, the scale-up and material safety are still extremely challenging especially when we design the multifunctional nanoemulsion delivery systems to combine the payload agents (drug or therapeutic nucleic acids) and targeting ligands. It is necessary that the scale-up and material safety need to be addressed before being transformed into the clinical application. In this study, the I.P

injection was used to treating pancreatic tumor mice. However, the translation of I.P injected nuclear acids formulation into clinic is extremely challenged even with the promising tumor accumulation by I.P injection in mice models. Hence, we can start with the I.V administration when moving to clinic. However, the rapid uptake of nanoemulsions by mononuclear phagocytic system (MPS) also impeded the translation to the clinic when giving by I.V. injection. In order to preventing the MPS uptake, we can stabilize the nanoemulsion with PEG, which also can improve the long blood circulation time.

Moreover, in this study, the intratracheal instillation was used for treating mice, we will use the inhalation in the future. The tumor penetration mechanism was evaluated by using EXO-1, the exocytosis inhibitors. Future directions will investigate the tumor penetration mechanism by using more of the other small inhibitors. Moreover, future directions will focus on the drug delivery using the emulsion that specifically targets lung and tumors. Moreover, PFOB emulsion can serve as an oxygen delivery system without apparent toxicity. For example, ICG&PFOB co-loaded nanoliposomes (LIP-PFOB-ICG) showed promising inhibition of the tumor growth via enhanced PDT&PTT synergistic therapy because of the excellent oxygen carrying ability of PFOB [326, 327]. Future directions will also focus on the PTT by formulating different PFOB nanoemulsions.

Bibliography

[1] N.W. Schluger, R. Koppaka, Lung disease in a global context. A call for public health action, Ann Am Thorac Soc 11(3) (2014) 407-16.
[2] M.J.R. Ruigrok, H.W. Frijlink, W.L.J. Hinrichs, Pulmonary administration of small interfering RNA: The route to go?, J Control Release 235 (2016) 14-23.
[3] O.M. Merkel, T. Kissel, Nonviral pulmonary delivery of siRNA, Acc Chem Res 45(7) (2012) 961-70.
[4] J. Chen, Y. Tang, Y. Liu, Y. Dou, Nucleic Acid-Based Therapeutics for Pulmonary Diseases, AAPS PharmSciTech 19(8) (2018) 3670-3680.
[5] T. Maes, K.G. Tournoy, G.F. Joos, Gene therapy for allergic airway diseases, Curr Allergy Asthma Rep 11(2) (2011) 163-72.
[6] Y. Xie, O.M. Merkel, Pulmonary Delivery of siRNA via Polymeric Vectors as Therapies of Asthma, Arch Pharm (Weinheim) 348(10) (2015) 681-8.
[7] K. Dua, R. Wadhwa, G. Singhvi, V. Rapalli, S.D. Shukla, M.D. Shastri, G. Gupta, S. Satija, M. Mehta, N. Khurana, R. Awasthi, P.K. Maurya, L. Thangavelu, R. S, M.M. Tambuwala, T. Collet, P.M. Hansbro, D.K. Chellappan, The potential of siRNA based drug delivery in respiratory disorders: Recent advances and progress, Drug Dev Res 80(6) (2019) 714-730.
[8] I. Villate-Beitia, J. Zarate, G. Puras, J.L. Pedraz, Gene delivery to the lungs: pulmonary gene therapy for cystic fibrosis, Drug Dev Ind Pharm 43(7) (2017) 1071-1081.
[9] S.D. Gioia, C. Sardo, S. Castellani, B. Porsio, G. Belgiovine, A. Carbone, G. Giammona, G. Cavallaro, M. Conese, From Genesis to Revelation: The Role of Inflammatory Mediators in Chronic Respiratory Diseases and their Control by Nucleic Acid-based Drugs, Curr Drug Deliv 14(2) (2017) 253-271.
[10] A. Bohr, N. Tsapis, I. Andreana, A. Chamarat, C. Foged, C. Delomenie, M. Noiray, N. El Brahmi, J.P. Majoral, S. Mignani, E. Fattal, Anti-Inflammatory Effect of Anti-TNF-α SiRNA Cationic Phosphorus Dendrimer Nanocomplexes Administered Intranasally in a Murine Acute Lung Injury Model, Biomacromolecules 18(8) (2017) 2379-2388.
[11] M. Mehta, Deeksha, D. Tewari, G. Gupta, R. Awasthi, H. Singh, P. Pandey, D.K. Chellappan, R. Wadhwa, T. Collet, P.M. Hansbro, S.R. Kumar, L. Thangavelu, P. Negi, K. Dua, S. Satija, Oligonucleotide therapy: An emerging focus area for drug delivery in chronic inflammatory respiratory diseases, Chem Biol Interact 308 (2019) 206-215.
[12] R. Itani, A. Al Faraj, siRNA Conjugated Nanoparticles-A Next Generation Strategy to Treat Lung Cancer, Int J Mol Sci 20(23) (2019).
[13] O.S. Usmani, Choosing the right inhaler for your asthma or COPD patient, Ther Clin Risk Manag 15 (2019) 461-472.
[14] S.M. Elbashir, W. Lendeckel, T. Tuschl, RNA interference is mediated by 21- and 22-nucleotide RNAs, Genes Dev 15(2) (2001) 188-200.
[15] S.M. Hoy, Patisiran: First Global Approval, Drugs 78(15) (2018) 1625-1631.
[16] M. Manoharan, RNA interference and chemically modified small interfering RNAs,

Curr Opin Chem Biol 8(6) (2004) 570-9.
[17] I. Urits, D. Swanson, M.C. Swett, A. Patel, K. Berardino, A. Amgalan, A.A. Berger, H. Kassem, A. Kaye, O. Viswanath, A Review of Patisiran (ONPATTRO®) for the Treatment of Polyneuropathy in People with Hereditary Transthyretin Amyloidosis, Neurol Ther (2020).
[18] L.J. Scott, Givosiran: First Approval, Drugs 80(3) (2020) 335-339.
[19] R.R. Nikam, K.R. Gore, Journey of siRNA: Clinical Developments and Targeted Delivery, Nucleic Acid Ther 28(4) (2018) 209-224.
[20] P.E. Saw, E.W. Song, siRNA therapeutics: a clinical reality, Sci China Life Sci 63(4) (2020) 485-500.
[21] D. Haussecker, Current issues of RNAi therapeutics delivery and development, J Control Release 195 (2014) 49-54.
[22] R. Kandil, O.M. Merkel, Pulmonary delivery of siRNA as a novel treatment for lung diseases, Ther Deliv 10(4) (2019) 203-206.
[23] N.R. Labiris, M.B. Dolovich, Pulmonary drug delivery. Part I: physiological factors affecting therapeutic effectiveness of aerosolized medications, Br J Clin Pharmacol 56(6) (2003) 588-99.
[24] O.M. Merkel, I. Rubinstein, T. Kissel, siRNA delivery to the lung: what's new?, Adv Drug Deliv Rev 75 (2014) 112-28.
[25] S.R. Youngren-Ortiz, N.S. Gandhi, L. España-Serrano, M.B. Chougule, Aerosol Delivery of siRNA to the Lungs. Part 1: Rationale for Gene Delivery Systems, Kona 33 (2016) 63-85.
[26] J.A. Whitsett, T. Alenghat, Respiratory epithelial cells orchestrate pulmonary innate immunity, Nat Immunol 16(1) (2015) 27-35.
[27] J.V. Fahy, B.F. Dickey, Airway mucus function and dysfunction, N Engl J Med 363(23) (2010) 2233-47.
[28] D. Vermette, P. Hu, M.F. Canarie, M. Funaro, J. Glover, R.W. Pierce, Tight junction structure, function, and assessment in the critically ill: a systematic review, Intensive Care Med Exp 6(1) (2018) 37.
[29] R. Guagliardo, P. Merckx, A. Zamborlin, L. De Backer, M. Echaide, J. Pérez-Gil, S.C. De Smedt, K. Raemdonck, Nanocarrier Lipid Composition Modulates the Impact of Pulmonary Surfactant Protein B (SP-B) on Cellular Delivery of siRNA, Pharmaceutics 11(9) (2019).
[30] P. Merckx, L. De Backer, L. Van Hoecke, R. Guagliardo, M. Echaide, P. Baatsen, B. Olmeda, X. Saelens, J. Pérez-Gil, S.C. De Smedt, K. Raemdonck, Surfactant protein B (SP-B) enhances the cellular siRNA delivery of proteolipid coated nanogels for inhalation therapy, Acta Biomater 78 (2018) 236-246.
[31] R. Guagliardo, J. Pérez-Gil, S. De Smedt, K. Raemdonck, Pulmonary surfactant and drug delivery: Focusing on the role of surfactant proteins, J Control Release 291 (2018) 116-126.
[32] A. Haczku, Protective role of the lung collectins surfactant protein A and surfactant

protein D in airway inflammation, J Allergy Clin Immunol 122(5) (2008) 861-79; quiz 880-1.
[33] L. De Backer, A. Cerrada, J. Pérez-Gil, S.C. De Smedt, K. Raemdonck, Bio-inspired materials in drug delivery: Exploring the role of pulmonary surfactant in siRNA inhalation therapy, J Control Release 220(Pt B) (2015) 642-50.
[34] L. De Backer, K. Braeckmans, M.C. Stuart, J. Demeester, S.C. De Smedt, K. Raemdonck, Bio-inspired pulmonary surfactant-modified nanogels: A promising siRNA delivery system, J Control Release 206 (2015) 177-86.
[35] C. McPherson, J.A. Wambach, Prevention and Treatment of Respiratory Distress Syndrome in Preterm Neonates, Neonatal Netw 37(3) (2018) 169-177.
[36] G. Hu, J.W. Christman, Editorial: Alveolar Macrophages in Lung Inflammation and Resolution, Front Immunol 10 (2019) 2275.
[37] C.D. Walkey, J.B. Olsen, H. Guo, A. Emili, W.C. Chan, Nanoparticle size and surface chemistry determine serum protein adsorption and macrophage uptake, J Am Chem Soc 134(4) (2012) 2139-47.
[38] G. Osman, J. Rodriguez, S.Y. Chan, J. Chisholm, G. Duncan, N. Kim, A.L. Tatler, K.M. Shakesheff, J. Hanes, J.S. Suk, J.E. Dixon, PEGylated enhanced cell penetrating peptide nanoparticles for lung gene therapy, J Control Release 285 (2018) 35-45.
[39] N. Kim, G.A. Duncan, J. Hanes, J.S. Suk, Barriers to inhaled gene therapy of obstructive lung diseases: A review, J Control Release 240 (2016) 465-488.
[40] C. Puisney, A. Baeza-Squiban, S. Boland, Mechanisms of Uptake and Translocation of Nanomaterials in the Lung, Adv Exp Med Biol 1048 (2018) 21-36.
[41] H.H. Gustafson, D. Holt-Casper, D.W. Grainger, H. Ghandehari, Nanoparticle Uptake: The Phagocyte Problem, Nano Today 10(4) (2015) 487-510.
[42] C. Kelly, A.B. Yadav, C. Lawlor, K. Nolan, J. O'Dwyer, C.M. Greene, N.G. McElvaney, N. Sivadas, J.M. Ramsey, S.A. Cryan, Therapeutic aerosol bioengineering of siRNA for the treatment of inflammatory lung disease by TNFα gene silencing in macrophages, Mol Pharm 11(11) (2014) 4270-9.
[43] S. Maghrebi, P. Joyce, M. Jambhrunkar, N. Thomas, C.A. Prestidge, Poly(lactic-co-glycolic) Acid-Lipid Hybrid Microparticles Enhance the Intracellular Uptake and Antibacterial Activity of Rifampicin, ACS Appl Mater Interfaces 12(7) (2020) 8030-8039.
[44] L. De Backer, T. Naessens, S. De Koker, E. Zagato, J. Demeester, J. Grooten, S.C. De Smedt, K. Raemdonck, Hybrid pulmonary surfactant-coated nanogels mediate efficient in vivo delivery of siRNA to murine alveolar macrophages, J Control Release 217 (2015) 53-63.
[45] D. Zhang, H. Lee, X. Wang, A. Rai, M. Groot, Y. Jin, Exosome-Mediated Small RNA Delivery: A Novel Therapeutic Approach for Inflammatory Lung Responses, Mol Ther 26(9) (2018) 2119-2130.
[46] Y. He, Y. Liang, R. Han, W.L. Lu, J.C.W. Mak, Y. Zheng, Rational particle design to overcome pulmonary barriers for obstructive lung diseases therapy, J Control Release 314 (2019) 48-61.

[47] X.M. Bustamante-Marin, L.E. Ostrowski, Cilia and Mucociliary Clearance, Cold Spring Harb Perspect Biol 9(4) (2017).
[48] P. Mastorakos, A.L. da Silva, J. Chisholm, E. Song, W.K. Choi, M.P. Boyle, M.M. Morales, J. Hanes, J.S. Suk, Highly compacted biodegradable DNA nanoparticles capable of overcoming the mucus barrier for inhaled lung gene therapy, Proc Natl Acad Sci U S A 112(28) (2015) 8720-5.
[49] N. Sanders, C. Rudolph, K. Braeckmans, S.C. De Smedt, J. Demeester, Extracellular barriers in respiratory gene therapy, Adv Drug Deliv Rev 61(2) (2009) 115-27.
[50] A.P.B. Almeida, G.B.R. Damaceno, A.F. Carneiro, A. Bohr, H.R. Gonçalves, M.C. Valadares, T.L. Nascimento, E.M. Lima, Mucopenetrating lipoplexes modified with PEG and hyaluronic acid for CD44-targeted local siRNA delivery to the lungs, J Biomater Appl 34(5) (2019) 617-630.
[51] C. Ge, J. Yang, S. Duan, Y. Liu, F. Meng, L. Yin, Fluorinated alpha-Helical Polypeptides Synchronize Mucus Permeation and Cell Penetration toward Highly Efficient Pulmonary siRNA Delivery against Acute Lung Injury, Nano Lett 20(3) (2020) 1738-1746.
[52] J.S. Suk, A.J. Kim, K. Trehan, C.S. Schneider, L. Cebotaru, O.M. Woodward, N.J. Boylan, M.P. Boyle, S.K. Lai, W.B. Guggino, J. Hanes, Lung gene therapy with highly compacted DNA nanoparticles that overcome the mucus barrier, J Control Release 178 (2014) 8-17.
[53] J.S. Suk, N.J. Boylan, K. Trehan, B.C. Tang, C.S. Schneider, J.M. Lin, M.P. Boyle, P.L. Zeitlin, S.K. Lai, M.J. Cooper, J. Hanes, N-acetylcysteine enhances cystic fibrosis sputum penetration and airway gene transfer by highly compacted DNA nanoparticles, Mol Ther 19(11) (2011) 1981-9.
[54] J.S. Suk, S.K. Lai, N.J. Boylan, M.R. Dawson, M.P. Boyle, J. Hanes, Rapid transport of muco-inert nanoparticles in cystic fibrosis sputum treated with N-acetyl cysteine, Nanomedicine (Lond) 6(2) (2011) 365-75.
[55] P. Wark, V.M. McDonald, Nebulised hypertonic saline for cystic fibrosis, Cochrane Database Syst Rev 9(9) (2018) Cd001506.
[56] S.Y. Graeber, Z. Zhou-Suckow, J. Schatterny, S. Hirtz, R.C. Boucher, M.A. Mall, Hypertonic saline is effective in the prevention and treatment of mucus obstruction, but not airway inflammation, in mice with chronic obstructive lung disease, Am J Respir Cell Mol Biol 49(3) (2013) 410-7.
[57] E. Daviskas, B.K. Rubin, Effect of inhaled dry powder mannitol on mucus and its clearance, Expert Rev Respir Med 7(1) (2013) 65-75.
[58] S. Xu, B.Z. Olenyuk, C.T. Okamoto, S.F. Hamm-Alvarez, Targeting receptor-mediated endocytotic pathways with nanoparticles: rationale and advances, Adv Drug Deliv Rev 65(1) (2013) 121-38.
[59] J. Bradbury, Detergent-lentiviral combination gives gene therapy hope for cystic fibrosis, Lancet 360(9342) (2002) 1306.
[60] D. Bardoliwala, V. Patel, A. Javia, S. Ghosh, A. Patel, A. Misra, Nanocarriers in effective pulmonary delivery of siRNA: current approaches and challenges, Ther Deliv

10(5) (2019) 311-332.
[61] P. Wu, X. Luo, H. Wu, F. Yu, K. Wang, M. Sun, D. Oupicky, Cholesterol Modification Enhances Antimetastatic Activity and siRNA Delivery Efficacy of Poly(ethylenimine)-Based CXCR4 Antagonists, Macromol Biosci 18(11) (2018) e1800234.
[62] G. Chen, K. Wang, Y. Wang, P. Wu, M. Sun, D. Oupický, Fluorination Enhances Serum Stability of Bioreducible Poly(amido amine) Polyplexes and Enables Efficient Intravenous siRNA Delivery, Adv Healthc Mater 7(5) (2018).
[63] G. Chen, K. Wang, Q. Hu, L. Ding, F. Yu, Z. Zhou, Y. Zhou, J. Li, M. Sun, D. Oupický, Combining Fluorination and Bioreducibility for Improved siRNA Polyplex Delivery, ACS Appl Mater Interfaces 9(5) (2017) 4457-4466.
[64] M. Durymanov, J. Reineke, Non-viral Delivery of Nucleic Acids: Insight Into Mechanisms of Overcoming Intracellular Barriers, Front Pharmacol 9 (2018) 971.
[65] J. Viger-Gravel, A. Schantz, A.C. Pinon, A.J. Rossini, S. Schantz, L. Emsley, Structure of Lipid Nanoparticles Containing siRNA or mRNA by Dynamic Nuclear Polarization-Enhanced NMR Spectroscopy, J Phys Chem B 122(7) (2018) 2073-2081.
[66] S. Patel, J. Kim, M. Herrera, A. Mukherjee, A.V. Kabanov, G. Sahay, Brief update on endocytosis of nanomedicines, Adv Drug Deliv Rev 144 (2019) 90-111.
[67] S.J. Hong, K.S. Cho, M.H. Ahn, S. Pal, P.H. Choung, J. Sangshetti, R.B. Arote, Targeted Delivery of siRNA Therapeutics using Ligand Mediated Biodegradable Polymeric Nanocarriers, Curr Pharm Des 24(16) (2018) 1788-1800.
[68] T.W.M. Keil, D. Baldassi, O.M. Merkel, T-cell targeted pulmonary siRNA delivery for the treatment of asthma, Wiley Interdiscip Rev Nanomed Nanobiotechnol (2020) e1634.
[69] F. Ercole, M.R. Whittaker, J.F. Quinn, T.P. Davis, Cholesterol Modified Self-Assemblies and Their Application to Nanomedicine, Biomacromolecules 16(7) (2015) 1886-914.
[70] C. Pichon, L. Billiet, P. Midoux, Chemical vectors for gene delivery: uptake and intracellular trafficking, Curr Opin Biotechnol 21(5) (2010) 640-5.
[71] R. Pellegrino, G. Viegi, V. Brusasco, R.O. Crapo, F. Burgos, R. Casaburi, A. Coates, C.P. van der Grinten, P. Gustafsson, J. Hankinson, R. Jensen, D.C. Johnson, N. MacIntyre, R. McKay, M.R. Miller, D. Navajas, O.F. Pedersen, J. Wanger, Interpretative strategies for lung function tests, Eur Respir J 26(5) (2005) 948-68.
[72] H. Fehrenbach, C. Wagner, M. Wegmann, Airway remodeling in asthma: what really matters, Cell Tissue Res 367(3) (2017) 551-569.
[73] M.S. Twigg, S. Brockbank, P. Lowry, S.P. FitzGerald, C. Taggart, S. Weldon, The Role of Serine Proteases and Antiproteases in the Cystic Fibrosis Lung, Mediators Inflamm 2015 (2015) 293053.
[74] S. Yuan, M. Hollinger, M.E. Lachowicz-Scroggins, S.C. Kerr, E.M. Dunican, B.M. Daniel, S. Ghosh, S.C. Erzurum, B. Willard, S.L. Hazen, X. Huang, S.D. Carrington, S. Oscarson, J.V. Fahy, Oxidation increases mucin polymer cross-links to stiffen airway mucus gels, Sci Transl Med 7(276) (2015) 276ra27.
[75] J.S. Suk, S.K. Lai, Y.Y. Wang, L.M. Ensign, P.L. Zeitlin, M.P. Boyle, J. Hanes, The

penetration of fresh undiluted sputum expectorated by cystic fibrosis patients by non-adhesive polymer nanoparticles, Biomaterials 30(13) (2009) 2591-7.
[76] V. Kim, G.J. Criner, Chronic bronchitis and chronic obstructive pulmonary disease, Am J Respir Crit Care Med 187(3) (2013) 228-37.
[77] D. Mei, W.S.D. Tan, Y. Tay, A. Mukhopadhyay, W.S.F. Wong, Therapeutic RNA Strategies for Chronic Obstructive Pulmonary Disease, Trends Pharmacol Sci 41(7) (2020) 475-486.
[78] B. Forbes, R. O'Lone, P.P. Allen, A. Cahn, C. Clarke, M. Collinge, L.A. Dailey, L.E. Donnelly, J. Dybowski, D. Hassall, D. Hildebrand, R. Jones, J. Kilgour, J. Klapwijk, C.C. Maier, T. McGovern, K. Nikula, J.D. Parry, M.D. Reed, I. Robinson, L. Tomlinson, A. Wolfreys, Challenges for inhaled drug discovery and development: Induced alveolar macrophage responses, Adv Drug Deliv Rev 71 (2014) 15-33.
[79] S.N. Georas, F. Rezaee, Epithelial barrier function: at the front line of asthma immunology and allergic airway inflammation, J Allergy Clin Immunol 134(3) (2014) 509-20.
[80] J. DeVincenzo, J.E. Cehelsky, R. Alvarez, S. Elbashir, J. Harborth, I. Toudjarska, L. Nechev, V. Murugaiah, A. Van Vliet, A.K. Vaishnaw, R. Meyers, Evaluation of the safety, tolerability and pharmacokinetics of ALN-RSV01, a novel RNAi antiviral therapeutic directed against respiratory syncytial virus (RSV), Antiviral Res 77(3) (2008) 225-31.
[81] T.R. Hawn, A.I. Matheson, S.N. Maley, O. Vandal, Host-directed therapeutics for tuberculosis: can we harness the host?, Microbiol Mol Biol Rev 77(4) (2013) 608-27.
[82] A.G. Rosas-Taraco, D.M. Higgins, J. Sánchez-Campillo, E.J. Lee, I.M. Orme, M. González-Juarrero, Local pulmonary immunotherapy with siRNA targeting TGFβ1 enhances antimicrobial capacity in Mycobacterium tuberculosis infected mice, Tuberculosis (Edinb) 91(1) (2011) 98-106.
[83] S. Habtemariam, I. Berindan-Neagoe, C.A. Cismaru, D. Schaafsma, S.F. Nabavi, S. Ghavami, M. Banach, S.M. Nabavi, Lessons from SARS and MERS remind us of the possible therapeutic effects of implementing a siRNA strategy to target COVID-19: Shoot the messenger!, J Cell Mol Med (2020).
[84] B.J. Zheng, Y. Guan, Q. Tang, C. Du, F.Y. Xie, M.L. He, K.W. Chan, K.L. Wong, E. Lader, M.C. Woodle, P.Y. Lu, B. Li, N. Zhong, Prophylactic and therapeutic effects of small interfering RNA targeting SARS-coronavirus, Antivir Ther 9(3) (2004) 365-74.
[85] B.J. Li, Q. Tang, D. Cheng, C. Qin, F.Y. Xie, Q. Wei, J. Xu, Y. Liu, B.J. Zheng, M.C. Woodle, N. Zhong, P.Y. Lu, Using siRNA in prophylactic and therapeutic regimens against SARS coronavirus in Rhesus macaque, Nat Med 11(9) (2005) 944-51.
[86] M.L. He, B.J. Zheng, Y. Chen, K.L. Wong, J.D. Huang, M.C. Lin, Y. Peng, K.Y. Yuen, J.J. Sung, H.F. Kung, Kinetics and synergistic effects of siRNAs targeting structural and replicase genes of SARS-associated coronavirus, FEBS Lett 580(10) (2006) 2414-20.
[87] R. Itani, M. Tobaiqy, A. Al Faraj, Optimizing use of theranostic nanoparticles as a life-saving strategy for treating COVID-19 patients, Theranostics 10(13) (2020) 5932-5942.
[88] K. Nahar, N. Gupta, R. Gauvin, S. Absar, B. Patel, V. Gupta, A. Khademhosseini, F.

Ahsan, *In vitro*, in vivo and ex vivo models for studying particle deposition and drug absorption of inhaled pharmaceuticals, Eur J Pharm Sci 49(5) (2013) 805-18.
[89] M. Hittinger, N. Schneider-Daum, C.M. Lehr, Cell and tissue-based *in vitro* models for improving the development of oral inhalation drug products, Eur J Pharm Biopharm 118 (2017) 73-78.
[90] A. Ray, A. Mandal, A.K. Mitra, Recent Patents in Pulmonary Delivery of Macromolecules, Recent Pat Drug Deliv Formul 9(3) (2015) 225-36.
[91] L. De Backer, K. Braeckmans, J. Demeester, S.C. De Smedt, K. Raemdonck, The influence of natural pulmonary surfactant on the efficacy of siRNA-loaded dextran nanogels, Nanomedicine (Lond) 8(10) (2013) 1625-38.
[92] J. Rosenecker, S. Naundorf, S.W. Gersting, R.W. Hauck, A. Gessner, P. Nicklaus, R.H. Müller, C. Rudolph, Interaction of bronchoalveolar lavage fluid with polyplexes and lipoplexes: analysing the role of proteins and glycoproteins, J Gene Med 5(1) (2003) 49-60.
[93] O.B. Garbuzenko, G. Mainelis, O. Taratula, T. Minko, Inhalation treatment of lung cancer: the influence of composition, size and shape of nanocarriers on their lung accumulation and retention, Cancer Biol Med 11(1) (2014) 44-55.
[94] H.A. Khan, R. Shanker, Toxicity of Nanomaterials, Biomed Res Int 2015 (2015) 521014.
[95] M. Mittal, M.R. Siddiqui, K. Tran, S.P. Reddy, A.B. Malik, Reactive oxygen species in inflammation and tissue injury, Antioxid Redox Signal 20(7) (2014) 1126-67.
[96] A.A. Bogdanov, Jr., S. Gupta, N. Koshkina, S.J. Corr, S. Zhang, S.A. Curley, G. Han, Gold nanoparticles stabilized with MPEG-grafted poly(l-lysine): *in vitro* and in vivo evaluation of a potential theranostic agent, Bioconjug Chem 26(1) (2015) 39-50.
[97] X. Wei, B. Shao, Z. He, T. Ye, M. Luo, Y. Sang, X. Liang, W. Wang, S. Luo, S. Yang, S. Zhang, C. Gong, M. Gou, H. Deng, Y. Zhao, H. Yang, S. Deng, C. Zhao, L. Yang, Z. Qian, J. Li, X. Sun, J. Han, C. Jiang, M. Wu, Z. Zhang, Cationic nanocarriers induce cell necrosis through impairment of Na(+)/K(+)-ATPase and cause subsequent inflammatory response, Cell Res 25(2) (2015) 237-53.
[98] Y.M. Gabal, A.O. Kamel, O.A. Sammour, A.H. Elshafeey, Effect of surface charge on the brain delivery of nanostructured lipid carriers in situ gels via the nasal route, Int J Pharm 473(1-2) (2014) 442-57.
[99] A. Kurtz-Chalot, C. Villiers, J. Pourchez, D. Boudard, M. Martini, P.N. Marche, M. Cottier, V. Forest, Impact of silica nanoparticle surface chemistry on protein corona formation and consequential interactions with biological cells, Mater Sci Eng C Mater Biol Appl 75 (2017) 16-24.
[100] Y. Liu, J. Hardie, X. Zhang, V.M. Rotello, Effects of engineered nanoparticles on the innate immune system, Semin Immunol 34 (2017) 25-32.
[101] Y. Zhang, H. Pan, P. Zhang, N. Gao, Y. Lin, Z. Luo, P. Li, C. Wang, L. Liu, D. Pang, L. Cai, Y. Ma, Functionalized quantum dots induce proinflammatory responses in vitro: the role of terminal functional group-associated endocytic pathways, Nanoscale 5(13) (2013)

5919-29.
[102] D. Landesman-Milo, D. Peer, Altering the immune response with lipid-based nanoparticles, J Control Release 161(2) (2012) 600-8.
[103] K.-y. Ng, K.A. Stringer, Z. Cohen, R. Serravo, B. Tian, J.D. Meyer, R. Falk, T. Randolph, M.C. Manning, D.C. Thompson, Alveolar macrophage cell line is not activated by exposure to polymeric microspheres, International journal of pharmaceutics 170(1) (1998) 41-49.
[104] N. Joshi, N. Shirsath, A. Singh, K.S. Joshi, R. Banerjee, Endogenous lung surfactant inspired pH responsive nanovesicle aerosols: pulmonary compatible and site-specific drug delivery in lung metastases, Sci Rep 4 (2014) 7085.
[105] L. Gomes Dos Reis, W.H. Lee, M. Svolos, L.M. Moir, R. Jaber, N. Windhab, P.M. Young, D. Traini, Nanotoxicologic Effects of PLGA Nanoparticles Formulated with a Cell-Penetrating Peptide: Searching for a Safe pDNA Delivery System for the Lungs, Pharmaceutics 11(1) (2019).
[106] S. Uchida, K. Itaka, Q. Chen, K. Osada, T. Ishii, M.A. Shibata, M. Harada-Shiba, K. Kataoka, PEGylated polyplex with optimized PEG shielding enhances gene introduction in lungs by minimizing inflammatory responses, Mol Ther 20(6) (2012) 1196-203.
[107] I.V. Chernikov, V.V. Vlassov, E.L. Chernolovskaya, Current Development of siRNA Bioconjugates: From Research to the Clinic, Front Pharmacol 10 (2019) 444.
[108] J.K. Lam, W. Liang, H.K. Chan, Pulmonary delivery of therapeutic siRNA, Adv Drug Deliv Rev 64(1) (2012) 1-15.
[109] D. Parashar, V. Rajendran, R. Shukla, R. Sistla, Lipid-based nanocarriers for delivery of small interfering RNA for therapeutic use, Eur J Pharm Sci 142 (2020) 105159.
[110] H.Y. Xue, S. Liu, H.L. Wong, Nanotoxicity: a key obstacle to clinical translation of siRNA-based nanomedicine, Nanomedicine (Lond) 9(2) (2014) 295-312.
[111] F. Mastrotto, C. Brazzale, F. Bellato, S. De Martin, G. Grange, M. Mahmoudzadeh, A. Magarkar, A. Bunker, S. Salmaso, P. Caliceti, In Vitro and in Vivo Behavior of Liposomes Decorated with PEGs with Different Chemical Features, Mol Pharm 17(2) (2020) 472-487.
[112] I.V. Chernikov, D.V. Gladkikh, M.I. Meschaninova, A.G. Ven'yaminova, M.A. Zenkova, V.V. Vlassov, E.L. Chernolovskaya, Cholesterol-Containing Nuclease-Resistant siRNA Accumulates in Tumors in a Carrier-free Mode and Silences MDR1 Gene, Mol Ther Nucleic Acids 6 (2017) 209-220.
[113] O.B. Garbuzenko, A. Kuzmov, O. Taratula, S.R. Pine, T. Minko, Strategy to enhance lung cancer treatment by five essential elements: inhalation delivery, nanotechnology, tumor-receptor targeting, chemo- and gene therapy, Theranostics 9(26) (2019) 8362-8376.
[114] A.D. Tagalakis, M.M. Munye, R. Ivanova, H. Chen, C.M. Smith, A.M. Aldossary, L.Z. Rosa, D. Moulding, J.L. Barnes, K.N. Kafetzis, S.A. Jones, D.L. Baines, G.W.J. Moss, C. O'Callaghan, R.J. McAnulty, S.L. Hart, Effective silencing of ENaC by siRNA delivered with epithelial-targeted nanocomplexes in human cystic fibrosis cells and in mouse lung, Thorax 73(9) (2018) 847-856.

[115] M. Otsuka, M. Shiratori, H. Chiba, K. Kuronuma, Y. Sato, Y. Niitsu, H. Takahashi, Treatment of pulmonary fibrosis with siRNA against a collagen-specific chaperone HSP47 in vitamin A-coupled liposomes, Exp Lung Res 43(6-7) (2017) 271-282.
[116] F.E. Ruiz, J.P. Clancy, M.A. Perricone, Z. Bebok, J.S. Hong, S.H. Cheng, D.P. Meeker, K.R. Young, R.A. Schoumacher, M.R. Weatherly, L. Wing, J.E. Morris, L. Sindel, M. Rosenberg, F.W. van Ginkel, J.R. McGhee, D. Kelly, R.K. Lyrene, E.J. Sorscher, A clinical inflammatory syndrome attributable to aerosolized lipid-DNA administration in cystic fibrosis, Hum Gene Ther 12(7) (2001) 751-61.
[117] I. d'Angelo, G. Costabile, E. Durantie, P. Brocca, V. Rondelli, A. Russo, G. Russo, A. Miro, F. Quaglia, A. Petri-Fink, B. Rothen-Rutishauser, F. Ungaro, Hybrid Lipid/Polymer Nanoparticles for Pulmonary Delivery of siRNA: Development and Fate Upon In Vitro Deposition on the Human Epithelial Airway Barrier, J Aerosol Med Pulm Drug Deliv 31(3) (2018) 170-181.
[118] C. Dormenval, A. Lokras, G. Cano-Garcia, A. Wadhwa, K. Thanki, F. Rose, A. Thakur, H. Franzyk, C. Foged, Identification of Factors of Importance for Spray Drying of Small Interfering RNA-Loaded Lipidoid-Polymer Hybrid Nanoparticles for Inhalation, Pharm Res 36(10) (2019) 142.
[119] J.E. Baatz, M.D. Bruno, P.J. Ciraolo, S.W. Glasser, B.R. Stripp, K.L. Smyth, T.R. Korfhagen, Utilization of modified surfactant-associated protein B for delivery of DNA to airway cells in culture, Proc Natl Acad Sci U S A 91(7) (1994) 2547-51.
[120] B. Olmeda, B. García-Álvarez, J. Pérez-Gil, Structure-function correlations of pulmonary surfactant protein SP-B and the saposin-like family of proteins, Eur Biophys J 42(2-3) (2013) 209-22.
[121] M. Martínez-Calle, B. Olmeda, P. Dietl, M. Frick, J. Pérez-Gil, Pulmonary surfactant protein SP-B promotes exocytosis of lamellar bodies in alveolar type II cells, Faseb j 32(8) (2018) 4600-4611.
[122] S.D. Revak, T.A. Merritt, C.G. Cochrane, G.P. Heldt, M.S. Alberts, D.W. Anderson, A. Kheiter, Efficacy of synthetic peptide-containing surfactant in the treatment of respiratory distress syndrome in preterm infant rhesus monkeys, Pediatr Res 39(4 Pt 1) (1996) 715-24.
[123] Y. Qiu, M.Y.T. Chow, W. Liang, W.W.Y. Chung, J.C.W. Mak, J.K.W. Lam, From Pulmonary Surfactant, Synthetic KL4 Peptide as Effective siRNA Delivery Vector for Pulmonary Delivery, Mol Pharm 14(12) (2017) 4606-4617.
[124] T.W.M. Keil, D.P. Feldmann, G. Costabile, Q. Zhong, S. da Rocha, O.M. Merkel, Characterization of spray dried powders with nucleic acid-containing PEI nanoparticles, Eur J Pharm Biopharm 143 (2019) 61-69.
[125] Y. Xie, N.H. Kim, V. Nadithe, D. Schalk, A. Thakur, A. Kılıç, L.G. Lum, D.J.P. Bassett, O.M. Merkel, Targeted delivery of siRNA to activated T cells via transferrin-polyethylenimine (Tf-PEI) as a potential therapy of asthma, J Control Release 229 (2016) 120-129.
[126] O.M. Merkel, A. Beyerle, D. Librizzi, A. Pfestroff, T.M. Behr, B. Sproat, P.J. Barth, T.

Kissel, Nonviral siRNA delivery to the lung: investigation of PEG-PEI polyplexes and their in vivo performance, Mol Pharm 6(4) (2009) 1246-60.
[127] X. Wang, D. Niu, C. Hu, P. Li, Polyethyleneimine-Based Nanocarriers for Gene Delivery, Curr Pharm Des 21(42) (2015) 6140-56.
[128] L. Xue, Y. Yan, P. Kos, X. Chen, D.J. Siegwart, PEI fluorination reduces toxicity and promotes liver-targeted siRNA delivery, Drug Deliv Transl Res (2020).
[129] L. Ding, C. Zhu, F. Yu, P. Wu, G. Chen, A. Ullah, K. Wang, M. Sun, J. Li, D. Oupický, Pulmonary delivery of polyplexes for combined PAI-1 gene silencing and CXCR4 inhibition to treat lung fibrosis, Nanomedicine 14(6) (2018) 1765-1776.
[130] C. Xu, P. Wang, J. Zhang, H. Tian, K. Park, X. Chen, Pulmonary Codelivery of Doxorubicin and siRNA by pH-Sensitive Nanoparticles for Therapy of Metastatic Lung Cancer, Small 11(34) (2015) 4321-33.
[131] V. Capel, D. Vllasaliu, P. Watts, P.A. Clarke, D. Luxton, A.M. Grabowska, G. Mantovani, S. Stolnik, Water-soluble substituted chitosan derivatives as technology platform for inhalation delivery of siRNA, Drug Deliv 25(1) (2018) 644-653.
[132] K. Miwata, H. Okamoto, T. Nakashima, D. Ihara, Y. Horimasu, T. Masuda, S. Miyamoto, H. Iwamoto, K. Fujitaka, H. Hamada, A. Shibata, T. Ito, T. Okuda, N. Hattori, Intratracheal Administration of siRNA Dry Powder Targeting Vascular Endothelial Growth Factor Inhibits Lung Tumor Growth in Mice, Mol Ther Nucleic Acids 12 (2018) 698-706.
[133] O.S. Muddineti, A. Shah, S.V.K. Rompicharla, B. Ghosh, S. Biswas, Cholesterol-grafted chitosan micelles as a nanocarrier system for drug-siRNA co-delivery to the lung cancer cells, Int J Biol Macromol 118(Pt A) (2018) 857-863.
[134] P.Y. Xu, R.K. Kankala, Y.J. Pan, H. Yuan, S.B. Wang, A.Z. Chen, Overcoming multidrug resistance through inhalable siRNA nanoparticles-decorated porous microparticles based on supercritical fluid technology, Int J Nanomedicine 13 (2018) 4685-4698.
[135] P. Mehta, S. Kadam, A. Pawar, C. Bothiraja, Dendrimers for pulmonary delivery: current perspectives and future challenges, New Journal of Chemistry 43(22) (2019) 8396-8409.
[136] V. Dzmitruk, E. Apartsin, A. Ihnatsyeu-Kachan, V. Abashkin, D. Shcharbin, M. Bryszewska, Dendrimers Show Promise for siRNA and microRNA Therapeutics, Pharmaceutics 10(3) (2018).
[137] D.S. Conti, D. Brewer, J. Grashik, S. Avasarala, S.R. da Rocha, Poly(amidoamine) dendrimer nanocarriers and their aerosol formulations for siRNA delivery to the lung epithelium, Mol Pharm 11(6) (2014) 1808-22.
[138] E. Bielski, Q. Zhong, H. Mirza, M. Brown, A. Molla, T. Carvajal, S.R.P. da Rocha, TPP-dendrimer nanocarriers for siRNA delivery to the pulmonary epithelium and their dry powder and metered-dose inhaler formulations, Int J Pharm 527(1-2) (2017) 171-183.
[139] M. Agnoletti, A. Bohr, K. Thanki, F. Wan, X. Zeng, J.P. Boetker, M. Yang, C. Foged, Inhalable siRNA-loaded nano-embedded microparticles engineered using microfluidics and spray drying, Eur J Pharm Biopharm 120 (2017) 9-21.

[140] D.P. Feldmann, Y. Cheng, R. Kandil, Y. Xie, M. Mohammadi, H. Harz, A. Sharma, D.J. Peeler, A. Moszczynska, H. Leonhardt, S.H. Pun, O.M. Merkel, In vitro and in vivo delivery of siRNA via VIPER polymer system to lung cells, J Control Release 276 (2018) 50-58.
[141] Y. Zhao, H. Gao, J. He, C. Jiang, J. Lu, W. Zhang, H. Yang, J. Liu, Co-delivery of LOX-1 siRNA and statin to endothelial cells and macrophages in the atherosclerotic lesions by a dual-targeting core-shell nanoplatform: A dual cell therapy to regress plaques, J Control Release 283 (2018) 241-260.
[142] Y.Y. Cheng, Fluorinated polymers in gene delivery, Acta Polymerica Sinica (2017) 1234-1245.
[143] Z. Li, Y. Wang, Y. Shen, C. Qian, D. Oupicky, M. Sun, Targeting pulmonary tumor microenvironment with CXCR4-inhibiting nanocomplex to enhance anti-PD-L1 immunotherapy, Sci Adv 6(20) (2020) eaaz9240.
[144] T. Singh, A.S.N. Murthy, H.J. Yang, J. Im, Versatility of cell-penetrating peptides for intracellular delivery of siRNA, Drug Deliv 25(1) (2018) 1996-2006.
[145] D.H. Kim, H.J. Park, S. Lim, J.H. Koo, H.G. Lee, J.O. Choi, J.H. Oh, S.J. Ha, M.J. Kang, C.M. Lee, C.G. Lee, J.A. Elias, J.M. Choi, Regulation of chitinase-3-like-1 in T cell elicits Th1 and cytotoxic responses to inhibit lung metastasis, Nat Commun 9(1) (2018) 503.
[146] S.A. Moschos, A.E. Williams, M.A. Lindsay, Cell-penetrating-peptide-mediated siRNA lung delivery, Biochem Soc Trans 35(Pt 4) (2007) 807-10.
[147] Z. Li, G. Chen, L. Ding, Y. Wang, C. Zhu, K. Wang, J. Li, M. Sun, D. Oupicky, Increased Survival by Pulmonary Treatment of Established Lung Metastases with Dual STAT3/CXCR4 Inhibition by siRNA Nanoemulsions, Mol Ther 27(12) (2019) 2100-2110.
[148] Y. Wang, L. Ding, Z. Li, G. Chen, M. Sun, D. Oupicky, Treatment of acute lung injury and early- and late-stage pulmonary fibrosis with combination emulsion siRNA polyplexes, J Control Release 314 (2019) 12-24.
[149] L. Wu, X. Wen, X. Wang, C. Wang, X. Sun, K. Wang, H. Zhang, T. Williams, A.J. Stacy, J. Chen, A.H. Schmieder, G.M. Lanza, B. Shen, Local Intratracheal Delivery of Perfluorocarbon Nanoparticles to Lung Cancer Demonstrated with Magnetic Resonance Multimodal Imaging, Theranostics 8(2) (2018) 563-574.
[150] Y. Yao, M. Zhang, T. Liu, J. Zhou, Y. Gao, Z. Wen, J. Guan, J. Zhu, Z. Lin, D. He, Perfluorocarbon-Encapsulated PLGA-PEG Emulsions as Enhancement Agents for Highly Efficient Reoxygenation to Cell and Organism, ACS Appl Mater Interfaces 7(33) (2015) 18369-78.
[151] N. Butz, C. Porté, H. Courrier, M.P. Krafft, T.F. Vandamme, Reverse water-in-fluorocarbon emulsions for use in pressurized metered-dose inhalers containing hydrofluoroalkane propellants, Int J Pharm 238(1-2) (2002) 257-69.
[152] R.A. Orizondo, C.I. Babcock, M.L. Fabiilli, L. Pavlovsky, J.B. Fowlkes, J.G. Younger, K.E. Cook, Characterization of a reverse-phase perfluorocarbon emulsion for the pulmonary delivery of tobramycin, J Aerosol Med Pulm Drug Deliv 27(5) (2014) 392-9.

[153] S.K. Ferguson, D.I. Pak, J.L. Hopkins, J.W. Harral, K.M. Redinius, Z. Loomis, K.R. Stenmark, M.A. Borden, T. Schroeder, D.C. Irwin, Pre-clinical assessment of a water-in-fluorocarbon emulsion for the treatment of pulmonary vascular diseases, Drug Deliv 26(1) (2019) 147-157.
[154] Y. Jiang, S. Huo, J. Hardie, X.J. Liang, V.M. Rotello, Progress and perspective of inorganic nanoparticle-based siRNA delivery systems, Expert Opin Drug Deliv 13(4) (2016) 547-59.
[155] O. Taratula, O.B. Garbuzenko, A.M. Chen, T. Minko, Innovative strategy for treatment of lung cancer: targeted nanotechnology-based inhalation co-delivery of anticancer drugs and siRNA, J Drug Target 19(10) (2011) 900-14.
[156] A. Frede, B. Neuhaus, T. Knuschke, M. Wadwa, S. Kollenda, R. Klopfleisch, W. Hansen, J. Buer, D. Bruder, M. Epple, A.M. Westendorf, Local delivery of siRNA-loaded calcium phosphate nanoparticles abates pulmonary inflammation, Nanomedicine 13(8) (2017) 2395-2403.
[157] J. Conde, F. Tian, Y. Hernández, C. Bao, D. Cui, K.P. Janssen, M.R. Ibarra, P.V. Baptista, T. Stoeger, J.M. de la Fuente, In vivo tumor targeting via nanoparticle-mediated therapeutic siRNA coupled to inflammatory response in lung cancer mouse models, Biomaterials 34(31) (2013) 7744-53.
[158] C.N. D'Alessandro-Gabazza, T. Kobayashi, D. Boveda-Ruiz, T. Takagi, M. Toda, P. Gil-Bernabe, Y. Miyake, A. Yasukawa, Y. Matsuda, N. Suzuki, H. Saito, Y. Yano, A. Fukuda, T. Hasegawa, H. Toyobuku, S.I. Rennard, P.D. Wagner, J. Morser, Y. Takei, O. Taguchi, E.C. Gabazza, Development and preclinical efficacy of novel transforming growth factor-β1 short interfering RNAs for pulmonary fibrosis, Am J Respir Cell Mol Biol 46(3) (2012) 397-406.
[159] M.P. Zafra, C. Mazzeo, C. Gámez, A. Rodriguez Marco, A. de Zulueta, V. Sanz, I. Bilbao, J. Ruiz-Cabello, J.M. Zubeldia, V. del Pozo, Gene silencing of SOCS3 by siRNA intranasal delivery inhibits asthma phenotype in mice, PLoS One 9(3) (2014) e91996.
[160] M.R. Khaitov, I.P. Shilovskiy, A.A. Nikonova, N.N. Shershakova, O.Y. Kamyshnikov, A.A. Babakhin, V.V. Zverev, S.L. Johnston, R.M. Khaitov, Small interfering RNAs targeted to interleukin-4 and respiratory syncytial virus reduce airway inflammation in a mouse model of virus-induced asthma exacerbation, Hum Gene Ther 25(7) (2014) 642-50.
[161] F.Y. Goh, K.L. Cook, N. Upton, L. Tao, L.C. Lah, B.P. Leung, W.S. Wong, Receptor-interacting protein 2 gene silencing attenuates allergic airway inflammation, J Immunol 191(5) (2013) 2691-9.
[162] X. Zhang, P. Shan, D. Jiang, P.W. Noble, N.G. Abraham, A. Kappas, P.J. Lee, Small interfering RNA targeting heme oxygenase-1 enhances ischemia-reperfusion-induced lung apoptosis, J Biol Chem 279(11) (2004) 10677-84.
[163] M.Y.T. Chow, Y. Qiu, F.F.K. Lo, H.H.S. Lin, H.K. Chan, P.C.L. Kwok, J.K.W. Lam, Inhaled powder formulation of naked siRNA using spray drying technology with l-leucine as dispersion enhancer, Int J Pharm 530(1-2) (2017) 40-52.
[164] T. Ito, T. Okuda, R. Takayama, H. Okamoto, Establishment of an Evaluation Method

for Gene Silencing by Serial Pulmonary Administration of siRNA and pDNA Powders: Naked siRNA Inhalation Powder Suppresses Luciferase Gene Expression in the Lung, J Pharm Sci 108(8) (2019) 2661-2667.
[165] K. Tahara, W. Hashimoto, H. Takeuchi, Inhalation Properties and Stability of Nebulized Naked siRNA Solution for Pulmonary Therapy, Chem Pharm Bull (Tokyo) 64(1) (2016) 63-7.
[166] S. Gharse, J. Fiegel, Large Porous Hollow Particles: Lightweight Champions of Pulmonary Drug Delivery, Curr Pharm Des 22(17) (2016) 2463-9.
[167] F. Ungaro, R. d'Emmanuele di Villa Bianca, C. Giovino, A. Miro, R. Sorrentino, F. Quaglia, M.I. La Rotonda, Insulin-loaded PLGA/cyclodextrin large porous particles with improved aerosolization properties: in vivo deposition and hypoglycaemic activity after delivery to rat lungs, J Control Release 135(1) (2009) 25-34.
[168] B. Patel, N. Gupta, F. Ahsan, Low-molecular-weight heparin (LMWH)-loaded large porous PEG-PLGA particles for the treatment of asthma, J Aerosol Med Pulm Drug Deliv 27(1) (2014) 12-20.
[169] B. Patel, V. Gupta, F. Ahsan, PEG-PLGA based large porous particles for pulmonary delivery of a highly soluble drug, low molecular weight heparin, J Control Release 162(2) (2012) 310-20.
[170] P.J. McKiernan, P. Lynch, J.M. Ramsey, S.A. Cryan, C.M. Greene, Knockdown of Gene Expression in Macrophages by microRNA Mimic-Containing Poly (Lactic-co-glycolic Acid) Microparticles, Medicines (Basel) 5(4) (2018).
[171] Y. Mi, C. Mu, J. Wolfram, Z. Deng, T.Y. Hu, X. Liu, E. Blanco, H. Shen, M. Ferrari, A Micro/Nano Composite for Combination Treatment of Melanoma Lung Metastasis, Adv Healthc Mater 5(8) (2016) 936-46.
[172] H. Lee, D. Zhang, D.L. Laskin, Y. Jin, Functional Evidence of Pulmonary Extracellular Vesicles in Infectious and Noninfectious Lung Inflammation, J Immunol 201(5) (2018) 1500-1509.
[173] H. Lee, D. Zhang, J. Minhas, Y. Jin, Extracellular Vesicles Facilitate the Intercellular Communications in the Pathogenesis of Lung Injury, Cell Dev Biol 5(2) (2016).
[174] B.K. Singh, A.L. Cooney, S. Krishnamurthy, P.L. Sinn, Extracellular Vesicle-Mediated siRNA Delivery, Protein Delivery, and CFTR Complementation in Well-Differentiated Human Airway Epithelial Cells, Genes (Basel) 11(4) (2020).
[175] S.R. Youngren-Ortiz, N.S. Gandhi, L. España-Serrano, M.B. Chougule, Aerosol Delivery of siRNA to the Lungs. Part 2: Nanocarrier-based Delivery Systems, Kona 34 (2017) 44-69.
[176] J. Gottlieb, M.R. Zamora, T. Hodges, A.W. Musk, U. Sommerwerk, D. Dilling, S. Arcasoy, J. DeVincenzo, V. Karsten, S. Shah, B.R. Bettencourt, J. Cehelsky, S. Nochur, J. Gollob, A. Vaishnaw, A.R. Simon, A.R. Glanville, ALN-RSV01 for prevention of bronchiolitis obliterans syndrome after respiratory syncytial virus infection in lung transplant recipients, J Heart Lung Transplant 35(2) (2016) 213-21.
[177] W. Liao, J. Dong, H.Y. Peh, L.H. Tan, K.S. Lim, L. Li, W.F. Wong, Oligonucleotide

Therapy for Obstructive and Restrictive Respiratory Diseases, Molecules 22(1) (2017).
[178] M.E. Ali, A. Lamprecht, Spray freeze drying for dry powder inhalation of nanoparticles, Eur J Pharm Biopharm 87(3) (2014) 510-7.
[179] M.Y. Chow, J.K. Lam, Dry Powder Formulation of Plasmid DNA and siRNA for Inhalation, Curr Pharm Des 21(27) (2015) 3854-66.
[180] D.M. Jensen, D. Cun, M.J. Maltesen, S. Frokjaer, H.M. Nielsen, C. Foged, Spray drying of siRNA-containing PLGA nanoparticles intended for inhalation, J Control Release 142(1) (2010) 138-45.
[181] D.K. Jensen, L.B. Jensen, S. Koocheki, L. Bengtson, D. Cun, H.M. Nielsen, C. Foged, Design of an inhalable dry powder formulation of DOTAP-modified PLGA nanoparticles loaded with siRNA, J Control Release 157(1) (2012) 141-8.
[182] W. Liang, M.Y. Chow, P.N. Lau, Q.T. Zhou, P.C. Kwok, G.P. Leung, A.J. Mason, H.K. Chan, L.L. Poon, J.K. Lam, Inhalable dry powder formulations of siRNA and pH-responsive peptides with antiviral activity against H1N1 influenza virus, Mol Pharm 12(3) (2015) 910-21.
[183] T. Okuda, Y. Suzuki, Y. Kobayashi, T. Ishii, S. Uchida, K. Itaka, K. Kataoka, H. Okamoto, Development of Biodegradable Polycation-Based Inhalable Dry Gene Powders by Spray Freeze Drying, Pharmaceutics 7(3) (2015) 233-54.
[184] D.A. Vishali, J. Monisha, S.K. Sivakamasundari, J.A. Moses, C. Anandharamakrishnan, Spray freeze drying: Emerging applications in drug delivery, J Control Release 300 (2019) 93-101.
[185] J. Wu, L. Wu, F. Wan, J. Rantanen, D. Cun, M. Yang, Effect of thermal and shear stresses in the spray drying process on the stability of siRNA dry powders, Int J Pharm 566 (2019) 32-39.
[186] T. Okuda, M. Morishita, K. Mizutani, A. Shibayama, M. Okazaki, H. Okamoto, Development of spray-freeze-dried siRNA/PEI powder for inhalation with high aerosol performance and strong pulmonary gene silencing activity, J Control Release 279 (2018) 99-113.
[187] M.Y.T. Chow, Y. Qiu, Q. Liao, P.C.L. Kwok, S.F. Chow, H.K. Chan, J.K.W. Lam, High siRNA loading powder for inhalation prepared by co-spray drying with human serum albumin, Int J Pharm 572 (2019) 118818.
[188] P.F. Wu, Z.P. Lu, B.B. Cai, L. Tian, C. Zou, K.R. Jiang, Y. Miao, Role of CXCL12/CXCR4 signaling axis in pancreatic cancer, Chin Med J (Engl) 126(17) (2013) 3371-4.
[189] M.T. Chow, A.D. Luster, Chemokines in cancer, Cancer Immunol Res 2(12) (2014) 1125-31.
[190] B.A. Teicher, S.P. Fricker, CXCL12 (SDF-1)/CXCR4 pathway in cancer, Clin Cancer Res 16(11) (2010) 2927-31.
[191] M. Kucia, R. Reca, K. Miekus, J. Wanzeck, W. Wojakowski, A. Janowska-Wieczorek, J. Ratajczak, M.Z. Ratajczak, Trafficking of normal stem cells and metastasis of cancer stem cells involve similar mechanisms: pivotal role of the SDF-1-CXCR4 axis, Stem Cells

23(7) (2005) 879-94.
[192] Y. Shi, D.J. Riese, 2nd, J. Shen, The Role of the CXCL12/CXCR4/CXCR7 Chemokine Axis in Cancer, Front Pharmacol 11 (2020) 574667.
[193] K. Asifullah, Z. Zhou, W. He, K. Gao, M.W. Khan, R. Faisal, H. Muhammad, M. Sun, CXCR4-Receptor-Targeted Liposomes for the Treatment of Peritoneal Fibrosis, Mol Pharm 16(6) (2019) 2728-2741.
[194] J. Jaffar, K. Griffiths, S. Oveissi, M. Duan, M. Foley, I. Glaspole, K. Symons, L. Organ, G. Westall, CXCR4(+) cells are increased in lung tissue of patients with idiopathic pulmonary fibrosis, Respir Res 21(1) (2020) 221.
[195] C.H. Liu, K.M. Chan, T. Chiang, J.Y. Liu, G.G. Chern, F.F. Hsu, Y.H. Wu, Y.C. Liu, Y. Chen, Dual-Functional Nanoparticles Targeting CXCR4 and Delivering Antiangiogenic siRNA Ameliorate Liver Fibrosis, Mol Pharm 13(7) (2016) 2253-62.
[196] P.Y. Chu, M.S. Joshi, D. Horlock, H. Kiriazis, D.M. Kaye, CXCR4 Antagonism Reduces Cardiac Fibrosis and Improves Cardiac Performance in Dilated Cardiomyopathy, Front Pharmacol 10 (2019) 117.
[197] J. Cao, W. Zhu, D. Yu, L. Pan, L. Zhong, Y. Xiao, Y. Gao, Y. Jiao, Q. Zhang, J. Ji, H. Yang, S. Zhang, J. Cao, The Involvement of SDF-1α/CXCR4 Axis in Radiation-Induced Acute Injury and Fibrosis of Skin, Radiat Res 192(4) (2019) 410-421.
[198] B. Mehrad, M.D. Burdick, D.A. Zisman, M.P. Keane, J.A. Belperio, R.M. Strieter, Circulating peripheral blood fibrocytes in human fibrotic interstitial lung disease, Biochem Biophys Res Commun 353(1) (2007) 104-8.
[199] F. Li, X. Xu, J. Geng, X. Wan, H. Dai, The autocrine CXCR4/CXCL12 axis contributes to lung fibrosis through modulation of lung fibroblast activity, Exp Ther Med 19(3) (2020) 1844-1854.
[200] R. Strippoli, I. Benedicto, M.L. Pérez Lozano, A. Cerezo, M. López-Cabrera, M.A. del Pozo, Epithelial-to-mesenchymal transition of peritoneal mesothelial cells is regulated by an ERK/NF-kappaB/Snail1 pathway, Dis Model Mech 1(4-5) (2008) 264-74.
[201] L. Qin, J. Qin, X. Zhen, Q. Yang, L. Huang, Curcumin protects against hepatic stellate cells activation and migration by inhibiting the CXCL12/CXCR4 biological axis in liver fibrosis：A study in vitro and in vivo, Biomed Pharmacother 101 (2018) 599-607.
[202] Y.C. Sung, Y.C. Liu, P.H. Chao, C.C. Chang, P.R. Jin, T.T. Lin, J.A. Lin, H.T. Cheng, J. Wang, C.P. Lai, L.H. Chen, A.Y. Wu, T.L. Ho, T. Chiang, D.Y. Gao, D.G. Duda, Y. Chen, Combined delivery of sorafenib and a MEK inhibitor using CXCR4-targeted nanoparticles reduces hepatic fibrosis and prevents tumor development, Theranostics 8(4) (2018) 894-905.
[203] J. Xu, A. Mora, H. Shim, A. Stecenko, K.L. Brigham, M. Rojas, Role of the SDF-1/CXCR4 axis in the pathogenesis of lung injury and fibrosis, Am J Respir Cell Mol Biol 37(3) (2007) 291-9.
[204] Z. Liang, W. Zhan, A. Zhu, Y. Yoon, S. Lin, M. Sasaki, J.M. Klapproth, H. Yang, H.E. Grossniklaus, J. Xu, M. Rojas, R.J. Voll, M.M. Goodman, R.F. Arrendale, J. Liu, C.C. Yun, J.P. Snyder, D.C. Liotta, H. Shim, Development of a unique small molecule modulator of

CXCR4, PLoS One 7(4) (2012) e34038.
[205] J.S. Song, C.M. Kang, H.H. Kang, H.K. Yoon, Y.K. Kim, K.H. Kim, H.S. Moon, S.H. Park, Inhibitory effect of CXC chemokine receptor 4 antagonist AMD3100 on bleomycin induced murine pulmonary fibrosis, Exp Mol Med 42(6) (2010) 465-72.
[206] F. Trautmann, M. Cojoc, I. Kurth, N. Melin, L.C. Bouchez, A. Dubrovska, C. Peitzsch, CXCR4 as biomarker for radioresistant cancer stem cells, Int J Radiat Biol 90(8) (2014) 687-99.
[207] X. Yu, D. Wang, X. Wang, S. Sun, Y. Zhang, S. Wang, R. Miao, X. Xu, X. Qu, CXCL12/CXCR4 promotes inflammation-driven colorectal cancer progression through activation of RhoA signaling by sponging miR-133a-3p, J Exp Clin Cancer Res 38(1) (2019) 32.
[208] F. Teng, W.Y. Tian, Y.M. Wang, Y.F. Zhang, F. Guo, J. Zhao, C. Gao, F.X. Xue, Cancer-associated fibroblasts promote the progression of endometrial cancer via the SDF-1/CXCR4 axis, J Hematol Oncol 9 (2016) 8.
[209] H. Shim, S.K. Lau, S. Devi, Y. Yoon, H.T. Cho, Z. Liang, Lower expression of CXCR4 in lymph node metastases than in primary breast cancers: potential regulation by ligand-dependent degradation and HIF-1alpha, Biochem Biophys Res Commun 346(1) (2006) 252-8.
[210] A.J. Wagstaff, Plerixafor: in patients with non-Hodgkin's lymphoma or multiple myeloma, Drugs 69(3) (2009) 319-26.
[211] Y. Chen, R.R. Ramjiawan, T. Reiberger, M.R. Ng, T. Hato, Y. Huang, H. Ochiai, S. Kitahara, E.C. Unan, T.P. Reddy, C. Fan, P. Huang, N. Bardeesy, A.X. Zhu, R.K. Jain, D.G. Duda, CXCR4 inhibition in tumor microenvironment facilitates anti-programmed death receptor-1 immunotherapy in sorafenib-treated hepatocellular carcinoma in mice, Hepatology 61(5) (2015) 1591-602.
[212] I.X. Chen, V.P. Chauhan, J. Posada, M.R. Ng, M.W. Wu, P. Adstamongkonkul, P. Huang, N. Lindeman, R. Langer, R.K. Jain, Blocking CXCR4 alleviates desmoplasia, increases T-lymphocyte infiltration, and improves immunotherapy in metastatic breast cancer, Proc Natl Acad Sci U S A 116(10) (2019) 4558-4566.
[213] E.A. Sison, D. Magoon, L. Li, C.E. Annesley, B. Romagnoli, G.J. Douglas, G. Tuffin, J. Zimmermann, P. Brown, POL5551, a novel and potent CXCR4 antagonist, enhances sensitivity to chemotherapy in pediatric ALL, Oncotarget 6(31) (2015) 30902-18.
[214] N. Zheng, W. Liu, B. Li, H. Nie, J. Liu, Y. Cheng, J. Wang, H. Dong, L. Jia, Co-delivery of sorafenib and metapristone encapsulated by CXCR4-targeted PLGA-PEG nanoparticles overcomes hepatocellular carcinoma resistance to sorafenib, J Exp Clin Cancer Res 38(1) (2019) 232.
[215] H. Zhu, T. Li, Y. Du, M. Li, Pancreatic cancer: challenges and opportunities, BMC Med 16(1) (2018) 214.
[216] A. Vincent, J. Herman, R. Schulick, R.H. Hruban, M. Goggins, Pancreatic cancer, Lancet 378(9791) (2011) 607-20.
[217] J. Kokkinos, R.M.C. Ignacio, G. Sharbeen, C. Boyer, E. Gonzales-Aloy, D. Goldstein,

A. Australian Pancreatic Cancer Genome Initiative, J.A. McCarroll, P.A. Phillips, Targeting the undruggable in pancreatic cancer using nano-based gene silencing drugs, Biomaterials 240 (2020) 119742.
[218] R. Xue, K. Jia, J. Wang, L. Yang, Y. Wang, L. Gao, J. Hao, A Rising Star in Pancreatic Diseases: Pancreatic Stellate Cells, Front Physiol 9 (2018) 754.
[219] P. Edwards, B.W. Kang, I. Chau, Targeting the Stroma in the Management of Pancreatic Cancer, Front Oncol 11 (2021) 691185.
[220] S. Vasseur, R. Tomasini, R. Tournaire, J.L. Iovanna, Hypoxia induced tumor metabolic switch contributes to pancreatic cancer aggressiveness, Cancers (Basel) 2(4) (2010) 2138-52.
[221] A.M. Waters, C.J. Der, KRAS: The Critical Driver and Therapeutic Target for Pancreatic Cancer, Cold Spring Harb Perspect Med 8(9) (2018).
[222] Y. Lei, L. Tang, Y. Xie, Y. Xianyu, L. Zhang, P. Wang, Y. Hamada, K. Jiang, W. Zheng, X. Jiang, Gold nanoclusters-assisted delivery of NGF siRNA for effective treatment of pancreatic cancer, Nat Commun 8 (2017) 15130.
[223] B. Hu, Y. Weng, X.H. Xia, X.J. Liang, Y. Huang, Clinical advances of siRNA therapeutics, J Gene Med 21(7) (2019) e3097.
[224] F. Mainini, M.R. Eccles, Lipid and Polymer-Based Nanoparticle siRNA Delivery Systems for Cancer Therapy, Molecules 25(11) (2020).
[225] A.D. Miller, Lipid-based nanoparticles in cancer diagnosis and therapy, J Drug Deliv 2013 (2013) 165981.
[226] D.K. Sung, W.H. Kong, K. Park, J.H. Kim, M.Y. Kim, H. Kim, S.K. Hahn, Noncovalenly PEGylated CTGF siRNA/PDMAEMA complex for pulmonary treatment of bleomycin-induced lung fibrosis, Biomaterials 34(4) (2013) 1261-9.
[227] P.O. Yoon, J.W. Park, C.M. Lee, S.H. Kim, H.N. Kim, Y. Ko, S.J. Bae, S. Yun, J.H. Park, T. Kwon, W.S. Kim, J. Lee, Q. Lu, H.R. Kang, W.K. Cho, J.A. Elias, J.S. Yang, H.O. Park, K. Lee, C.G. Lee, Self-assembled Micelle Interfering RNA for Effective and Safe Targeting of Dysregulated Genes in Pulmonary Fibrosis, J Biol Chem 291(12) (2016) 6433-46.
[228] Z. Ju, J. Ma, C. Wang, J. Yu, Y. Qiao, F. Hei, Exosomes from iPSCs Delivering siRNA Attenuate Intracellular Adhesion Molecule-1 Expression and Neutrophils Adhesion in Pulmonary Microvascular Endothelial Cells, Inflammation 40(2) (2017) 486-496.
[229] G. Shim, H.W. Choi, S. Lee, J. Choi, Y.H. Yu, D.E. Park, Y. Choi, C.W. Kim, Y.K. Oh, Enhanced intrapulmonary delivery of anticancer siRNA for lung cancer therapy using cationic ethylphosphocholine-based nanolipoplexes, Mol Ther 21(4) (2013) 816-24.
[230] M.D.I. Manunta, A.D. Tagalakis, M. Attwood, A.M. Aldossary, J.L. Barnes, M.M. Munye, A. Weng, R.J. McAnulty, S.L. Hart, Delivery of ENaC siRNA to epithelial cells mediated by a targeted nanocomplex: a therapeutic strategy for cystic fibrosis, Sci Rep 7(1) (2017) 700.
[231] C. Ge, J. Yang, S. Duan, Y. Liu, F. Meng, L. Yin, Fluorinated α-Helical Polypeptides Synchronize Mucus Permeation and Cell Penetration toward Highly Efficient Pulmonary

siRNA Delivery against Acute Lung Injury, Nano Lett 20(3) (2020) 1738-1746.
[232] B. Oh, M. Lee, Combined delivery of HMGB-1 box A peptide and S1PLyase siRNA in animal models of acute lung injury, J Control Release 175 (2014) 25-35.
[233] S. Das, M. Kumar, V. Negi, B. Pattnaik, Y.S. Prakash, A. Agrawal, B. Ghosh, MicroRNA-326 regulates profibrotic functions of transforming growth factor-β in pulmonary fibrosis, Am J Respir Cell Mol Biol 50(5) (2014) 882-92.
[234] J. Dong, W. Liao, L.H. Tan, A. Yong, W.Y. Peh, W.S.F. Wong, Gene silencing of receptor-interacting protein 2 protects against cigarette smoke-induced acute lung injury, Pharmacol Res 139 (2019) 560-568.
[235] Y. Asai-Tajiri, K. Matsumoto, S. Fukuyama, O.K. Kan, T. Nakano, K. Tonai, T. Ohno, M. Azuma, H. Inoue, Y. Nakanishi, Small interfering RNA against CD86 during allergen challenge blocks experimental allergic asthma, Respir Res 15(1) (2014) 132.
[236] W. Wu, H. Chen, Y.M. Li, S.Y. Wang, X. Diao, K.G. Liu, Intranasal sirna targeting c-kit reduces airway inflammation in experimental allergic asthma, Int J Clin Exp Pathol 7(9) (2014) 5505-14.
[237] W.A. Wuyts, M. Wijsenbeek, B. Bondue, D. Bouros, P. Bresser, C.R. Cordeiro, O. Hilberg, J. Magnusson, E.D. Manali, A. Morais, Idiopathic pulmonary fibrosis: Best practice in monitoring and managing a relentless fibrotic disease, Respiration 99(1) (2020) 73-82.
[238] C. Zhang, Z. Wu, J.W. Li, K. Tan, W. Yang, H. Zhao, G.Q. Wang, Discharge may not be the end of treatment: Pay attention to pulmonary fibrosis caused by severe COVID-19, J Med Virol (2020).
[239] P.M. George, A.U. Wells, R.G. Jenkins, Pulmonary fibrosis and COVID-19: the potential role for antifibrotic therapy, Lancet Respir Med 8(8) (2020) 807-815.
[240] Y.-S. Kim, H. Cha, H.-J. Kim, J.-M. Cho, H.-R. Kim, The Anti-Fibrotic Effects of CG-745, an HDAC Inhibitor, in Bleomycin and PHMG-Induced Mouse Models, Molecules 24(15) (2019) 2792.
[241] X. Chen, H. Xu, J. Hou, H. Wang, Y. Zheng, H. Li, H. Cai, X. Han, J. Dai, Epithelial cell senescence induces pulmonary fibrosis through Nanog-mediated fibroblast activation, Aging (Albany NY) 12(1) (2020) 242.
[242] M. Selman, A. Pardo, Idiopathic pulmonary fibrosis: an epithelial/fibroblastic cross-talk disorder, Respiratory research 3(1) (2001) 1-8.
[243] T.M. Maher, M.E. Strek, Antifibrotic therapy for idiopathic pulmonary fibrosis: time to treat, Respiratory research 20(1) (2019) 1-9.
[244] L. Wollin, E. Wex, A. Pautsch, G. Schnapp, K.E. Hostettler, S. Stowasser, M. Kolb, Mode of action of nintedanib in the treatment of idiopathic pulmonary fibrosis, European Respiratory Journal 45(5) (2015) 1434-1445.
[245] J. Milara, B. Ballester, A. Morell, J.L. Ortiz, J. Escrivá, E. Fernández, F. Perez-Vizcaino, A. Cogolludo, E. Pastor, E. Artigues, E. Morcillo, J. Cortijo, JAK2 mediates lung fibrosis, pulmonary vascular remodelling and hypertension in idiopathic pulmonary fibrosis: an experimental study, Thorax 73(6) (2018) 519-529.
[246] J. Tao, M. Zhang, Z. Wen, B. Wang, L. Zhang, Y. Ou, X. Tang, X. Yu, Q. Jiang,

Inhibition of EP300 and DDR1 synergistically alleviates pulmonary fibrosis in vitro and in vivo, Biomed Pharmacother 106 (2018) 1727-1733.
[247] R. Tian, Y. Zhu, J. Yao, X. Meng, J. Wang, H. Xie, R. Wang, NLRP3 participates in the regulation of EMT in bleomycin-induced pulmonary fibrosis, Exp Cell Res 357(2) (2017) 328-334.
[248] J. DeVincenzo, R. Lambkin-Williams, T. Wilkinson, J. Cehelsky, S. Nochur, E. Walsh, R. Meyers, J. Gollob, A. Vaishnaw, A randomized, double-blind, placebo-controlled study of an RNAi-based therapy directed against respiratory syncytial virus, Proc Natl Acad Sci U S A 107(19) (2010) 8800-8805.
[249] L. Ding, S. Tang, T.A. Wyatt, D.L. Knoell, D. Oupický, Pulmonary siRNA delivery for lung disease: Review of recent progress and challenges, J Control Release 330 (2021) 977-991.
[250] R.A. Day, D.A. Estabrook, C. Wu, J.O. Chapman, A.J. Togle, E.M. Sletten, Systematic Study of Perfluorocarbon Nanoemulsions Stabilized by Polymer Amphiphiles, ACS Appl Mater Interfaces 12(35) (2020) 38887-38898.
[251] D.A. Estabrook, A.F. Ennis, R.A. Day, E.M. Sletten, Controlling nanoemulsion surface chemistry with poly(2-oxazoline) amphiphiles, Chem. Sci. 10(14) (2019) 3994-4003.
[252] X. Liang, M. Chen, P. Bhattarai, S. Hameed, Z. Dai, Perfluorocarbon@Porphyrin Nanoparticles for Tumor Hypoxia Relief to Enhance Photodynamic Therapy against Liver Metastasis of Colon Cancer, ACS Nano 14(10) (2020) 13569-13583.
[253] X. Ma, M. Yao, J. Shi, X. Li, Y. Gao, Q. Luo, R. Hou, X. Liang, F. Wang, High Intensity Focused Ultrasound-Responsive and Ultrastable Cerasomal Perfluorocarbon Nanodroplets for Alleviating Tumor Multidrug Resistance and Epithelial-Mesenchymal Transition, ACS Nano 14(11) (2020) 15904-15918.
[254] X. Li, F. Qin, L. Yang, L. Mo, L. Li, L. Hou, Sulfatide-containing lipid perfluorooctylbromide nanoparticles as paclitaxel vehicles targeting breast carcinoma, International journal of nanomedicine 9 (2014) 3971.
[255] R.A. Day, E.M. Sletten, Perfluorocarbon nanomaterials for photodynamic therapy For Nanobubbles and nanodroplets issue, Current Opinion in Colloid & Interface Science (2021) 101454.
[256] R.M. Strieter, B.N. Gomperts, M.P. Keane, The role of CXC chemokines in pulmonary fibrosis, The Journal of clinical investigation 117(3) (2007) 549-556.
[257] G. Burgstaller, B. Oehrle, M. Gerckens, E.S. White, H.B. Schiller, O. Eickelberg, The instructive extracellular matrix of the lung: basic composition and alterations in chronic lung disease, European Respiratory Journal 50(1) (2017).
[258] K. Griffiths, D. Habiel, J. Jaffar, U. Binder, W. Darby, C. Hosking, A. Skerra, G. Westall, C. Hogaboam, M. Foley, Anti-fibrotic effects of CXCR4-targeting i-body AD-114 in preclinical models of pulmonary fibrosis, Scientific reports 8(1) (2018) 1-15.
[259] J. Xu, A. Mora, H. Shim, A. Stecenko, K.L. Brigham, M. Rojas, Role of the SDF-1/CXCR4 axis in the pathogenesis of lung injury and fibrosis, American journal of

respiratory cell and molecular biology 37(3) (2007) 291-299.
[260] J. Jaffar, K. Griffiths, S. Oveissi, M. Duan, M. Foley, I. Glaspole, K. Symons, L. Organ, G. Westall, CXCR4+ cells are increased in lung tissue of patients with idiopathic pulmonary fibrosis, Respiratory Research 21(1) (2020) 1-16.
[261] D. Chakraborty, B. Šumová, T. Mallano, C.-W. Chen, A. Distler, C. Bergmann, I. Ludolph, R.E. Horch, K. Gelse, A. Ramming, Activation of STAT3 integrates common profibrotic pathways to promote fibroblast activation and tissue fibrosis, Nature communications 8(1) (2017) 1-16.
[262] A. Xiong, Z. Yang, Y. Shen, J. Zhou, Q. Shen, Transcription factor STAT3 as a novel molecular target for cancer prevention, Cancers 6(2) (2014) 926-957.
[263] J. Milara, G. Hernandez, B. Ballester, A. Morell, I. Roger, P. Montero, J. Escrivá, J.M. Lloris, M. Molina-Molina, E. Morcillo, The JAK2 pathway is activated in idiopathic pulmonary fibrosis, Respiratory research 19(1) (2018) 24.
[264] Y. Wang, J. Li, Y. Chen, D. Oupický, Balancing polymer hydrophobicity for ligand presentation and siRNA delivery in dual function CXCR4 inhibiting polyplexes, Biomater Sci 3(7) (2015) 1114-23.
[265] Y. Xie, Y. Wang, J. Li, Y. Hang, L. Jaramillo, C.J. Wehrkamp, M.A. Phillippi, A.M. Mohr, Y. Chen, G.A. Talmon, J.L. Mott, D. Oupický, Cholangiocarcinoma therapy with nanoparticles that combine downregulation of MicroRNA-210 with inhibition of cancer cell invasiveness, Theranostics 8(16) (2018) 4305-4320.
[266] T.A. Wyatt, K.L. Bailey, S.M. Simet, K.J. Warren, J.M. Sweeter, J.M. DeVasure, J.A. Pavlik, J.H. Sisson, Alcohol potentiates RSV-mediated injury to ciliated airway epithelium, Alcohol 80 (2019) 17-24.
[267] M.E. Price, A.J. Case, J.A. Pavlik, J.M. DeVasure, T.A. Wyatt, M.C. Zimmerman, J.H. Sisson, S-nitrosation of protein phosphatase 1 mediates alcohol-induced ciliary dysfunction, Sci Rep 8(1) (2018) 9701.
[268] X. Li, Z. Sui, X. Li, W. Xu, Q. Guo, J. Sun, F. Jing, Perfluorooctylbromide nanoparticles for ultrasound imaging and drug delivery, International journal of nanomedicine 13 (2018) 3053.
[269] Y. Xie, Y. Hang, Y. Wang, R. Sleightholm, D.R. Prajapati, J. Bader, A. Yu, W. Tang, L. Jaramillo, J. Li, R.K. Singh, D. Oupický, Stromal Modulation and Treatment of Metastatic Pancreatic Cancer with Local Intraperitoneal Triple miRNA/siRNA Nanotherapy, ACS Nano 14(1) (2020) 255-271.
[270] Y. Wang, S.T. Hazeldine, J. Li, D. Oupicky, Development of Functional Poly(amido amine) CXCR4 Antagonists with the Ability to Mobilize Leukocytes and Deliver Nucleic Acids, Adv Healthc Mater 4(5) (2015) 729-38.
[271] J. Li, D. Oupický, Effect of biodegradability on CXCR4 antagonism, transfection efficacy and antimetastatic activity of polymeric Plerixafor, Biomaterials 35(21) (2014) 5572-9.
[272] J. Li, Y. Zhu, S.T. Hazeldine, C. Li, D. Oupicky, Dual-function CXCR4 antagonist polyplexes to deliver gene therapy and inhibit cancer cell invasion, Angew. Chem. Int. Ed.

Engl. 51(35) (2012) 8740-3.
[273] Y. Wang, S. Kumar, S. Rachagani, B.R. Sajja, Y. Xie, Y. Hang, M. Jain, J. Li, M.D. Boska, S.K. Batra, D. Oupicky, Polyplex-mediated inhibition of chemokine receptor CXCR4 and chromatin-remodeling enzyme NCOA3 impedes pancreatic cancer progression and metastasis, Biomaterials 101 (2016) 108-120.
[274] R. Guagliardo, L. Herman, J. Penders, A. Zamborlin, H. De Keersmaecker, T. Van de Vyver, S. Verstraeten, P. Merckx, M.P. Mingeot-Leclercq, M. Echaide, J. Pérez-Gil, M.M. Stevens, S.C. De Smedt, K. Raemdonck, Surfactant Protein B Promotes Cytosolic SiRNA Delivery by Adopting a Virus-like Mechanism of Action, ACS Nano 15(5) (2021) 8095-8109.
[275] Q. Lu, A.H. El-Hashash, Cell-based therapy for idiopathic pulmonary fibrosis, Stem Cell Investigation 6 (2019).
[276] R.T. Kendall, C.A. Feghali-Bostwick, Fibroblasts in fibrosis: novel roles and mediators, Frontiers in pharmacology 5 (2014) 123.
[277] K. Kis, X. Liu, J.S. Hagood, Myofibroblast differentiation and survival in fibrotic disease, Expert reviews in molecular medicine 13 (2011) e27.
[278] D.V. Pechkovsky, C.M. Prêle, J. Wong, C.M. Hogaboam, R.J. McAnulty, G.J. Laurent, S.S.-M. Zhang, M. Selman, S.E. Mutsaers, D.A. Knight, STAT3-mediated signaling dysregulates lung fibroblast-myofibroblast activation and differentiation in UIP/IPF, The American journal of pathology 180(4) (2012) 1398-1412.
[279] O.M. Merkel, I. Rubinstein, T. Kissel, siRNA delivery to the lung: what's new?, Advanced drug delivery reviews 75 (2014) 112-128.
[280] L. Nuhn, S. Van Herck, A. Best, K. Deswarte, M. Kokkinopoulou, I. Lieberwirth, K. Koynov, B.N. Lambrecht, B.G. De Geest, FRET Monitoring of Intracellular Ketal Hydrolysis in Synthetic Nanoparticles, Angew Chem Int Ed Engl 57(33) (2018) 10760-10764.
[281] C.R. Navarrette, J.H. Sisson, E. Nance, D. Allen-Gipson, J. Hanes, T.A. Wyatt, Particulate matter in cigarette smoke increases ciliary axoneme beating through mechanical stimulation, J Aerosol Med Pulm Drug Deliv 25(3) (2012) 159-68.
[282] J.F. Ellena, V.V. Obraztsov, V.L. Cumbea, C.M. Woods, D.S. Cafiso, Perfluorooctyl bromide has limited membrane solubility and is located at the bilayer center. Locating small molecules in lipid bilayers through paramagnetic enhancements of NMR relaxation, Journal of medicinal chemistry 45(25) (2002) 5534-5542.
[283] S. Min-hong, J. Ning, L. Hong-tao, W. Zhen-guo, X. Yu-fen, Z. Xiao-bin, T. Chang-li, H. Jin, Intraperitoneal injection of bleomycin induces pulmonary fibrosis in mice: a long-term stability evaluation, Chinese Journal of Tissue Engineering Research 21(4) (2017) 512.
[284] M. Wilson, T. Wynn, Pulmonary fibrosis: pathogenesis, etiology and regulation, Mucosal immunology 2(2) (2009) 103.
[285] C. Dees, S. Pötter, Y. Zhang, C. Bergmann, X. Zhou, M. Luber, T. Wohlfahrt, E. Karouzakis, A. Ramming, K. Gelse, TGF-β–induced epigenetic deregulation of SOCS3 facilitates STAT3 signaling to promote fibrosis, The Journal of Clinical Investigation 130(5)

(2020).
[286] F. Salton, M.C. Volpe, M. Confalonieri, Epithelial–Mesenchymal Transition in the Pathogenesis of Idiopathic Pulmonary Fibrosis, Medicina 55(4) (2019) 83.
[287] P. Rawla, T. Sunkara, V. Gaduputi, Epidemiology of Pancreatic Cancer: Global Trends, Etiology and Risk Factors, World J Oncol 10(1) (2019) 10-27.
[288] A. Adamska, A. Domenichini, M. Falasca, Pancreatic ductal adenocarcinoma: current and evolving therapies, International journal of molecular sciences 18(7) (2017) 1338.
[289] W. Wang, L. Li, N. Chen, C. Niu, Z. Li, J. Hu, J. Cui, Nerves in the Tumor Microenvironment: Origin and Effects, Frontiers in Cell and Developmental Biology 8 (2020) 1630.
[290] R.D. Cervantes-Villagrana, D. Albores-García, A.R. Cervantes-Villagrana, S.J. García-Acevez, Tumor-induced neurogenesis and immune evasion as targets of innovative anti-cancer therapies, Signal transduction and targeted therapy 5(1) (2020) 1-23.
[291] R.A. Bradshaw, J. Pundavela, J. Biarc, R.J. Chalkley, A. Burlingame, H. Hondermarck, NGF and ProNGF: Regulation of neuronal and neoplastic responses through receptor signaling, Advances in biological regulation 58 (2015) 16-27.
[292] N.H. Molloy, D.E. Read, A.M. Gorman, Nerve growth factor in cancer cell death and survival, Cancers 3(1) (2011) 510-530.
[293] M. Llovera, Y. De Pablo, J. Egea, M. Encinas, S. Peiró, D. Martín-Zanca, N. Rocamora, J.X. Comella, Trk is a calmodulin-binding protein: implications for receptor processing, Journal of neurochemistry 88(2) (2004) 422-433.
[294] Y. Lei, L. Tang, Y. Xie, Y. Xianyu, L. Zhang, P. Wang, Y. Hamada, K. Jiang, W. Zheng, X. Jiang, Gold nanoclusters-assisted delivery of NGF siRNA for effective treatment of pancreatic cancer, Nature communications 8(1) (2017) 1-15.
[295] Z.W. Zhu, H. Friess, L. Wang, T. Bogardus, M. Korc, J. Kleeff, M.W. Büchler, Nerve growth factor exerts differential effects on the growth of human pancreatic cancer cells, Clin Cancer Res 7(1) (2001) 105-12.
[296] R.S. Banh, D.E. Biancur, K. Yamamoto, A.S.W. Sohn, B. Walters, M. Kuljanin, A. Gikandi, H. Wang, J.D. Mancias, R.J. Schneider, M.E. Pacold, A.C. Kimmelman, Neurons Release Serine to Support mRNA Translation in Pancreatic Cancer, Cell 183(5) (2020) 1202-1218.e25.
[297] Y. Xie, Y. Hang, Y. Wang, R. Sleightholm, D.R. Prajapati, J. Bader, A. Yu, W. Tang, L. Jaramillo, J. Li, Stromal modulation and treatment of metastatic pancreatic cancer with local intraperitoneal triple miRNA/siRNA nanotherapy, ACS nano 14(1) (2020) 255-271.
[298] R.L. Sleightholm, B.K. Neilsen, J. Li, M.M. Steele, R.K. Singh, M.A. Hollingsworth, D. Oupicky, Emerging roles of the CXCL12/CXCR4 axis in pancreatic cancer progression and therapy, Pharmacol. Ther. 179 (2017) 158-170.
[299] J. Zhang, C. Liu, X. Mo, H. Shi, S. Li, Mechanisms by which CXCR4/CXCL12 cause metastatic behavior in pancreatic cancer, Oncology letters 15(2) (2018) 1771-1776.

[300] X. Sun, G. Cheng, M. Hao, J. Zheng, X. Zhou, J. Zhang, R.S. Taichman, K.J. Pienta, J. Wang, CXCL12/CXCR4/CXCR7 chemokine axis and cancer progression, Cancer and Metastasis Reviews 29(4) (2010) 709-722.
[301] Y. Hang, S. Tang, W. Tang, D. Větvička, C. Zhang, Y. Xie, F. Yu, A. Yu, D. Sil, J. Li, Polycation fluorination improves intraperitoneal siRNA delivery in metastatic pancreatic cancer, Journal of Controlled Release 333 (2021) 139-150.
[302] Z. Lu, J. Wang, M.G. Wientjes, J.L. Au, Intraperitoneal therapy for peritoneal cancer, Future oncology 6(10) (2010) 1625-1641.
[303] H. Sun, D. Zhang, C. Huang, Y. Guo, Z. Yang, N. Yao, X. Dong, R. Cheng, N. Zhao, J. Meng, B. Sun, J. Hao, Hypoxic microenvironment induced spatial transcriptome changes in pancreatic cancer, Cancer Biol Med 18(2) (2021) 616-30.
[304] I. Mäger, K. Langel, T. Lehto, E. Eiríksdóttir, Ü. Langel, The role of endocytosis on the uptake kinetics of luciferin-conjugated cell-penetrating peptides, Biochimica et Biophysica Acta (BBA)-Biomembranes 1818(3) (2012) 502-511.
[305] Y. Feng, S. Yu, T.K. Lasell, A.P. Jadhav, E. Macia, P. Chardin, P. Melancon, M. Roth, T. Mitchison, T. Kirchhausen, Exo1: a new chemical inhibitor of the exocytic pathway, Proc Natl Acad Sci U S A 100(11) (2003) 6469-74.
[306] S. Descamps, R.A. Toillon, E. Adriaenssens, V. Pawlowski, S.M. Cool, V. Nurcombe, X. Le Bourhis, B. Boilly, J.P. Peyrat, H. Hondermarck, Nerve growth factor stimulates proliferation and survival of human breast cancer cells through two distinct signaling pathways, J Biol Chem 276(21) (2001) 17864-70.
[307] N.H. Molloy, D.E. Read, A.M. Gorman, Nerve growth factor in cancer cell death and survival, Cancers (Basel) 3(1) (2011) 510-30.
[308] M. Abraham, S. Klein, B. Bulvik, H. Wald, I.D. Weiss, D. Olam, L. Weiss, K. Beider, O. Eizenberg, O. Wald, E. Galun, A. Avigdor, O. Benjamini, A. Nagler, Y. Pereg, S. Tavor, A. Peled, The CXCR4 inhibitor BL-8040 induces the apoptosis of AML blasts by downregulating ERK, BCL-2, MCL-1 and cyclin-D1 via altered miR-15a/16-1 expression, Leukemia 31(11) (2017) 2336-2346.
[309] W.W. Tseng, D. Winer, J.A. Kenkel, O. Choi, A.H. Shain, J.R. Pollack, R. French, A.M. Lowy, E.G. Engleman, Development of an orthotopic model of invasive pancreatic cancer in an immunocompetent murine host, Clin Cancer Res 16(14) (2010) 3684-95.
[310] M.P. Torres, S. Rachagani, J.J. Souchek, K. Mallya, S.L. Johansson, S.K. Batra, Novel pancreatic cancer cell lines derived from genetically engineered mouse models of spontaneous pancreatic adenocarcinoma: applications in diagnosis and therapy, PLoS One 8(11) (2013) e80580.
[311] G.R. Dakwar, M. Shariati, W. Willaert, W. Ceelen, S.C. De Smedt, K. Remaut, Nanomedicine-based intraperitoneal therapy for the treatment of peritoneal carcinomatosis—Mission possible?, Advanced drug delivery reviews 108 (2017) 13-24.
[312] W. Yuan, D. Yang, Q. Su, X. Zhu, T. Cao, Y. Sun, Y. Dai, W. Feng, F. Li, Intraperitoneal administration of biointerface-camouflaged upconversion nanoparticles for contrast enhanced imaging of pancreatic cancer, Advanced Functional Materials 26(47)

(2016) 8631-8642.
[313] S. Suklabaidya, P. Dash, B. Das, V. Suresh, P.K. Sasmal, S. Senapati, Experimental models of pancreatic cancer desmoplasia, Laboratory Investigation 98(1) (2018) 27-40.
[314] P. Shah, D. Bhalodia, P. Shelat, Nanoemulsion: a pharmaceutical review, Systematic Reviews in Pharmacy 1(1) (2010).
[315] N.D. Ebelt, V. Zamloot, E.R. Manuel, Targeting desmoplasia in pancreatic cancer as an essential first step to effective therapy, Oncotarget 11(38) (2020) 3486.
[316] M.F. Flessner, The transport barrier in intraperitoneal therapy, American Journal of Physiology-Renal Physiology 288(3) (2005) F433-F442.
[317] K. Aoki, S. Furuhata, K. Hatanaka, M. Maeda, J.-S. Remy, J. Behr, M. Terada, T. Yoshida, Polyethylenimine-mediated gene transfer into pancreatic tumor dissemination in the murine peritoneal cavity, Gene Therapy 8(7) (2001) 508-514.
[318] S. Salatin, S. Maleki Dizaj, A. Yari Khosroushahi, Effect of the surface modification, size, and shape on cellular uptake of nanoparticles, Cell biology international 39(8) (2015) 881-890.
[319] S. Han, B. Kang, E. Jang, J. Ki, E. Kim, M.Y. Jeong, Y.M. Huh, H.Y. Son, S. Haam, Convenient Monitoring System of Intracellular microRNA Expression during Adipogenesis via Mechanical Stimulus-Induced Exocytosis of Lipovesicular miRNA Beacon, Adv Healthc Mater 7(5) (2018).
[320] M. Ayres Pereira, I.I.C. Chio, Metastasis in pancreatic ductal adenocarcinoma: Current standing and methodologies, Genes 11(1) (2020) 6.
[321] E. Tezel, K. Hibi, T. Nagasaka, A. Nakao, PGP9.5 as a prognostic factor in pancreatic cancer, Clin Cancer Res 6(12) (2000) 4764-7.
[322] J. Pundavela, S. Roselli, S. Faulkner, J. Attia, R.J. Scott, R.F. Thorne, J.F. Forbes, R.A. Bradshaw, M.M. Walker, P. Jobling, H. Hondermarck, Nerve fibers infiltrate the tumor microenvironment and are associated with nerve growth factor production and lymph node invasion in breast cancer, Mol Oncol 9(8) (2015) 1626-35.
[323] X. Tan, S. Sivakumar, J. Bednarsch, G. Wiltberger, J.N. Kather, J. Niehues, J. de Vos-Geelen, L. Valkenburg-van Iersel, S. Kintsler, A. Roeth, G. Hao, S. Lang, M.E. Coolsen, M. den Dulk, M.R. Aberle, J. Koolen, N.T. Gaisa, S.W.M. Olde Damink, U.P. Neumann, L.R. Heij, Nerve fibers in the tumor microenvironment in neurotropic cancer-pancreatic cancer and cholangiocarcinoma, Oncogene 40(5) (2021) 899-908.
[324] Q. Xu, Z. Wang, X. Chen, W. Duan, J. Lei, L. Zong, X. Li, L. Sheng, J. Ma, L. Han, W. Li, L. Zhang, K. Guo, Z. Ma, Z. Wu, E. Wu, Q. Ma, Stromal-derived factor-1α/CXCL12-CXCR4 chemotactic pathway promotes perineural invasion in pancreatic cancer, Oncotarget 6(7) (2015) 4717-32.
[325] Q. Xu, Z. Wang, X. Chen, W. Duan, J. Lei, L. Zong, X. Li, L. Sheng, J. Ma, L. Han, Stromal-derived factor-1α/CXCL12-CXCR4 chemotactic pathway promotes perineural invasion in pancreatic cancer, Oncotarget 6(7) (2015) 4717.
[326] D. Sheng, T. Liu, L. Deng, L. Zhang, X. Li, J. Xu, L. Hao, P. Li, H. Ran, H. Chen, Z. Wang, Perfluorooctyl bromide & indocyanine green co-loaded nanoliposomes for

enhanced multimodal imaging-guided phototherapy, Biomaterials 165 (2018) 1-13.
[327] Y. Qin, B. Cao, J. Li, S. Liao, C. Lin, X. Qing, Q. Zhang, X. Yu, An Oxygen-Enriched Photodynamic Nanospray for Postsurgical Tumor Regression, ACS Biomater Sci Eng 6(11) (2020) 6415-6423.